A solid oxide fuel cell- sCO_2 Brayton cycle hybrid system

System concepts and analysis

S.I. Schöffer

TUDelft

A solid oxide fuel cell- sCO_2 Brayton cycle hybrid system

System concepts and analysis

by

S.I. Schöffer

to obtain the degree of Master of Science
at the Delft University of Technology,
to be defended publicly on Friday August 18, 2017 at 9:00 AM.

Student number:	4098676	
Project duration:	November 1, 2016 – August 18, 2017	
Thesis committee:	Prof. dr. ir. S. Klein,	TU Delft, supervisor
	Dr. P. V. Aravind,	TU Delft
	Dr. ir. C.A. Infante Ferreira	TU Delft

TU Delft

Abstract

New technologies are being developed to produce electricity cleaner and more efficient. A promising technology among these is the solid oxide fuel cell (SOFC). It electrochemically converts chemical energy into electricity. This process is highly efficient and several types of fuel are suitable. Furthermore, the SOFC operates at a high temperature, thus producing high quality excess heat which can be converted into electricity in a thermodynamic power cycle to increase the efficiency. Commonly this is done by a directly coupled gas turbine (GT).

The supercritical carbon dioxide (sCO_2) Brayton cycle has recently received attention for its potential as a next generation power cycle. It combines the advantages of the steam Rankine cycle and air Brayton cycle. So far, two heat sources are mainly considered for this cycle: Nuclear and concentrated solar power (CSP).

The aim of this study is to investigate the potential of integrating a SOFC with a sCO_2 Brayton cycle.

A thermodynamic model of the SOFC- sCO_2 Brayton cycle hybrid system (SSHS) is developed to explore and analyze different concepts that effect the integration of both systems.

Methane is converted to syngas in an indirect internal reforming (IIR) setup. The steam required for this process is either fed by a heat recovery steam generator (HRSG) or supplied by recirculating anodic exhaust gas. Both options are considered. Recirculating the exhaust of the cathode is another options that is explored and analyzed.

Two sCO_2 cycle setups are analyzed in combination with the SOFC system: A simple recuperative cycle and a recompression cycle.

Different setups of the SSHS are compared on efficiency, complexity of the system and size of the exchangers. For comparison, a directly coupled solid oxide fuel cell (SOFC)- GT hybrid system is considered as well.

It is found that the recompression cycle in combination with SOFC system is more efficient than the simple recuperative cycle but significantly increases the complexity of the heat exchanger network, recirculating cathodic air decreases the size of the heat exchangers and increases the efficiency and supplying steam through a HRSG decreases the efficiency.

Compared to a directly coupled SOFC-GT system the SSHS is a significantly more complex system. However, it does not require a pressurized SOFC since the sCO_2 Brayton cycle is indirectly coupled to the SOFC. The most efficient setup of the SSHS, combining the recompression cycle with cathode recirculation, has a higher LHV efficiency than the directly coupled SOFC- GT hybrid system, 66.58% over 62.38%. This setup of the SSHS is rather complex though. Other setups of the SSHS show efficiencies similar to that of the directly coupled SOFC- GT hybrid system.

A promising result, but the practical feasibility of the SSHS is something that should be carefully considered in future research and practice.

Contents

List of Figures

List of Tables

Acronyms

AC alternating current

ASR area specific resistance

BoP balance of plant

CHP combined heat and power

CSP concentrated solar power

DC direct current

DIR direct internal reforming

ER external reforming

GT gas turbine

hex heat exchanger

HHV higher heating value

HP high pressure

HRSG heat recovery steam generator

HT high temperature

HTC high temperature compressor

HTR high temperature recuperator

IIR indirect internal reforming

LHV lower heating value

LMTD logarithmic mean temperature difference

LP low pressure

LT low temperature

LTC low temperature compressor

LTR low temperature recuperator

MCFC molten carbonate fuel cell

MSR methane steam reforming

ORC organic Rankine cycle

PCHE printed circuit heat exchanger

PFD process flow diagram

PR pressure ratio

sCO_2 supercritical carbon dioxide

SOFC solid oxide fuel cell

SSHS SOFC- sCO_2 Brayton cycle hybrid system

ST steam turbine

STHE shell and tube heat exchanger

TIT turbine inlet temperature

TOT turbine outlet temperature

WGS water-gas shift

Nomenclature

Normal script

A area

CP isobaric heat capacity

C_P specific isobaric heat capacity

δ electron path length

ΔG^0 Gibbs free energy of formation

ΔH^0 enthalpy of formation

E potential

η efficiency

F Faraday constant

h specific enthalpy

$I, II, III, \ldots$ rank in temperature from low to high

I current

i current density

K chemical equilibrium constant

N number of

$\dot{n}$ molar flow rate

P pressure

$\dot{Q}$ heat

R ohmic resistance

$\bar{R}$ universal gas constant

r recirculation ratio

ρ resistivity

S/C steam to carbon ratio

T temperature

$\bar{U}$ overall heat transfer coefficient

U_f fuel utilization ratio

V volume

$\dot{W}$ work

x concentration

ξ extent of reaction

Subscripts

0 environment

aft afterburner

an anode

C cold stream

ca cathode

com compressor

E entering stream

e electric

FC fuel cell

fd feed

$flue$ flue gas

gen generator

H hot stream

hex heat exchanger

ic interconnection

L leaving stream

N Nernst

Ω ohmic

pre preheater

rf reformer

tur turbine

Superscripts

int interval

k component k

1
Introduction

On December 12, 2015, the United Nations Framework Convention on Climate Change reached an agreement to mitigate climate change. Key in reaching this goal is a cleaner and more efficient way of producing electricity. Traditional ways of electricity will be phased out and replaced by renewable energy sources and cleaner fuel conversion systems.

Among other technologies, the solid oxide fuel cell (SOFC) has received attention as a potentially clean and highly efficient method of converting chemical energy to electricity.

The supercritical carbon dioxide (sCO_2) Brayton cycle has received attention as a promising power cycle. It combines the advantages of the steam Rankine cycle and air Brayton cycle but does not suffer from the drawbacks of these cycles.

The aim of this study is to investigate the potential of integrating these two aforementioned technologies.

1.1. Background information

1.1.1. The sCO_2 Brayton cycle

The most common way of producing electricity today is to convert chemical energy into heat by combustion and converting heat into work in a thermodynamic cycle after which work is converted into electricity in a generator.

The efficiency of conversion of heat into work is limited by the theoretical Carnot cycle. This theoretical cycle features the four main processes that occur in real thermodynamic cycles: Compression, heat addition, expansion and heat rejection. The efficiency is limited by the hot and cold temperatures of the cycle.

$$\eta = 1 - \frac{T_C}{T_H} \tag{1.1}$$

Practical cycles all have their own peculiarities but share the key concepts of the Carnot cycle. It also provides a useful rule of thumb, the efficiency of the cycle increases if the hot temperature of the cycle, the turbine inlet temperature (TIT), increases. [1]

Two common practical cycles are the steam Rankine cycle, powering a steam turbine (ST), and the air Brayton cycle, powering a gas turbine (GT).

The steam Rankine cycle benefits from the fact that compression occurs in the liquid phase, requiring little pump work and thus increasing the efficiency of the cycle. Heat addition and rejection mostly occur at a constant temperature, evaporation and condensation, limiting the range of operating temperatures. State of the art steam Rankine cycles operating at a temperature up to 600 °C and pressure up to 300 bar reach efficiencies of around 46% [2].

The air Brayton cycle operates entirely in the gas phase. Because of this, compression work increases significantly. This reduces the efficiency but it can be compensated by the fact that heat addition is not tied to an evaporation process. This makes higher TITs possible and thus increases the efficiency. So even though an air Brayton cycle is not limited in temperature range theoretically by a phase change process, it is in practice bound to operate at a high TIT, ~1250 °C, in order to achieve efficiencies of ~35-45 %. [1] [3]

The temperature limitations of these two cycles make them less suitable to utilize waste heat. The steam Rankine cycle requires the majority of the heat input above relatively high temperature, the evaporation temperature. The boiling temperature of water being 100 °C at atmospheric pressure and the critical point at 373.95 °C and 220.64 bar. All heat available below this temperature is wasted. The air Brayton cycle simply requires a TIT too high for waste heat recovery application.

Different power cycles are being developed that are more suitable for waste heat recovery applications. One of these new technologies is the organic Rankine cycle (ORC). In an ORC water is replaced by an organic fluid as working fluid. This organic fluid is chosen so that the phase change occurs at lower temperatures, making it more suitable for low grade heat applications, such as waste heat recovery.

Another option is to develop cycles that operate near the critical point. Different working fluids, that have a suitable critical point, are being considered for this. A promising development in this field is the sCO_2 Brayton cycle. Carbon dioxide has the advantage of a low critical temperature, 30.98 °C, and suitable critical pressure, 73.77 bar. [4]

This critical temperature allows operation near the critical point. Near the critical point, the gas has a high density, significantly reducing the compression work. The cycle is supercritical, which means it operates entirely above the critical point and no phase change occurs. The sCO_2 therefore combines the advantages of the steam Rankine cycle, low compression work, and the air Brayton cycle, no phase change, but does not need a high TIT to achieve high efficiencies. The high density of the sCO_2 also makes for small and relatively simple turbomachinery.

Furthermore, carbon dioxide is abundantly available, cheap, stable and non-toxic. [5]

The simplest cycle setup is a recuperative cycle, figure 1.1a[1]. The fluid is compressed (1-2) and preheated (2-3) in the recuperator by the hot gas leaving the turbine. Heat from an external source is received (3-4) to bring the working fluid up to TIT. Expansion in the turbine (4-5) produces work. The hot exhaust, as said, is cooled down in the recuperator (5-6) and heat is rejected in the cooler (6-1). More advanced cycles to improve the efficiency have been studied. It is found that the recompression

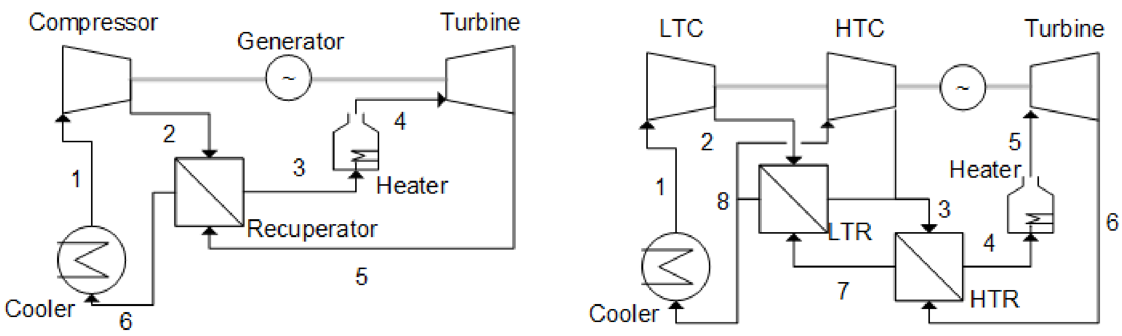

(a) *Simple recuperative cycle*

(b) *Simple recuperative cycle*

Figure 1.1: *process flow diagram (PFD)s*

cycle, figure 1.1b[2], is the most efficient for a high pressure ratio (PR) and TIT. Other more complex cycles reach similar efficiencies but the recompression cycle receives the most interest because of its relative simplicity and high efficiency [5][6][7][8][9][10].

In the recompression cycle the flow is split before it enters the cooler (8). The majority of the flow is cooled down (8-1) and compressed in the low temperature compressor (LTC) (1-2), as in the simple recuperative cycle. It is heated up to (2-3) the outlet temperature of the high temperature compressor (HTC) in the low temperature recuperator (LTR). Here the other part of the flow that is split before entering the cooler and compressed in the HTC (8-3) is added before entering the high temperature

[1]See figure 4.3 for a temperature-entropy diagram
[2]See figure 4.12 for a temperature-entropy diagram

recuperator (HTR) (3-4). Similar to the simple recuperative cycle heat is added (4-5) and work is produced in the turbine (5-6) by expansion. The hot outlet of turbine is cooled down in the HTR (6-7) and LTR (7-8) before the flow is split.

The cycle is more efficient because less heat is rejected by splitting the flow before entering the cooler. This is partly offset by the increased compression work at a higher temperature away from the critical point. It does however achieve a net gain in efficiency.

The sCO_2 Brayton cycle is still in its early developmental stages with very few actual systems constructed and tested. The largest system is a 10 MW pilot program looking to investigate and demonstrate the sCO_2 Brayton cycle. It's aim is to achieve efficiencies of over 50 % at a TIT of 700 °C. [11]

The two main heat sources considered for the sCO_2 Brayton cycle are nuclear [5] and concentrated solar power (CSP) [11]. Other fields such as coal power, waste heat recovery, geothermal energy and high temperature fuel cells are considered as well [6]. Prior studies on high temperature fuel cells and the sCO_2 Brayton cycle will be discussed in more detail in section 1.1.3.

1.1.2. The SOFC system

Fuel cells convert chemical energy directly into electricity by an electrochemical process, *skipping* the conversion steps of a heat engine. This makes a fuel cell potentially more efficient than traditional power cycles. Its efficiency is not limited by the Carnot efficiency but by the maximum obtainable work from a chemical reaction, the Gibbs free energy of formation [12].

$$\eta = \frac{\Delta G^0}{\Delta H^0} = 1 - \frac{T\Delta S^0}{\Delta H^0} \tag{1.2}$$

A single fuel cell consists of an electrolyte in contact on one side with the anode, the negative electrode, and the cathode, the positive electrode, on the other side. The fuel, the reducer in the electrochemical reaction, is supplied on the anode side. On the cathode side an oxidizer is supplied; usually oxygen either as a component in air or pure. Ions transfered in the electrochemical reaction are conducted by the electrolyte, electrons are not and flow through an external electrical circuit, producing electric power.

A concept very similar to that of a battery. Contrary to a battery, a fuel cell can not store energy but it converts chemical energy into electricity as long as fuel and an oxidizer are supplied.

Different types of fuel cells are characterized by the type of electrolyte, type of fuel and operating temperature. Table 1.1 shows the most important types of fuel cells [12].

As can be seen in table 1.1, the SOFC operates in a high temperature range. This high temperature is required for the electrolyte to conduct the mobile oxygen ions. These oxygen ions move from

Type	Mobile ion	Operating temperature °C	Applications
Alkaline fuel cell	OH^-	50-200	Space vehicles
Proton exchange membrane fuel cell	H^+	30-100	Vehicles and mobile applications
Direct methanol fuel cell	H^+	20-90	Portable systems requiring low power and long running time
Phosphoric acid fuel cell	H^+	~220	~200 kW combined heat and power (CHP) systems
Molten carbonate fuel cell (MCFC)	CO_3^{2-}	~650	~200 kW-1 MW CHP systems
SOFC	O^{2-}	600-1000	~2 kW- several MW CHP systems

Table 1.1: *Different types of fuel cells [12]*

the cathode, through the electrolyte, to the anode. The electrons needed to form these oxygen ions are supplied by an external electrical circuit connected to the anode. If hydrogen is used as fuel, which it commonly is, the anode half reaction is:

$$H_2 + O^{2-} \rightarrow H_2O + 2e^- \tag{1.3}$$

the cathode half reaction:

$$\frac{1}{2}O_2 + 2e^- \rightarrow O^{2-} \tag{1.4}$$

so the complete reaction is [12]:

$$H_2 + \frac{1}{2}O_2 \rightarrow H_2O \tag{1.5}$$

This reaction produces electricity and heat.

Besides hydrogen a wide range of fuels can be used by a SOFC system. Natural gas, consisting mainly of methane, is the most common fuel for SOFC systems. Before it can be utilized in the actual cell, it must be reformed to syngas. The most common way to do is, is through a steam reforming process. In this highly endothermic process methane and steam are converted to a mixture of hydrogen, steam, methane, carbon monoxide and carbon dioxide. Higher temperatures, in the same range as the operating temperature of the SOFC, produce syngas with higher concentrations of hydrogen. Therefore the syngas enters the anode channel of the fuel cell at a high temperature[3].

The steam needed for this process can be supplied externally or by recirculating part of the anode flow. In this way the steam formed in the anode half reaction can be used.

The heat needed for this process can be supplied externally, external reforming (ER), or the reformer can be thermally coupled to the fuel cell so that part of the the produced heat in the electrochemical process can be used for the steam reforming process. The latter setup is referred to as an indirect internal reforming (IIR) system. Integrating the reformer and anode completely, thus allowing the steam reforming reactions to take place in the anode simultaneously with the electrochemical reaction, is referred to as a direct internal reforming (DIR) system. This is potentially the most efficient. However, this causes problems with carbon deposition and thermal management.

Similar reforming processes can be applied for higher hydrocarbons in fuel mixes. The gasification products of solid fuels can be utilized in a SOFC as well. Impurities in the fuel such as sulphur components should be treated as these can damage the fuel cell. [13]

Thermal management is an important aspect in all types of fuel cells. The materials of the electrolyte and electrodes have different thermal expansion coefficients. Thermal compatibility of the materials is important in choosing these, but even then thermal stress cannot be avoided completely. In order to limit the thermal stress, large temperature difference must be avoided in a fuel cell. This is achieved by cooling the fuel cell. This is commonly done by air, which is used to supply the oxygen as well. To avoid high temperature differences the air must be preheated before entering the cathode channel of the fuel cell [14].

All cells must be arranged in stacks and connected electrically. Different cell geometries, the two most common being tubular and planar cells, are possible, as are different setups to stack them. Figure 1.2 is an example of these two cell designs and common ways to stack them. Aspects like thermal management, fabrication processes and electrical losses should all be considered when designing a SOFC stack and system [15].

The first SOFC demonstration plant developed by Siemens Westinghouse, in the Netherlands, produced 100 kW. In 1998 it operated for over 15 000 hours, demonstrating the feasibility of the technology [16]. Today, SOFC systems are also becoming commercially available [17], however it is not a widespread technology yet.

Problems to overcome are reliability issues and costs. These are challenges for the cell itself and other system components such as interconnectors and seals. Research mainly focuses on electrolyte and electrode materials and reducing the issues with high temperatures [18].

[3]From a perspective of thermal management it is also beneficial that the syngas enters at a high temperature

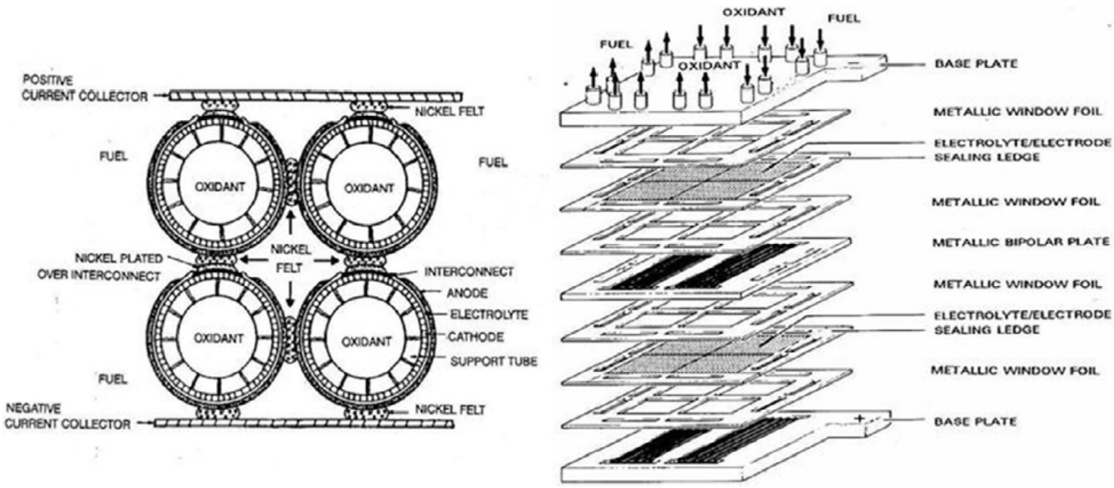

Figure 1.2: *Example of a tubular stack (l) and planar stack (r)*

1.1.3. SOFC hybrid systems

Since a SOFC operates on high temperatures, it also produces high quality heat. Furthermore, not all fuel is used in a SOFC so some of it can be still be combusted. Many concepts for utilizing this heat have been suggested and studied [19][20]. A useful way to utilize this heat is by converting it into electricity in a bottoming cycle.

Different concepts exist and can be categorized based on several characteristics of the system, i.e. the method of reforming as mentioned in section 1.1.2 and the way the SOFC system is coupled to the bottoming cycle.

A SOFC can either be directly coupled to a gas turbine (GT) or indirectly to a bottoming cycle, such as a steam Rankine cycle. In a directly coupled system, the hot exhaust gas of the fuel cell is fed directly into a GT. The remaining fuel is combusted and the gas is expanded through the turbine. This requires the fuel cell to operate at an elevated pressure and makes the system less flexible and thus harder to operate.

In case of an indirect coupling, the excess heat from the SOFC system is transferred by heat exchangers to a power cycle. This setup requires a more complicated system, more heat exchangers, than a directly coupled system but it has some advantages as well. The two subsystems can operate independently, making the complete setup more flexible, the fuel cell can operate on atmospheric pressure and different working fluids in the thermodynamic cycle such as water and carbon dioxide are possible.

Table 1.2 gives a summary of selected studies reviewed in [19]. All systems use methane as fuel. Most research focuses on directly coupled hybrid systems since these have higher efficiencies and a less complex system setup, making them less expensive. Control strategies however prove to be difficult, making these systems unattractive for part-load operation. Conversely, indirect coupled systems are more complex and less efficient but are more flexible in operation.

	Reforming system	SOFC hybrid setup	TIT(°C)	Turbine PR	Efficiency[4]
Calise *et al.* [18]	DIR/Anode recirculation	Direct	1250	7.8	67.5%
Chan *et al.* [21]	DIR/Anode recirculation	Direct	1193	4.58	62.2%
Chan *et al.* [22]	DIR/HRSG	Direct	948	3.71	61.9%

[4]Electric system efficiency

Song *et al.* [23]	IIR/Anode recirculation	Direct	840	2.9	60.2%
Jia *et al.* [24]		None			49%
	DIR/HRSG	Direct	998	2.87	60.65%
		Direct + Rankine cycle	965/340	2.83/254	60.40%
Yang *et al.* [25]	IIR/Anode recirculation	Direct	750-1150	3.5	42-70%
	ER/Anode recirculation		750-1150	3.5	32-60%
Arsalis [26]	DIR/Anode recirculation	Direct + Rankine cycle			66-74%
Park and Kim [27]	IIR/Anode recirculation	Direct	700-1350	3.5-10.5	55-72%
		Indirect air Brayton cycle	600-1050	3.5-10.5	47-66%
Facchinetti *et al.* [28]	ER/HRSG	Anode coupling [5]	800/1200	2.4/2.3	66.0/68.0%
	ER/HRSG	Cathode coupling [6]	800/1200	5.0/5.5	63.8/65.5%

Table 1.2: *Overview of selected studies reviewed in [19]*

SOFC/GT hybrid systems have been studied most extensively. However, only very few actual systems have been built. The fuel cells are still very expensive and the systems complexity and turbomachinery make it hard to scale down to lab size.

A first proof of concept of a hybrid SOFC-GT system developed by Siemens Westinghouse in 1999 shows a high (52.1%) but lower than expected (>57%) efficiency at a power of 200 kW [16] [29].

Another 200 kW test setup has successfully operated at an efficiency of 50%. Higher efficiencies on a scale of multiple megawatts of over 70% are even deemed feasible [30].

A smaller 5 kW system has successfully been built and tested as well. Data on efficiency has not been published though [31].

Clearly this technology is still developing and a fully commercially operational hybrid SOFC/GT system does not exist yet.

Integration of a SOFC system and sCO_2 Brayton cycle has, to the authors knowledge, not been studied yet. But a sCO_2 Brayton cycle in combination with another high temperature fuel cell, a MCFC, has been.

Bae *et al.* [32] have studied various cycle layouts as a bottoming cycle for a MCFC system. The heat available from the MCFC is kept constant and treated as an external heat source though. Consequently, integration concepts and variation in the MCFC operation and its effect on the sCO_2 could not be studied.

Bae *et al.* concluded that the performance of the sCO_2 Brayton cycle is better than that of an indirectly coupled air Brayton cycle. Furthermore they introduced a cascading sCO_2 Brayton/Rankine cycle in which the cooler of the sCO_2 is also the heater in a steam Rankine cycle. This setup proved to perform similarly or even better than the recompression cycle in terms of efficiency. In terms of specific power, an indication of how large the heat exchangers will be, a transcritical simple recuperative cycle performed best. The recompression cycle and the cascading sCO_2 Brayton/Rankine cycle have lower specific powers. From this Bae *et al.* conclude that not one cycle can be selected to meet a wide range of design requirements. Finally, they recommend that the operating conditions of the MCFC can be optimized to match the operating characteristics of the sCO_2 Brayton cycle. However, full integration of both systems is not considered, the exhaust of the MCFC is regarded as an external heat source.

[5] The outlet of anode is connected to a compressor and turbine, the fuel cell operates at ambient pressure
[6] The outlet of cathode is connected to a compressor and turbine, the fuel cell operates at ambient pressure

1.2. Motivation and scope

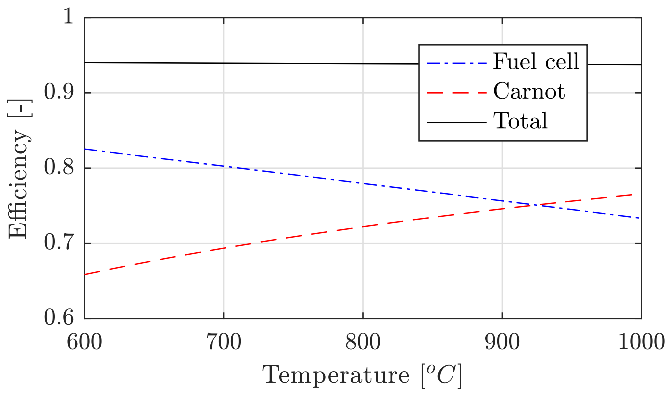

Figure 1.3: *Maximum theoretical efficiency*

Figure 1.3 shows the maximum obtainable efficiency of a fuel cell, heat engine and combination of the two. The maximum efficiency of the fuel cell is defined as the ratio between the Gibbs free energy of formation of the oxidation of hydrogen at standard pressure and the lower heating value (LHV) of hydrogen, equation 1.2 and 1.5. The total efficiency is defined by assuming that all heat generated in the reaction is transfered to an ideal Carnot heat engine.

Clearly an actual system will not operate so ideally, but figure 1.3 does illustrate that both systems have the potential to work complementary and achieve very high efficiencies.

Furthermore, the temperature range of the SOFC, 600 - 1000 °C, produces waste heat at these high temperatures. This matches well with the operating temperatures, 32 to 700 °C, of the sCO_2 Brayton cycle.

The concept of a SOFC- sCO_2 Brayton cycle hybrid system (SSHS) is relatively unknown. The focus is to look at the interaction between the two systems. Therefore, only parameters that affect this interaction are studied. The goal is to identify qualitative properties of the SSHS under the effect of different operating parameters. That is not the say that quantitative properties are not of interest, but these should be considered with care as they are only as good as the assumptions regarding the thermodynamics behind the system. Comparison of quantitative properties of different cases, under the same assumptions, does provide an insight into the quality of each case.

Since both system have been studied separately, it is outside of the scope of this study to investigate the effects of parameters that only affect one of the two systems. Typical characteristics and dependencies of each system are taken from literature.

Different cases are compared on the basis of efficiency, heat exchanger area and the systems complexity. A cost estimation is not included because both technologies are in the developmental stages; any cost estimation would be haphazard.

1.3. Thesis outline

TheSSHS is explained and its model is described in chapter 2. The model of the SOFC is validated in chapter 3. Different cases are discussed and compared in chapter 4. In chapter 5 a conclusion is drawn and recommendations are made.

2

Model description

A model is developed to study a SSHS. This chapter describes the equations, assumptions and choices behind this model. Its aim is to understand the interaction between the SOFC system and the sCO_2 Brayton cycle and to get an idea of its potential. More detailed study on each component will be necessary but is outside the scope of this study.

Section 2.1 discusses the general concept of the SSHS and assumptions applicable to all components. The SOFC system is described in section 2.2 and section 2.3 describes the sCO_2 Brayton cycle. The integration strategy and balance of plant (BoP) components will be discussed in section 2.4. Finally, the modeling approach is discussed in section 2.5.

2.1. System concept and general assumptions

2.1.1. System concept

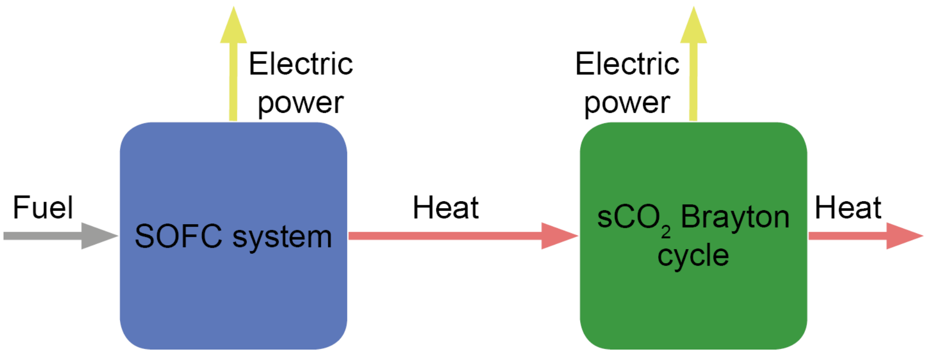

Figure 2.1: *System concept*

Figure 2.1 shows the general concept of the SSHS. In the SOFC system fuel is converted into electric power and heat. Part of this excess heat is converted in the sCO_2 Brayton cycle into electric power, the remaining heat is rejected to the environment.

2.1.2. General assumptions

In order to model the system, assumptions have to be made. Assumptions listed here are valid for every component in the system. Specific assumptions for a component are given in the respective section.

- All components are perfectly thermally insulated, therefore there is no heat transfer with the environment

- Fluid properties are taken from Lemmon *et al.* [33] if temperature and pressure are within range of the database
- When temperature and pressure are out of range for Lemmon *et al.* [33], the properties are determined by the GasMix method
  - The GasMix method applies the ideal gas law and temperature dependent specific heats

$$PV = \bar{R}T \tag{2.1}$$

$$C_P = C_1 + C_2 T + C_3 T^2 + C_4 T^3 \tag{2.2}$$

  - Constants are from Chase *et al.* [34] and are valid from 300 to 5000 K
- The fuel supplied to the SOFC system is pure methane
- Components are modeled by a lumped parameter approach
- A reference environment is defined as a gas mixture of nitrogen, oxygen, water vapor and carbon dioxide at standard temperature and pressure

$$T_0 = 298.15\,\mathrm{K} \tag{2.3}$$

$$P_0 = 1.013\,25\,\mathrm{bar} \tag{2.4}$$

$$[x_0^{N_2}, x_0^{O_2}, x_0^{H_2O}, x_0^{CO_2}] = [0.7649, 0.2035, 0.0313, 0.003] \tag{2.5}$$

2.2. The solid oxide fuel cell system

Besides the actual fuel cell, a SOFC is made up of several other components, depending on the exact setup of the system. Figure 2.2 shows the key components of a typical SOFC system.

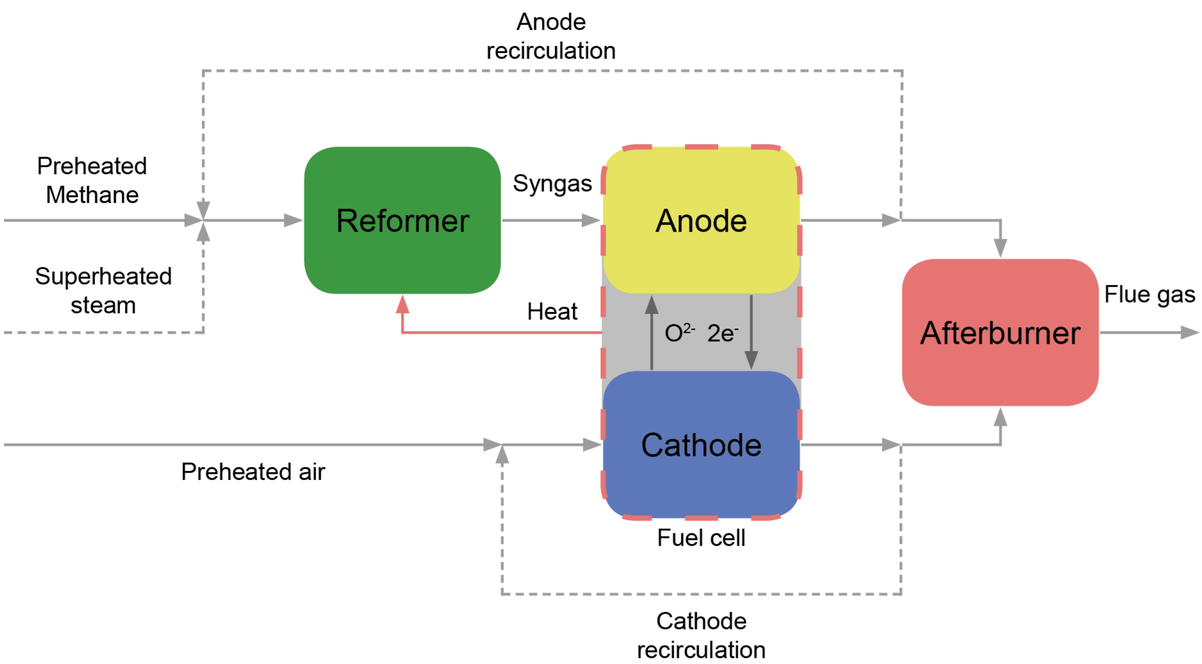

Figure 2.2: *SOFC system concept*

In this study pure methane is used as fuel. This has to be reformed to a hydrogen rich mixture, syngas. Three options exist for a reforming system. In an ER system, the reformer is separated from the SOFC entirely. Heat required for the reforming process is supplied by a heat exchanger.

In an IIR system, the reformer is thermally coupled to the SOFC, but the flows are separated. The heat required by the reformer is supplied directly by the excess heat generated in the SOFC. The advantage of this setup over an ER system is that it is more compact, more efficient and reduces the cooling requirement of the SOFC.

The third option is lining the anode with a catalyst so that the reforming process can take place in the anode itself. This setup is potentially even more efficient and compact but has some drawbacks. The highly endothermic reforming process can lead to cold spots in the fuel cell, complicating the thermal management and potentially damaging the cell. Furthermore, undesirable reactions are more likely to occur. Such reactions might cause carbon deposition in the anode, blocking its active area and making it less efficient.

In this work, an IIR system is adopted because it shows a good trade off between efficiency and practical feasibility.

The reforming process requires steam. This can either be supplied externally by a heat recovery steam generator (HRSG) or by recirculating anode exhaust gas. In the latter case, the steam formed in the electrochemical reaction in the SOFC is utilized in the reforming reactions. The advantage of supplying steam by anode recirculation is that it does not require a heat recovery steam generator (HRSG). However, supplying steam externally in a HRSG does provide more flexibility in operation. Both options will be considered in this work.

Large temperature differences in the SOFC should be avoided to keep thermal stress within limits. Part of the cooling is achieved by supplying heat to the reformer in the IIR setup but additional cooling is required. Air is not only required to supply oxygen for the electrochemical reaction, it is also used to cool the fuel cell. This air has to be preheated to avoid a large temperature difference. Therefore the temperature difference between the in- and outlet of the cathode is not large, consequently a high equivalence ratio of air must be supplied in order to cool the SOFC.

The option to recirculate part of the air from the outlet of the cathode will be considered in this study as well.

Not all fuel is utilized in the fuel cell. Part of the hydrogen is not consumed in order to maintain a partial pressure of hydrogen. Furthermore, carbon monoxide is assumed not to react electrochemically in the fuel cell. And finally, a very small amount of methane might be left in the mixture. These combustible products are burned in an afterburner.

Modeling of the operation of the SOFC is split into two. Section 2.2.1 discusses the reforming process and section 2.2.2 the actual fuel cell

2.2.1. Reforming process

Methane and steam enter the reformer as a fuel mix. In the reformer heat is added, making the highly endothermic methane steam reforming (MSR) reaction possible. More hydrogen is produced in the reformer through the slightly exothermic water-gas shift (WGS) reaction. The produced syngas leaves the reformer and enters the anode. In the anode the hydrogen is consumed in the fuel cells electrochemical reaction. The WGS reaction will also still take place in the anode, the MSR will not in absence of a catalyst. The exhaust of the anode is partially recirculated and the rest is fed to the afterburner.

To determine the compositions of the fuel mix, syngas and anode exhaust gas, some assumptions have to be made.

- The outlet of the reformer is the chemical equilibrium of only two reactions assumed to take place [35]
  - The MSR reaction
  $$CH_4 + H_2O \leftrightarrows CO + 3H_2 \tag{2.6}$$
  - The WGS reaction
  $$CO + H_2O \leftrightarrows CO_2 + H_2 \tag{2.7}$$
- The reformer is at a constant temperature

- The steam to carbon ratio at the inlet of the reformer is 1.7 [35]
- Two reactions take place in the anode, the WGS reaction (equation 2.7) and the anode half reaction

$$H_2 + O^{2-} \rightarrow H_2O + 2e^- \tag{2.8}$$

- The fuel utilization ratio is fixed at 85% [36]
- The outlet of the anode is the chemical equilibrium of the WGS reaction

The chemical equilibrium of the MSR- and WGS- reactions are given by its constants, equation 2.9 and 2.10.

$$K_{MSR} = \frac{x_{rf,L}^{CO}(x_{rf,L}^{H_2})^3}{x_{rf,L}^{CH_4} x_{rf,L}^{H_2O}}(\frac{P}{P_0})^2 \tag{2.9}$$

$$K_{WGS} = \frac{x_{rf,L}^{CO_2} x_{rf,L}^{H_2}}{x_{rf,L}^{CO} x_{rf,L}^{H_2O}} \tag{2.10}$$

The equilibrium constants depend on temperature, equation 2.11 [37]. Its constants are in table 2.1.

$$\log K = C_1 T + C_2 T^+ C_3 T^3 + C_4 T^4 + C_5 \tag{2.11}$$

	MSR reaction	WGS reaction
C_1	$1.950\,28 \times 10^{-1}$	-3.915×10^{-2}
C_2	$-2.252\,32 \times 10^{-4}$	$4.637\,42 \times 10^{-5}$
C_3	$1.240\,65 \times 10^{-7}$	$-2.574\,79 \times 10^{-8}$
C_4	$-2.631\,21 \times 10^{-11}$	$5.473\,01 \times 10^{-12}$
C_5	-66.1395	13.2097

Table 2.1: *Constants for equation 2.9 and 2.10*

A set of equations and variables can be defined and solved in order to determine the gas compositions and mass flows at the inlet/outlet of the reformer and anode. Using the fuel- and water- feed, extent of reactions, fuel utilization-, steam to carbon- and anode recirculation- ratio a mass balance for each component can defined, equation 2.12 to 2.16.

$$\dot{n}_{rf,L}^{CH_4} = \dot{n}_{rf,L}^{CH_4} r_{an} + \dot{n}_{fd}^{CH_4} - \xi_{MSR} \tag{2.12}$$

$$\dot{n}_{rf,L}^{H_2O} = (\dot{n}_{rf,L}^{H_2O} - \xi_{WGS,an} + \frac{I}{2F}) r_{an} + \dot{n}_{fd}^{H_2O} - \xi_{MSR} - \xi_{WGS,rf} \tag{2.13}$$

$$\dot{n}_{rf,L}^{CO} = (\dot{n}_{rf,L}^{CO} - \xi_{WGS,an}) r_{an} + \xi_{MSR} - \xi_{WGS,rf} \tag{2.14}$$

$$\dot{n}_{rf,L}^{CO_2} = (\dot{n}_{rf,L}^{CO_2} + \xi_{WGS,an}) r_{an} + \xi_{WGS,rf} \tag{2.15}$$

$$\dot{n}_{rf,L}^{H_2} = (\dot{n}_{rf,L}^{H_2} + \xi_{WGS,an} - \frac{I}{2F}) r_{an} + 3\xi_{MSR} + \xi_{WGS,rf} \tag{2.16}$$

The fuel utilization ratio is defined as the ratio between the current and the maximum theoretically current assuming all combustible products oxidize:

$$U_f = \frac{I}{2F(\dot{n}_{rf,L}^{H_2} + 4\dot{n}_{rf,L}^{CH_4} + \dot{n}_{rf,L}^{CO})} \tag{2.17}$$

The steam to carbon ratio is defined as the ratio between steam and methane at the inlet of the reformer:

$$S/C = \frac{\dot{n}_{rf,E}^{H_2O}}{\dot{n}_{rf,E}^{CH_4}} = \frac{(\dot{n}_{rf,L}^{H_2O} - \xi_{WGS,an} + \frac{I}{2F}) r_{an} + \dot{n}_{fd}^{H_2O}}{\dot{n}_{rf,L}^{CH_4} r_{an} + \dot{n}_{fd}^{CH_4}} \tag{2.18}$$

The concentration is defined as:

$$x^k = \frac{\dot{n}^k}{\sum_k \dot{n}^k} \tag{2.19}$$

For a given outlet temperature of the reformer the set of equations 2.9 to 2.19 can be solved. This determines the molar flow rates of each component at the inlet of the reformer, the outlet of the reformer/inlet of the anode and the outlet of the anode.

2.2.2. Fuel cell

Geometry

Different cell geometries and stack designs for SOFC systems have been developed. Each design has its advantages and disadvantages. For stationary power production, ease of scaling up is important. For this reasons, the tubular design, as shown in figure 2.3 is chosen. [15]

The tubular design, as designed by Siemens Westinghouse is shown in figure 2.3. The sizes of the

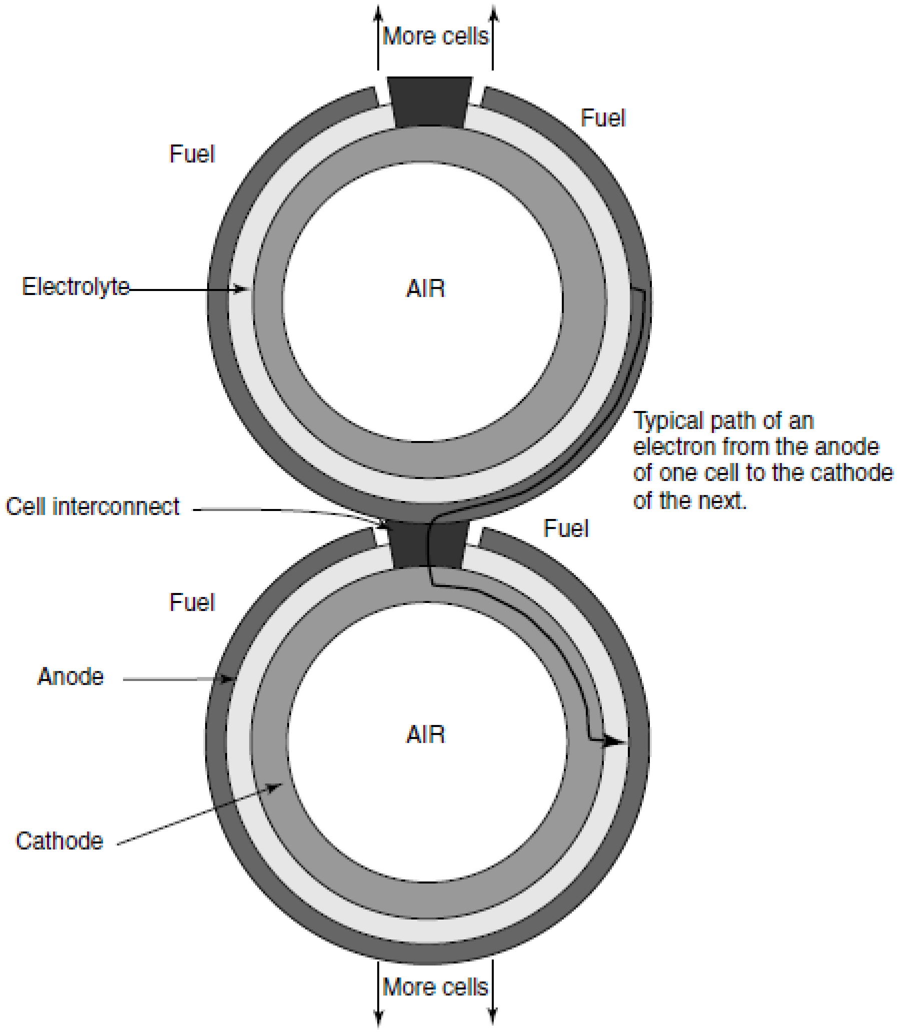

Figure 2.3: *Tubular design as produced by Siemens Westinghouse [12]*

components of this design differ. Table 2.2 shows the sizes chosen in this study.

Electrochemical operation

As mentioned in section 2.2.1 it is assumed that only one electrochemical reaction takes place in the fuel cell. The anode half reaction is given by equation 2.8. The electrons produced in this reaction are not conducted by the electrolyte and flow through an external circuit powering an electric load. The

Cell length	150 cm [14]
Cell outer diameter	2.2 cm [14]
Cathode thickness	2 mm [14]
Electrolyte thickness	40 μm [14]
Anode thickness	150 μm [14]
Interconnection thickness	100 μm [14]
Interconnection angle	30° [38]

Table 2.2: *Component sizes of a tubular cell in this study*

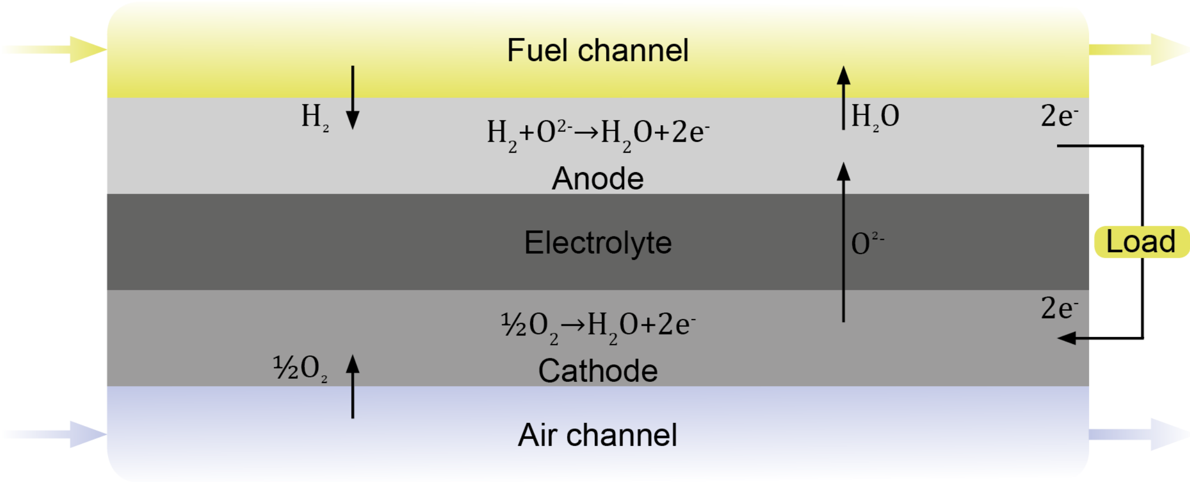

Figure 2.4: *Electrochemical operation of a SOFC*

oxygen ions needed for this reaction however are conducted by the electrolyte and are formed in the cathode half reaction, equation 2.20.

$$\frac{1}{2}O_2 + 2e^- \rightarrow O^{2-} \tag{2.20}$$

The total reaction in the fuel cell is the sum of both half reactions, equation 2.21

$$H_2 + \frac{1}{2}O_2 \rightarrow H_2O \tag{2.21}$$

To determine the performance of a fuel cell an ideal cell voltage, also referred to as Nernst voltage, is defined. If the fuel cell would operate ideally, it would produce an amount of electrical power equal to the Gibbs free energy of formation of the electrochemical reaction taking place. The voltage related to that, is the Nernst voltage. In case of the oxidation of hydrogen this is equation 2.22:

$$E_N = -\frac{\Delta G^0(T_{FC}, P_0)}{2F} + \frac{\bar{R}T_{FC}}{2F}\ln\frac{P_{H_2O}\sqrt{P_{O_2}}}{P_{H_2}} \tag{2.22}$$

The Nernst voltage consists of two terms. The Gibbs free energy of formation at the fuel cells working temperature and standard pressure and a term correcting for the concentrations of the components taking place in the reaction. The latter term is defined under the assumption of the ideal gas law and that fugacity can be approached by partial pressures in case of the relatively low operating pressures of a fuel cell. Both terms are divided by the amount of electrons being transfered in one reaction and the Faraday constant, to convert from energy to voltage.

For high temperature fuel cells, such as a SOFC, the potential loss due to the low concentrations of hydrogen, water and oxygen can be significant.

As current is drawn, losses occur, also referred to as overpotential. There are three sources of overpotential in fuel cells, namely ohmic, activation and concentration overpotential. In order to determine the operating characteristics of the SOFC, some assumptions are made.

- The partial pressure of each component is determined by Raoult's law [39]. This law states that the partial pressure of a component is proportional to its concentration.
- A lumped parameter approach is assumed, section 2.1.2, this has the following consequences:
  - The fuel cell temperature is constant in all directions
  - The current density is constant
  - The potential is constant and therefore determined by the outlet compositions of the fuel and air flow since at this point Nernst voltage is at its minimum
- Under normal operating conditions the overpotential is dominated by ohmic overpotential.
  - Concentration overpotential only becomes significant when the limiting current density is approached [14]. It is assumed that the fuel cell is operated far from this limiting current density. Therefore concentration overpotential is neglected.
  - Activation overpotential in high temperature fuel cells is very insignificant [14] and therefore neglected
- As mentioned in section 2.2.1 the fuel utilization ratio is fixed
- DC/AC conversion efficiency is 97% [36]

Ohm's law determines the ohmic overpotential.

$$E_{\Omega} = IR^{FC} \tag{2.23}$$

Figure 2.3 shows a typical electron path in a tubular geometry. An equivalent electrical circuit shown in figure 2.5 represents this path. Two of these circuits in parallel form the equivalent circuit of the fuel cell [40]. Each resistance depends on the components resistivity, surface and the path length of the electron.

$$R^k = \frac{\delta^k \rho^k}{A^k} \tag{2.24}$$

Resistivity of each component depends on temperature [38]. See table 2.3 for the values of the constants.

$$\rho^k = C_1 \exp \frac{C_2}{T_{FC}} \tag{2.25}$$

Subtracting the overpotential from the ideal potential gives the actual cell potential, equation 2.26.

	C_1 (Ωcm)	C_2 (K)
Anode	2.98×10^{-3}	-1392
Cathode	8.114×10^{-3}	600
Electrolyte	2.94×10^{-3}	10350
Interconnect	1.256×10^{-1}	4690

Table 2.3: *Constants for equation 2.25*

$$E_{FC} = E_N - E_{\Omega} \tag{2.26}$$

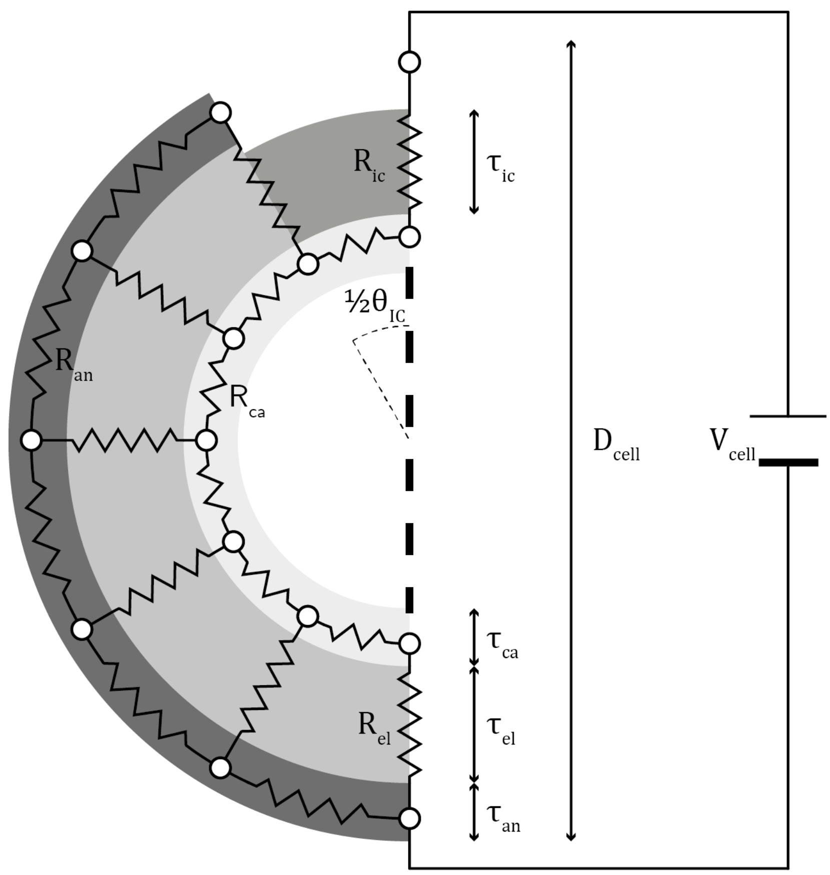

Figure 2.5: *Equivalent electrical circuit*

Cooling

Not all chemical energy in the fuel is converted to electricity, a significant part is converted to heat. Part of it due to the irreversibilities in the electrochemical reaction and part by the heat generated by the ohmic resistance. This heat is absorbed by the air and fuel flow. As mentioned before, large temperature differences in the fuel cell cause thermal stress that will damage the fuel cell [12]. Exactly how and where in the fuel cell this heat is generated is a complicated matter. Some assumptions regarding the thermal management of the fuel cell are made to simplify this [41]:

- The entering temperatures of the anode and cathode flow are equal, so are their leaving temperatures
- The temperature difference between the in- and outlet of the anode and cathode flows is 100 °C
- The fuel cells temperature is midway between the entering and leaving temperatures of the fuel and air flow
- Air used by the system has the same composition as the environment, equation 2.5

To determine how much air is needed to cool the fuel cell, the energy balance of the fuel cell must be solved.

$$\dot{n}_{an,E}h_{an,E} + \dot{n}_{ca,E}h_{ca,E} = \dot{W}_{FC,e} + \dot{Q}_{rf} + \dot{n}_{an,L}h_{an,L} + \dot{n}_{ca,L}h_{ca,L} \tag{2.27}$$

Since the oxygen concentration at the outlet of the cathode affects the Nernst potential and thus the electrochemical operation, the cooling is affected as well. The composition of the gas at the cathode outlet determines its specific enthalpy, since the temperature and pressure are imposed. Therefore the mass balance of the cathode (equation 2.28), and more specifically of the oxygen in the cathode (equation 2.29), have to be solved simultaneously with the fuel cells energy balance and and its overall electrochemical operation.

$$\dot{n}_{air,pre,L} + r_{ca}\dot{n}_{ca,L} = \frac{I}{4F} + \dot{n}_{ca,L} \tag{2.28}$$

$$x_{air}^{O_2}\dot{n}_{air,pre,L} + r_{ca}x_{ca,L}^{O_2}\dot{n}_{ca,L} = \frac{I}{4F} + x_{ca,L}^{O_2}\dot{n}_{ca,L} \tag{2.29}$$

2.3. The sCO_2 Brayton cycle

As mentioned in section 1.1.1, different setups for the sCO_2 Brayton cycle are possible. In this study, two setups are considered, the simple recuperative cycle and the recompression cycle. Both cycles will operate entirely above the critical point (73.77 bar, 30.98 °C).

Since the cycle will be integrated with the SOFC system, the heat exchanger setup of the cycle is not necessarily the same as when it would operate as a stand alone system with an external heat source. Therefore, only the compressor(s) and turbine(s) operating conditions will be defined initially. The resulting hot and cold streams will be integrated with the SOFC system.

Some assumptions regarding the turbomachinery have to be made:

- Minimum pressure and temperature of the cycle is a little above the critical point at 80 bar and 32 °C
- Maximum pressure and temperature of the cycle is 250 bar and 700 °C [42]
- Isentropic efficiency of a compressor is 80 % and assumed to be constant for all operating conditions [43]
- Isentropic efficiency of a turbine is 90 % and assumed to be constant for all operating conditions [42]
- Efficiency of the generator is 95 % and assumed to be constant for all operating conditions [44]
- Mechanical losses in the shaft are assumed to be negligible

2.4. Balance of plant

2.4.1. Pinch analysis

With the SOFC system defined and the compressors and turbines of the sCO_2 Brayton cycle defined, a network of heat exchangers must be designed. A pinch analysis [45] will be used to determine the mass flow in the sCO_2 Brayton cycle and a maximum total efficiency.

In a pinch analysis a system of hot streams, that need to be cooled down, and cold streams, that need to be heated up, is analyzed. It aims to maximize the heat transfer between the hot and cold streams in order to minimize external hot and/or cold utilities.

Important in the pinch analysis is the thermodynamic pinch point of the system. In order to find this point, a composite temperature-enthalpy curve of all the hot streams is determined. This is done by evaluating the enthalpy change in a certain temperature interval of all the hot stream combined. Similarly this done for all the cold streams. The pinch point of the system is found where both temperature enthalpy curves, hot and cold, have an imposed minimal temperature difference. No other point can have a smaller temperature difference.

The pinch point of the system represents the point where the design of the heat exchanger network is at its most critical. After all, this is where the temperature difference is at its minimum. It also splits the design problem into two, above and below the pinch. Heat should not be transfered across the pinch. This means that for the problem above the pinch, no external cold utility is necessary because all hot flows should can be cooled down just by supplying heat to the cold flows without violating the imposed minimal temperature difference. An external hot utility might be needed to supply sufficient heat to the cold streams. Vice versa there will be no need for an external hot utility for the problem below the pinch.

A simple example of a pinch analysis can be found in section A.1. It should be noted that a pinch analysis does not determine a heat exchanger network but only provides a useful starting point to design one.

Specific to this study is that the mass flow through the sCO_2 Brayton cycle is unknown. This is determined by solving the pinch problem for a specified minimum temperature difference. The problem is constrained by the fact that there will no external hot utility.

2.4.2. Heat exchangers

Different heat exchanger types will have to be employed in this system. For the low pressure (LP) flows a common shell and tube heat exchanger (STHE) will be used [46]. The high pressure (HP) flows in the sCO_2 Brayton cycle require a different heat exchanger though.

One such heat exchanger designed for the high temperatures and pressures involved in this system is a PCHE. Heatric [47] makes PCHEs, its maximum operating temperature and pressure are 1160 K and 650 bar respectively [47].

A single plate of a PCHE is made by etching channels photo-chemically into both sides of the plate. Dependent on the design requirements different types channels and flow configuration are possible. The plates are joined together by a process called diffusion bonding, creating one solid block.

Because of this manufacturing process, a PCHE is compact, highly efficient and capable of operating at very high pressures and temperatures [48].

Estimating the size of heat exchangers is commonly done by determining the overall heat transfer coefficient. Different methods for evaluating the overall heat transfer coefficient of a PCHE have been compared with data from Heatric [47] by Bahamonde Noriega *et al.* [7].

Results from Bahamonde Noriega *et al.* [7] show that a relation suggested by Hesselgreaves *et al.* [48] performs the best. However, this comparison in only made for a sCO_2 recuperator. Furthermore, the suggested relation by Hesselgreaves *et al.* [48] is based on work by Oyakawa *et al.* [50] in which relations are established for flows with Reynolds numbers in the order of $10^4 - 10^5$. The air flow for example will have far lower Reynolds numbers for reasonable flow velocities.

Since determining a heat transfer coefficient is uncertain at best and the goal of this work is to compare different setups with one another, not designing an actual system, it is chosen to estimate an overall heat transfer coefficient and not determine it.

Heatric supplies estimates for heat transfer coefficients in case of LP gas PCHE, a HP gas PCHE and a water/water PCHE. There is an exact value found by testing for a sCO_2 recuperator; this value is used in this work [47][51].

The heaters that are needed in a SSHS involve a LP and HP gas stream. Heatric estimates the overall heat transfer coefficient lower for for LP flows than for HP flows. Therefore the heat transfer coefficient of a heater is assumed to be lower than that of a HP recuperator. The lower limit of the estimate for LP flows from Heatric is used.

The heat transfer coefficient of the sCO_2 cooler is assumed to be higher than that of the recuperator since the cold stream in this PCHE is water. It also found that the heat transfer coefficient of sCO_2 near the critical point is similar to that of water [5]. For this reason, the heat transfer coefficient of the sCO_2 cooler is estimated at the lower limit of the estimate by Heatric for a water/water PCHE. These heat

	$\bar{U}$ ($W\,m^{-2}\,K^{-1}$)
Esitmates by Heatric [47]	
LP gas PCHE	500-1000
HP gas PCHE	1000-4000
Water/water PCHE	7000-10 000
Values used in present work	
PCHE recuperator	754 [47][51]
PCHE heater	500
PCHE cooler	7000
STHE gas to gas	20 [52]
STHE gas to water	30 [52]

Table 2.4: *Typical overall heat transfer coefficients*

transfer coefficients are assumed to be constant in every heat exchanger. This not the case for flows

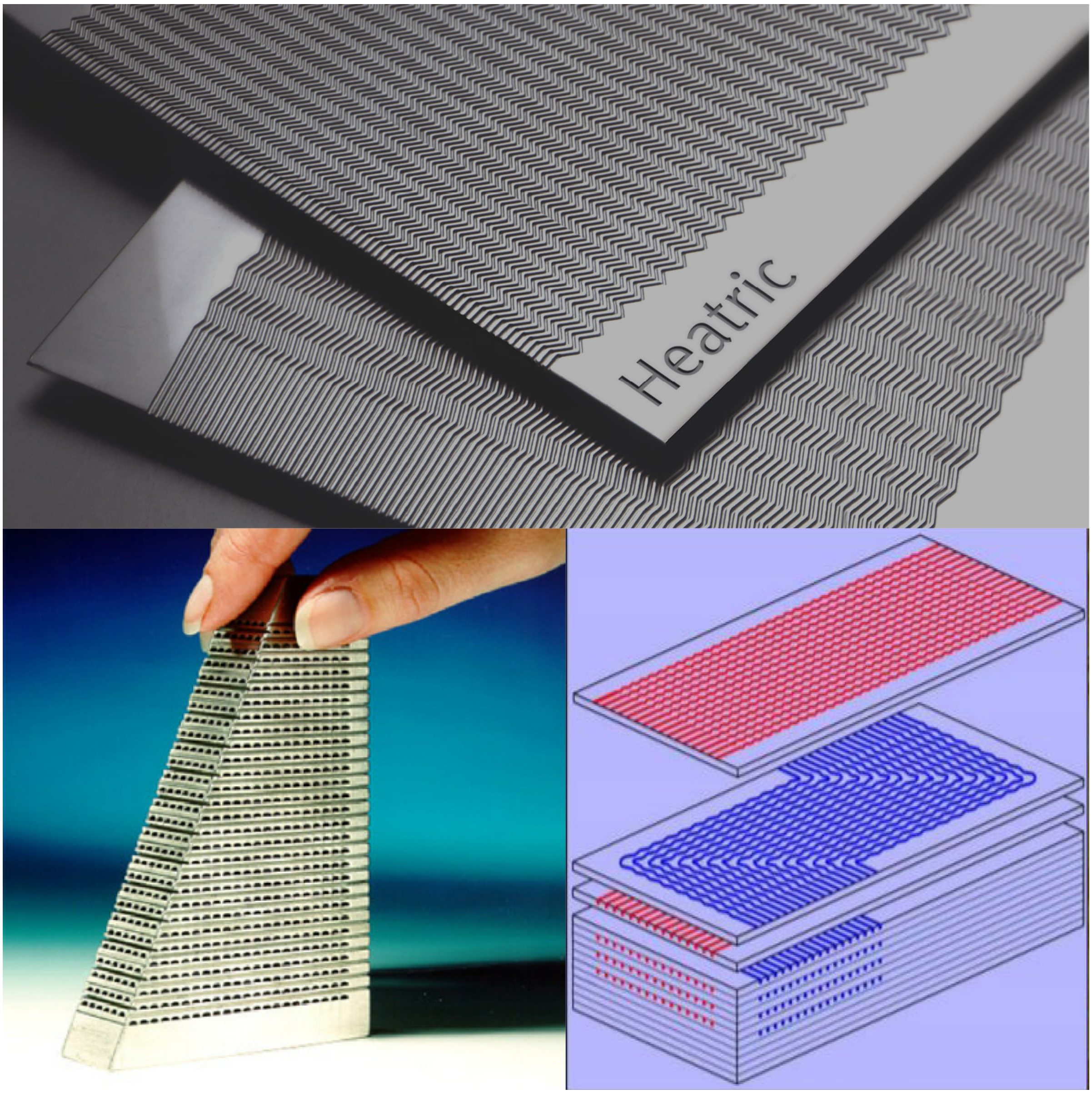

Figure 2.6: *A PCHE plate (t), assembled PCHE (l) and plate stacking arrangement (r)*[47][49]

near the critical point, but as mentioned before, attempts at making a more accurate estimation have not shown very good results and have only been done for specific cases.

When the overall heat transfer coefficient is known, it is common practice to determine the area of a heat exchanger with the logarithmic mean temperature difference (LMTD) [52]. However, this method assumes a constant specific heat capacity of the fluids, which is not a valid assumption near the critical point. Equation 2.30 shows the integral of which the LMTD is the solution if constant specific heat capacities are assumed.

$$A = \int_0^X \frac{d\dot{Q}}{\bar{U}(T_H(x) - T_C(x))} dx \tag{2.30}$$

This equation can also be solved without assuming constant heat capacities. Numerically this is done by dividing the heat exchanger into small cells, figure 2.7. The cells are split in such a way that the transfered heat in each is constant.

$$\Delta\dot{Q}(k) = constant \tag{2.31}$$

As a consequence, the specific enthalpy of both streams changes linearly over the cells. This naturally refines the grid with respect to the temperature profile of the flow when the heat capacity of a flow increases, such as near the critical point.

The temperature of both flows is a function of enthalpy and pressure. For pressure loss, see section 2.4.4.

$$T = f(h(x), P) \tag{2.32}$$

The surface of each cell is determined by the temperature difference and heat transfer coefficient.

$$\Delta A(k) = \frac{\Delta\dot{Q}}{\bar{U}(T_H(k) - T_C(k))} \tag{2.33}$$

The total surface of the heat exchanger is the sum of the surface of all cells.

$$A = \sum_{k=1}^{K} \Delta A(k) \tag{2.34}$$

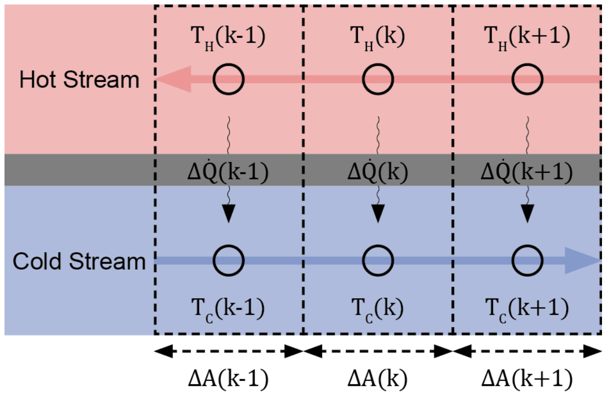

Figure 2.7: *Numerical discretization of a heat exchanger*

All heat exchangers have a counter flow setup, as in figure 2.7.

$$T_C(0) = T_{C,E} \tag{2.35}$$

$$T_H(0) = T_{H,L} \tag{2.36}$$

2.4.3. Afterburner and mixers

In the afterburner the mix of the anode and cathode exhaust is combusted. Full combustion of methane, carbon monoxide and hydrogen is assumed.

$$CH_4 + 2O_2 \rightarrow 2H_2O + CO_2 \tag{2.37}$$

$$CO + \frac{1}{2}O_2 \rightarrow CO_2 \tag{2.38}$$

$$H_2 + \frac{1}{2}O_2 \rightarrow H_2O \tag{2.39}$$

Equation 2.40 shows the energy balance of the afterburner.

$$(1 - r_{ca})\dot{n}_{ca,L}h_{aft,E} + (1 - r_{an})\dot{n}_{an,L}h_{aft,E} = \dot{n}_{aft,L}h_{aft,L} \tag{2.40}$$

Mixing occurs in at least a few places and depending on the design of the heat exchangers network even more. The recirculated anode gas mixes with the fuel feed. If cathodic air is recirculated it mixes with the air feed and the outlet of the anode and cathode mix. Furthermore, flows will be split in order to design a heat exchanger network. It assumed that mixers work perfectly; the enthalpy of mixing is zero and there is no pressure drop.

2.4.4. Pressure drop

In all components of the system pressure drop occurs. The pressure drop in each component depends on its geometric specifics. Since the exact setup of the system is not yet determined, an estimate for the pressure drop in each flow is determined a priori. Table 2.5 shows the assumed values.

To simplify the design of a heat exchanger network, a pressure drop for a hot and cold flow is estimated independent of the heat exchangers it flows through and the pressure drop of mixing and splitting

	Pressure drop (%)
Cold/Hot flows	2 [7]
Fuel cell/reformer	4 [44]
Afterburner	5 [44]
Mixing/splitting	0

Table 2.5: *Pressure drop in different components*

a flow is assumed to be zero. The assumed pressure drop of a hot or cold flow can be viewed as an all inclusive pressure drop, including heat exchangers, splitters, mixers and connectors.

The relative change in pressure of the flow is assumed to be equal to the relative change in enthalpy.

$$\frac{\delta P}{\delta h} = C \tag{2.41}$$

2.5. Model development

The described model is developed in MATLAB, [53]. An object oriented programming approach is applied. Figure 2.8 shows the steps taken to design a SSHS.

As input, the operating temperature of the fuel cell is given. Since a temperature difference over the fuel cell is assumed, this also determines the in- and outlet temperatures of the anode, cathode and reformer are determined. The fuel cell does not operate at an elevated pressure, therefore pressures are determined only assuming the pressure drops as delineated in section 2.4.4.

From this the compositions of the in- and outlet of the reformer and anode are determined. As is the the total current produced in the fuel cell, the anode recirculation ratio and the heat required by the reformer.

Adding the current density and cathode recirculation as input, the electrochemical operation of the fuel cell is determined. With this, the equivalence ratio is determined as well.

And so, the complete operation of the SOFC cell is determined. This includes the hot flows of the SOFC system: The exhaust being cooled down before entering the afterburner and the flue gas; and the cold flows: The air- and fuel feed.

Defining the setup of the sCO_2 cycle, the mass flow through this cycle is determined by a pinch analysis. From the result of the pinch analysis a heat exchanger network is designed. Though there is not just one way to do is, a general strategy is discussed in section 4.1.4.

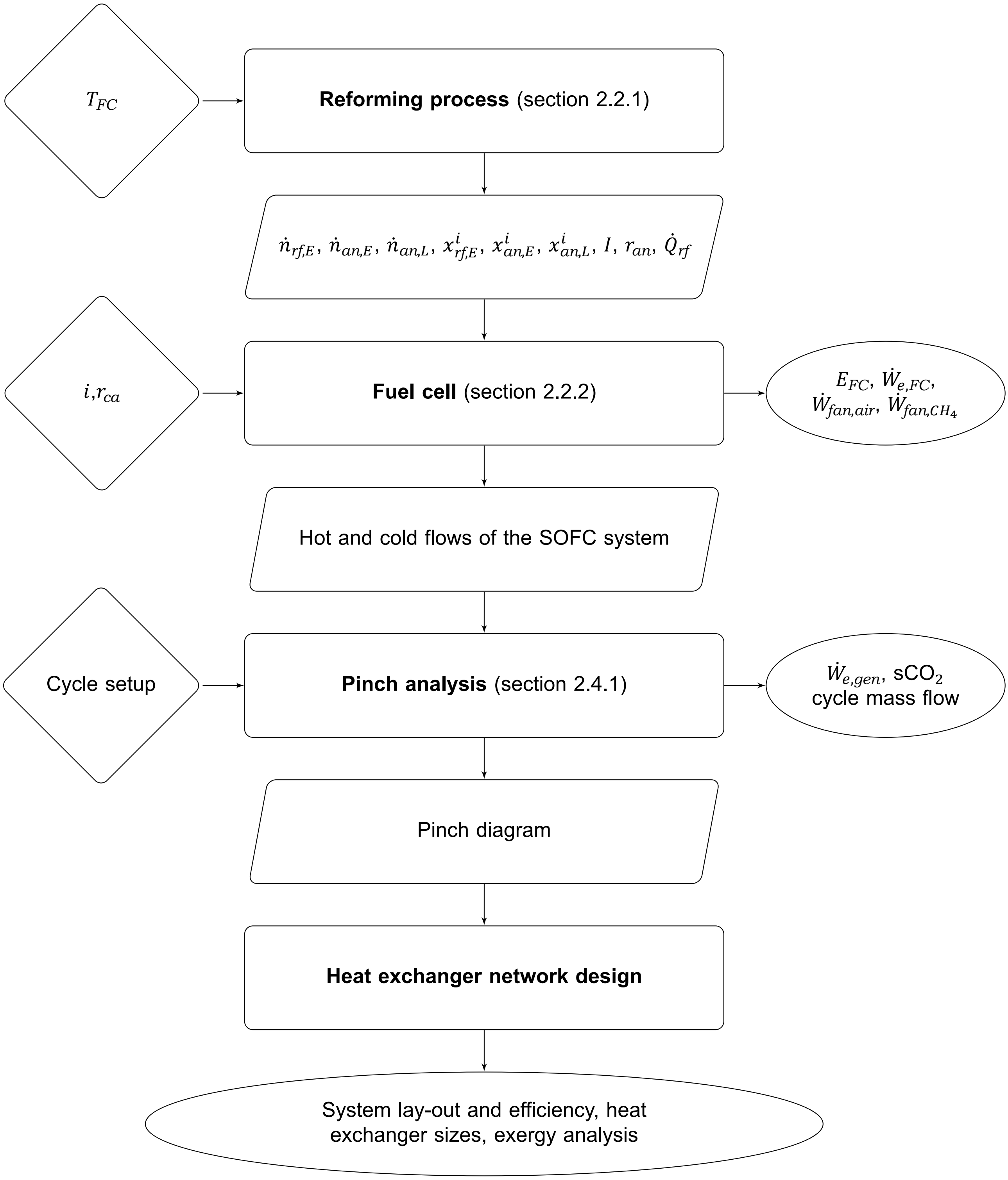

Figure 2.8: *Model flow diagram*

3
Model validation

This chapter discusses the validation of the model. The results of this model of the fuel cell are compared to other models found in research literature in section 3.1.1 and to test data in section 3.1.2.

In appendix B a discussion on the numerical discretization of the equivalent electrical circuit, figure 2.5, and the area of the heat exchangers, figure 2.7, can be found.

3.1. The solid oxide fuel cell system

Since the geometry of every fuel cell, fuel composition and other operating conditions have their own specifics and characteristics it is hard to verify this model for a wide range of operating conditions and fuel compositions. Furthermore, exact data of fuel cell geometry, fuel compositions and corresponding electrochemical performance is hard to get by. Therefore any comparison should be considered with care.

3.1.1. Comparison with other models

The model of this study is compared to other similar models. A summary of the comparisons is given in table 3.1.

Comparison with Campanari and Iora [40]

Input (T_{FC}(°C)/i(A m^{-2}))	**Output** (Ohmic overpotential (mV))		
	Campanari and Iora	This study	Difference (%)
706/1635	169	164.5	-2.48
754/2135	178	173.7	-2.54
836/2321	161	152.8	-4.92
891/2099	132	127.7	-3.06
939/1481	89	86.1	-3.70
Input	**Output**		
	Campanari and Iora	This study	Difference (%)
Operating pressure, anode- inlet flow composition and outlet temperature and fuel utilization ratio	$x_{an,L}^{CH_4} = 0.00$	0.00	0.00
	$x_{an,L}^{H_2O} = 0.5128$	0.5075	-1.04
	$x_{an,L}^{CO} = 0.0853$	0.0772	-9.48
	$x_{an,L}^{CO_2} = 0.2420$	0.2466	+1.88
	$x_{an,L}^{H_2} = 0.1143$	0.1171	+2.45
	$I = 1.72 \times 10^5$ A	1.72×10^5 A	0.00
Input (T_{FC}(°C)/i(A cm^{-2})[7]	**Output** (Power density (mW cm^{-2}))		

[7] Concentration of hydrogen, water and oxygen as well as total current is as calculated in present work

	Campanari and Iora	This study	Difference (%)
796.5/179.2	123.6	133.23	+7.77
739/179.2	123.6	132.54	+7.22
835/179.2	123.6	132.37	+7.08
Comparison with Chan *et al.* [21]			
Input	**Output**		
Operating pressure, anode inlet flow composition, anode outlet and stack temperature, fuel utilization ratio and number of cells	Chan *et al.*	This study	Difference (%)
	$x_{an,L}^{CH_4} = 0.0006$	0	-
	$x_{an,L}^{H_2O} = 0.6175$	0.6553	+4.42
	$x_{an,L}^{CO} = 0.0499$	0.0414	-17.8
	$x_{an,L}^{CO_2} = 0.1619$	0.1733	+7.02
	$x_{an,L}^{H_2} = 0.1569$	0.1268	-19.17
	$i = 141.6\,\mathrm{A\,m^{-2}}$	$154.3\,\mathrm{A\,m^{-2}}$	+8.94
	$E_{FC} = 0.738\,\mathrm{V}$	0.7367 V	-3.56
	$\eta_{FC} = 52.19\%$	54.83%	+5.06%
Comparison with Aguiar *et al.* [54]			
Input	**Output**		
Operating pressure, reformer inlet composition, reformer and anode outlet temperature, cell operating voltage and current density	Aguiar *et al.*	This study	Difference (%)
	$x_{rf,L}^{CH_4} = 0.00$	0.00	0.00
	$x_{rf,L}^{CO} = 0.25$	0.32	+28.4
	$x_{rf,L}^{H_2} = 0.45$	0.37	-17.01
	$x_{an,L}^{CH_4} = 0.00$	0.00	0.00
	$x_{an,L}^{CO} = 0.12$	0.09	-26.00
	$x_{an,L}^{H_2} = 0.15$	0.13	-14.27
	$\eta_{FC} = 46.5\%$	46.45%	-0.1
Comparison with Aguiar *et al.* [55]			
Input	**Output**		
Operating pressure, anode inlet composition, anode outlet temperature, cell operating voltage and current density	Aguiar *et al.*	This study	Difference (%)
	$x_{an,L}^{CH_4} = 0.00$	0.00	0.00
	$x_{an,L}^{H_2O} = 0.65$	0.63	-2.36
	$x_{an,L}^{CO} = 0.04$	0.035	-13.42
	$x_{an,L}^{CO_2} = 0.16$	0.17	+3.35
	$x_{an,L}^{H_2} = 0.15$	0.17	+10.24
	$\eta_{FC} = 46.8\%$	47.8%	+2.18
Comparison with Asimptote [56]			
Input	**Output**		
Reformer inlet conditions, fuel cell and reformer operating pressures and temperatures, fuel utilization ratio, ohmic resistance and current density	Asimptote	This study	Difference (%)
	$x_{an,L}^{CH_4} = 0.0018$	0.0019	+5.56
	$x_{an,L}^{H_2O} = 0.6005$	0.6005	0.00
	$x_{an,L}^{CO} = 0.0387$	0.0385	-0.52
	$x_{an,L}^{CO_2} = 0.2940$	0.2942	+0.07
	$x_{an,L}^{H_2} = 0.0650$	0.0649	-0.15
	$\dot{W}_{FC,e} = 442.86\,\mathrm{kW}$	400.11	-9.65

Table 3.1: *Comparison with other models*

First a comparison is made with the model from Campanari and Iora [40], as it uses the same equivalent electrical circuit as in figure 2.5. Campanari and Iora [40] have developed a model where the stack temperature and current density vary locally. Furthermore, activation and concentration losses are not neglected.

All geometry inputs are listed by Campanari and Iora [40], except for which angle the interconnection is sprayed on the cathode – an important parameter, since this determines the area of the interconnection through which the current flows. Especially since the interconnection material is less conductive than the electrodes. In combination with a relatively small area, the interconnection determines for a large portion the resistance of the cell.

Local stack temperatures and current densities from the results of Campanari and Iora [40] are used as input. The ohmic overpotential determined by this study is than compared with the ohmic overpotential results from Campanari and Iora [40]. It is found that an angle of 15° for the interconnection shows a reasonable match. Differences can be caused by the discretization and/or the unknown angle of the interconnection. The error is considered within acceptable range.

A second comparison is made by comparing the outlet composition of the anode flow and the total drawn current. As an input, a given syngas composition is used. Contrary to this study, the extent of the MSR reaction is determined by a reaction rate localized in the cell and not by assuming an equilibrium out the outlet. More importantly, electrochemical oxidation of carbon monoxide is assumed to take place in the anode.

This is reflected in slightly different concentrations. But the total current is the same since the fuel utilization ratio is defined as the ratio of the current over the total amount of combustible products entering the anode, equation 2.17.

A comparison for the overall performance of the cell is also made by comparing the power densities. Campanari and Iora [40] do not assume a constant stack temperature or current density. In fact, the stack temperature, anode- and cathode gas temperature all vary along the cell, contrary to the assumption that the stack temperature is halfway between the in- and outlet temperature of the anode- and cathode flow.

Three assumptions regarding an average stack temperature will now be compared. First, assuming the average stack temperature is halfway between the in- and outlet stack temperature (796.5 °C), secondly the temperature is halfway between the in- and outlet temperature of the anode flow (739 °C) and similarly for the cathode flow (835 °C) as given by Campanari and Iora [40].

This study calculates higher power densities. This makes sense since concentration and activation losses are neglected. Furthermore, this study predicts a slightly lower ohmic resistance. The different average temperatures do not seem to have much effect. A higher temperature will lead to a lower resistance but also a lower Nernst voltage.

Chan *et al.* also us a lumped modeling approach. Contrary to this study, Chan *et al.* [21] determine a stack temperature and do not neglect concentration and activation losses.

A DIR reforming process is assumed, so to be able to compare, the same will be done for this study. The same equilibrium conditions are assumed, but the concentrations differ slightly. This study predicts a slightly higher total current, which is also reflected in the lower hydrogen and methane concentration. It should be noted though that the chemical equilibrium assumed by Chan *et al.* [21] is not satisfied in their own work. The methane concentration is too high, explaining the lower total current density.

So even if concentration and activation losses are neglected in this study, a higher total efficiency, assuming the same number of cells, is achieved. The difference is deemed to be within an acceptable range.

Aguiar *et al.* [54] have developed an IIR SOFC planar model. The reforming process is modeled using local reactions rates and mass and energy balances. Two more reactions are assumed to take place as well: An additional reforming reaction and the electrochemical oxidation of carbon monoxide.

The different reforming process is reflected in a different syngas composition. Paradoxically, the carbon monoxide oxidation being neglected in this present work leads to a lower carbon monoxide concentration. This can be explained by the fact that under the same fuel utilization ratio, more hydrogen is consumed when neglecting the carbon monoxide oxidation. This leads to lower higher hydrogen concentrations, favoring the forward WGS reaction.

Since Aguiar *et al.* [54] use a planar fuel cell, only a comparison based on the same voltage and current density is made. It is found that this study only requires a very little extra amount of methane to operate on the same current density, reflected in a very small difference in overall efficiency.

Aguiar *et al.* [55] have developed a DIR planar SOFC model. All the same reactions are assumed to take place but are modeled by reaction rates. A comparison shows that the chemical equilibrium have a close match with the reaction rates model.

Finally, a comparison with software developed by Delft University of Technology is made [56]. The composition of the anode exhaust gas shows a near perfect match. The produced power shows a difference, even though the cells resistance is the same, as this is given as an input. The difference is in the fact that Asimptote [56] makes different assumptions regarding the current density and Nernst voltage.

In general, it can be concluded that the developed in this study performs well when compared to aforementioned other works. Concentration of components do differ slightly in some comparisons but not to such an extent that it is reason for concern. The small differences can be explained by slightly different modeling approaches and assumptions.

The overall performance of the cell differs very little in most comparisons. Only when compared to Campanari and Iora [40] and Asimptote [56] the overall efficiency does show a slightly significant deviation. In the former comparison, this study shows a higher efficiency, in the latter a lower. Overall, these differences are not considered significant enough to adjust the model.

3.1.2. Comparison with experimental data

The results of the model are compared to measured data from a typical tubular SOFC [57]. The measured data concern three temperatures, a fuel composition of 89% hydrogen, 11% water, a fuel utilization ratio of 85% and air is used as oxidant with an equivalence ratio of 4. Figure 3.1 shows the measured data, their linear fits and the results of the model under the same operating conditions.

All component sizes are assumed to be as delineated in table 2.2.

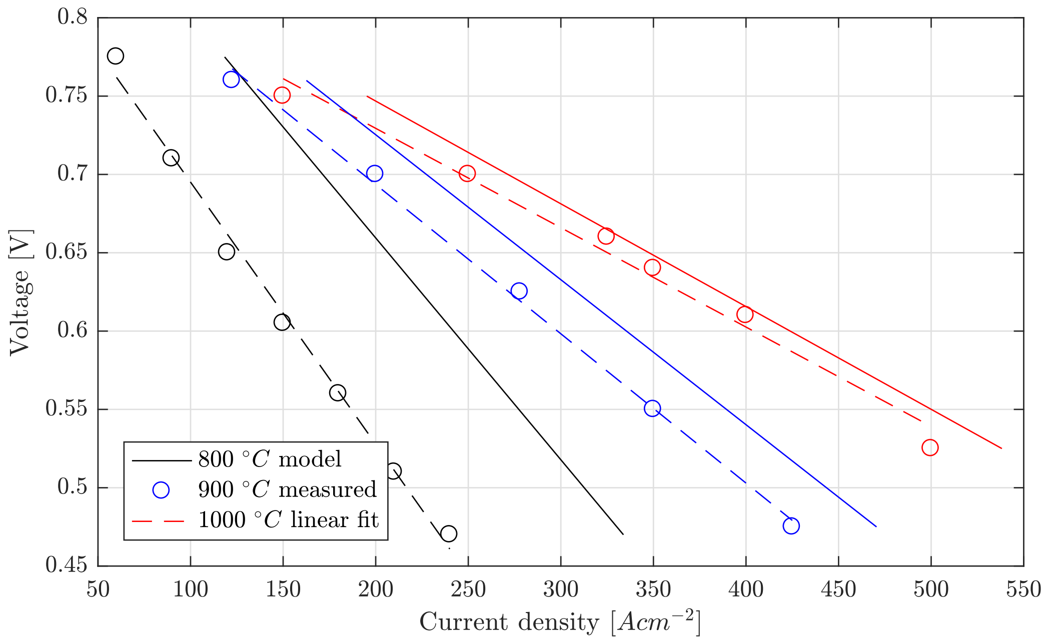

Figure 3.1: IV curve of the model and measured data

Assuming all overpotentials except ohmic can be neglected, the slope of the IV curve represents the area specific resistance (ASR) of the fuel cell. Table 3.2 shows the difference between the slope of the linear fit of the measured data and that of the model. As can be seen, the model shows a higher voltage than the test data do. One reason is that the model neglects activation and concentration losses. In the case of 800 and 900 °C, the ohmic resistance is lower than it is in the test data.

A reason for this deviation is that in reality the stack temperature is not constant. This causes the ohmic resistance to vary along the cells length. In the model, the ohmic resistance is approached by assuming an average stack temperature. Simple assumptions like this will inevitably be different from reality.

	800 °C	900 °C	1000 °C
Measured ASR (Ωcm^2)	1.673	0.9530	0.6342
Model ASR (Ωcm^2)	1.416	0.925	0.656
Difference (%)	-15.34	-2.89	+3.41

Table 3.2: *Comparison between the model and measured data*

Finally, the temperature dependence of the specific resistivity of the components is also an attempt at approaching the reality. Again, this is bound to differ from reality.

The difference between the model and tested data is in some cases quite significant. However, these deviations can be explained (at least partly). The comparison does confirm however that the model shows a performance in the same order of magnitude. In combination with the fact that the model performs comparable to other models in research literature, section 3.1.1, there is enough reason to validate the model for its purpose. One must also keep in mind that this study aims to investigate the interaction between a SOFC system and sCO_2 Brayton cycle and not to study the behavior of a SOFC.

4

Case studies

This chapter discusses the performance and specifics of different setups of the SSHS. Different cases will be analyzed to study the effect of a specific parameter on the system. Many parameters can be varied in combinations with each other, giving rise to myriad of system setups. For the purpose of this study it is chosen to analyze system behavior when changing parameters that effect the interaction between the two systems.

The operating temperature of the SOFC is an important parameter for its performance. Firstly, it has an effect on the reforming reactions. This is reflected by a slight change in the concentration of hydrogen and water at the outlet of the anode and total current. Secondly, the Nernst voltage decreases quite significantly for higher operating temperatures. Thirdly, the ohmic resistance also decreases significantly. See figure C.1. The effect of the decreasing ohmic resistance outweighs that of the decreasing Nernst voltage. Figure 4.1 shows that the performance of the SOFC improves with higher temperatures. Only for a very high number of cells this is not the case. This can be explained by the fact that a high number of cells corresponds to a low current density. A low current density reduces the effect of the ohmic resistance to such an extent that the effect of the decreasing Nernst voltage becomes dominant over the decreasing ohmic resistance.

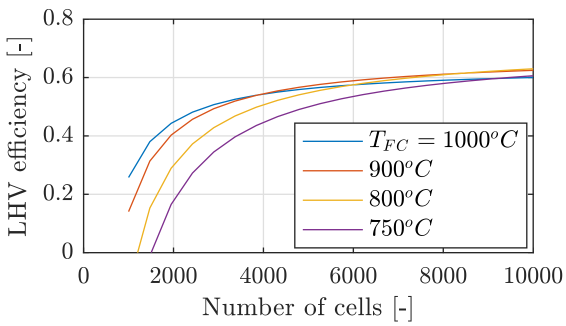

Figure 4.1:
Effect of the fuel cells operating temperature on the performance

Operating with more cells (low current density) is more expensive and the marginal improvement in performance decreases rapidly. For a reasonable number of cells, the fuel cells performance improves with higher operating temperatures. Therefore, the operating temperature of the fuel cell in each case is fixed so that the outlet temperature of the anode and cathode corresponds to the maximum operating temperature of the PCHE (1160 K/886.85 °C). Under the assumption that temperature difference between the in- and outlet of the fuel cell is 100 °C and the operating temperature is the average of this, the fuel cell's operating temperature is fixed at 836.185 °C.

The operating pressure of the fuel cell is also fixed, the only increase in pressure is to overcome the pressure losses in the system. One of the advantages of the SSHS is the indirect coupling. It is therefore not required to operate the SOFC at an elevated pressure, which would increase the complexity and cost of the system.

Two adjustments to the SOFC system will be considered, namely cathode recirculation and supplying steam through a HRSG instead of by recirculating anode gas.

An ER setup would change the interaction between systems when compared to an IIR setup. However, it will not be considered. It is found that when these two setups are compared, an ER setup makes the system more complex by adding a heat exchanger, significantly increasing the air flow due to increased need for cooling of the fuel cell and decreases efficiency [25].

To continue, two sCO_2 Brayton cycle setups will be considered. A simple recuperative cycle and a recompression cycle. As mentioned in section 1.1.1, the recompression cycle is considered the most efficient while relatively simple.

Section 4.1 discusses the hybrid simple in its most basic setup. No HRSG, no cathode recirculation and a simple recuperative cycle. The performance of a recompression cycle compared to the basic setup is analyzed in section 4.2. In section 4.3 the effect of cathode recirculation is analyzed. Combining a recompression cycle and cathode recirculation is discussed in section 4.4. A HRSG to supply steam to the reformer is analyzed in section 4.5. A different design approach than a pinch analysis for each case is discussed in section 4.6. Finally, a reference case of a directly coupled GT under the same assumptions and operating conditions is developed in section 4.7. A comparison of all cases is made in section 4.8.

Case	**Section**
I: Basic setup	4.1
II: Recompression cycle	4.2
III: Case Cathode recirculation ratio	4.3
IV: Steam feed	4.5
V: Recompression cycle + cathode recirculation	4.4
VI: Heat exchanger network design	4.6
VII : Directly couple GT	4.7

Table 4.1: *Overview of studied cases*

Additional details of each case can be found in appendix C.

4.1. Case I: Basic setup

4.1.1. The SOFC system

As mentioned before, the operating temperature and pressure of the fuel cell are fixed. The current density and related number of cells still have to be determined. Based on figure C.2 and C.3 the choice has been made to operate at a current density of 225 mA cm^{-2}. This is considered to be a reasonable trade-off between efficiency and number of cells. Costs are not part of this study, but cost considerations should not be neglected.

Table 4.2 shows the operating characteristics of the SOFC in this case. The LHV efficiency refers to the fuel (methane) to alternating current (AC) efficiency. The high equivalence ratio is a consequence of the cooling requirement to maintain a temperature difference of 100 °C. For the compositions of the flows in the SOFC system the reader is referred to table C.2.

Operating temperature	836.85 °C
Operating pressure	1.110 55 bar
Operating voltage	553 mV
Current density	225 mA cm^{-2}
Power density	124 mW cm^{-2}
LHV AC Efficiency	47.30 %
Nernst voltage	822 mV
Ohmic resistance	1.20 Ω cm^2
Anode recirculation ratio	0.4847
Equivalence ratio	10.44
Number of cells	3 035

Table 4.2: *Operating characteristics of the SOFC (case I: Basic setup)*

4.1.2. The sCO_2 Brayton cycle

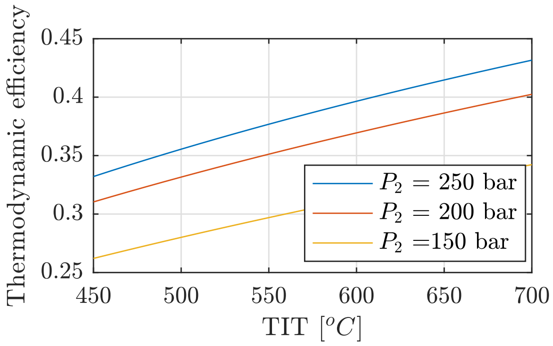

Figure 4.2: *Effect of the outlet pressure of the compressor (P_2) and TIT*

In this case a simple recuperative cycle is adopted. It is found that the efficiency of the cycle increases if the inlet of the compressor is as close as possible to the critical point [7]. Near the critical point the fluid is compressed when the density is high, decreasing the work of the compressor. The inlet of the compressor is therefore at the assumed minimum possible temperature, 32 °C, and pressure, 80 bar.

Figure 4.2 shows that increasing the outlet pressure of the compressor (P_2) and increasing the TIT increases the efficiency. Therefore the outlet pressure of the compressor will be the assumed maximum pressure, 250 bar, and the TIT is the assumed maximum temperature, 700 °C. With an assumed pressure drop of 2%, the inlet pressure of the turbine is 245 bar. The recuperator and heater are yet to be determined, as these will be integrated with the SOFC system. Figure 4.3 shows the T-s diagram of this cycle. The thermodynamic efficiency of the cycle is 43.16 % for a minimal temperature difference of 10 °C. The vast majority of the SOFC system is available at temperatures above the inlet temperature of the fuel cell. This temperature is above the TIT of 700 °C. Section 4.6.1 discusses this in more detail.

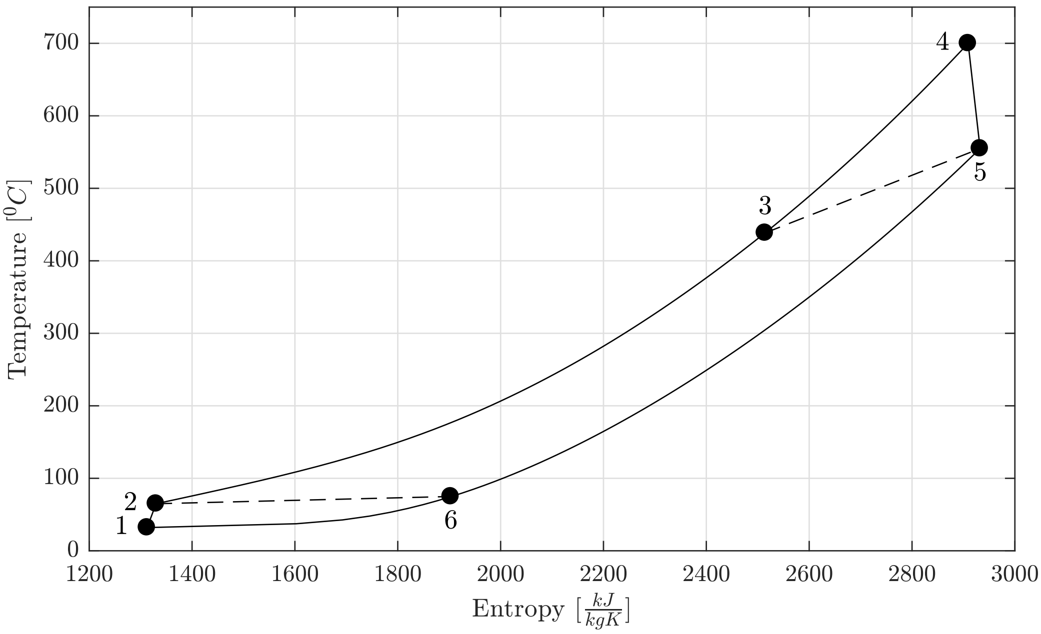

Figure 4.3: *T-s diagram (simple recuperative cycle, the numbers refer to the PFD, figure 1.1a)*

4.1.3. Pinch analysis

The key variable in the pinch analysis is the minimum temperature difference of the heat exchanger network. The smaller this difference is, the more heat can be transfered in the system, the higher the efficiency. The drawback is that a smaller temperature difference requires larger heat exchangers as the driving force, the temperature difference, decreases. An optimal trade off between efficiency and the higher cost associated with bigger heat exchangers is commonly found between 10 and 30 °C [46].

For this case a minimum temperature difference of 10 °C is chosen. A mass flow through the sCO_2 Brayton cycle is determined by solving the pinch problem for this minimal temperature difference. The pinch point of the system is at the outlet of the sCO_2 compressor. Figure 4.4 shows the resulting pinch diagram. The interval temperatures correspond to the shifted interval temperatures of the streams, see the example in section A.1.

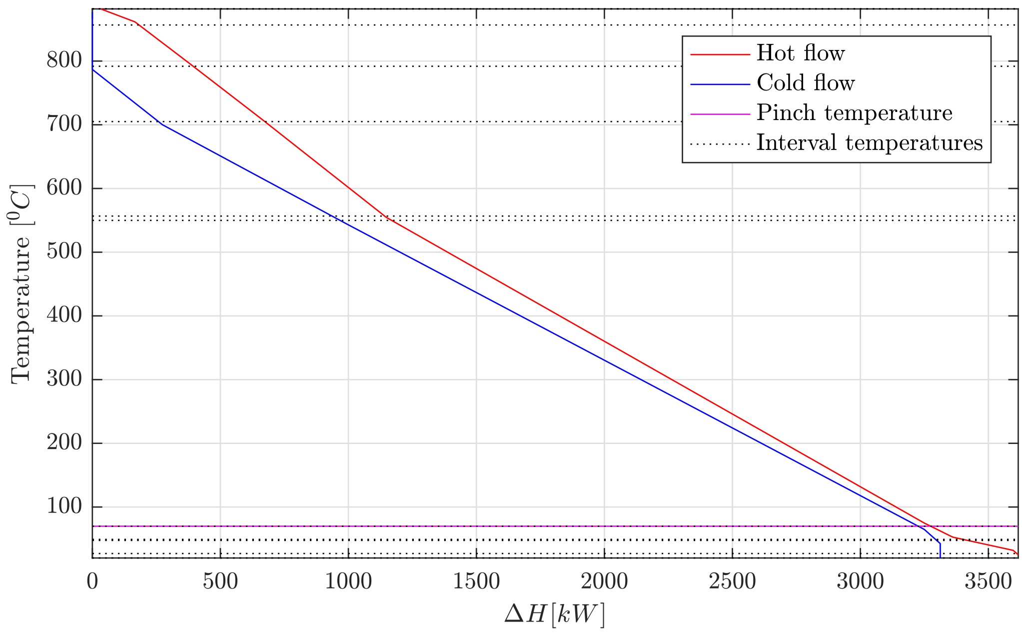

Figure 4.4: *Pinch diagram (case I: Basic setup, ΔT_{hex} =10 °C)*

Figure 4.5 shows the hot and cold stream of this case. Air and fuel are preheated before entering the reformer and cathode respectively. Part of the anode exhaust is recirculated and mixed with the fuel, hence the lower temperature of the fuel feed outlet. The rest of the anode exhaust is mixed with the cathode exhaust and exhausted by the fuel cell. The temperature of the stream leaving the fuel cell is set at the maximum temperature allowed by the PCHE. Before the fuel still left in this mixture is combusted in the afterburner, increasing the temperature in the process, it must be cooled down in order not to exceed the maximum temperature of the PCHE. It is cooled down to a temperature so that the outlet temperature of the afterburner matches with the maximum temperature of the PCHE. The in- and outlet temperature of each flow as well as the temperature at the pinch are shown. The

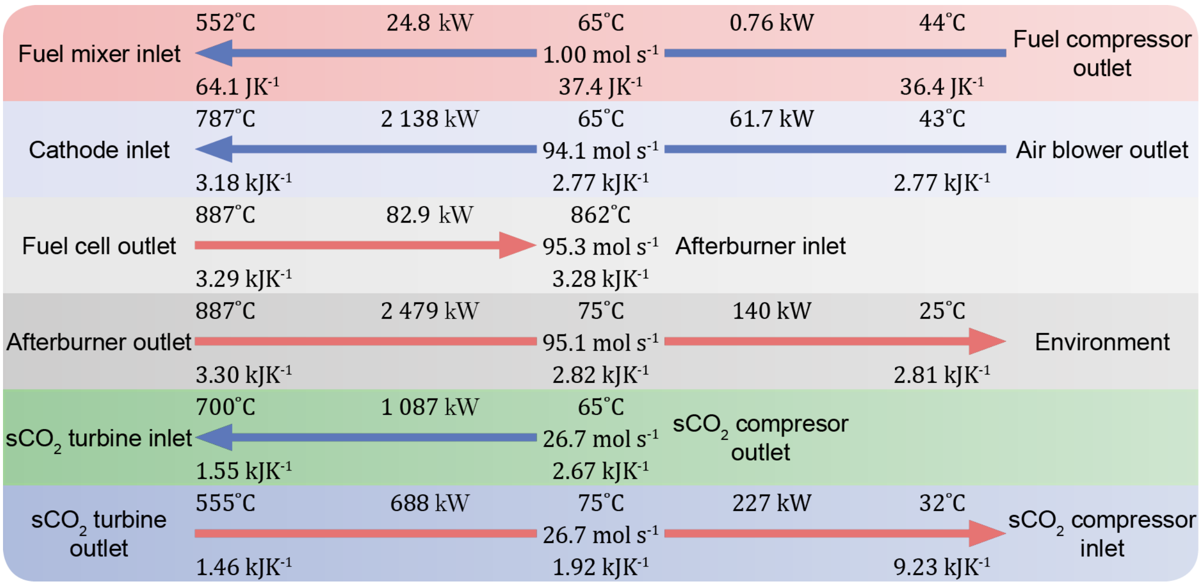

Figure 4.5: *Heat flows (case I: Basic setup, ΔT_{hex} =10 °C)*

temperature difference between the hot and cold flows is indeed 10 °C at the pinch. The heat duty of each flow above as well as below the pinch is displayed as well.

4.1.4. Heat exchanger network

In order to make the heat flows in figure 4.5 possible, a network of heat exchangers must be designed. There is not just one specific way to do this, but there are some guidelines and rules of thumb to help out [45].

As mentioned in section 2.4.1, the pinch point splits the design problem in two. Above and below the pinch, heat should not be transferred across the pinch. Above the pinch, all heat required by the cold flows can be supplied by cooling down the hot flows. This is the case because the system is designed without a hot utility above the pinch. Below the pinch, more heat is available in the hot flows than required by the cold. As in any power cycle, heat must be rejected at low temperatures. This can be achieved by exhausting the flue gas before it has reached environmental temperature or by cooling the sCO_2 with water.

Since the pinch is the point where the design is at its most constrained, it is easiest to *design away from the pinch*. This means that one has to start at the pinch point and match streams to form a heat exchanger from there. When matching hot and cold streams, two things are useful to keep in mind. When moving away from and above the pinch, the heat capacity of the hot flow should be lower than or equal than that of the cold flow, equation 4.2.

$$CP = C_P \dot{n} \tag{4.1}$$

$$CP_H \leq CP_C \tag{4.2}$$

In case of constant heat capacities this rule ensures that there will not be a temperature crossover. Heat capacities are not constant in this case, but this rule still provides a useful insight in matching streams.

When a hot stream has a higher heat capacity than all cold streams it must be split in order satisfy this rule. However, the number of hot streams above the pinch should be equal to or smaller than the number of cold streams above the pinch.

$$N_H \leq N_C \tag{4.3}$$

Consequently, splitting a hot stream to satisfy one rule, equation 4.2, could result in also splitting a cold stream to satisfy the other, equation 4.3. For designing the network below the pinch, these rules must be mirrored.

Splitting a flow might seem a good option from a thermodynamic point of view. For practical reasons it should be considered with care though. While splitting a flow and consequently using more heat exchangers, piping and valves, might decrease the total heat exchanger area, it also increases the systems complexity. This is a trade off that should be considered in a design. The designs in this study aim to limit the amount of heat exchangers, even if this means that the total area of the heat exchangers increases.

When matching streams to form a heat exchanger, it is found that the total area of the heat exchanger tends be minimal when the heat capacities of the hot and cold stream roughly match. It therefore makes sense to proportionally divide streams in favor of minimizing the area of one particular heat exchanger, consequently increasing that of another.

Finally it should be noted that the dew temperature of the flue gas in this case is 33.6 °C. This is below the inlet temperatures of the air and fuel feed, meaning that condensation in the flue gas will not occur before it is exhausted.

Taking all of the above into account, a heat exchanger network is designed. Figure 4.6 and 4.7 show the result. The data of all the points in the PFD, figure 4.7, can be found in section C.2.

Figure 4.5 serves as the basis in the designing the heat exchanger network. The design problem above the pinch has more flows and no external heat utilities, therefore the design process is started above the pinch. At the pinch, the heat capacity of the flue gas is too large to be cooled down by supplying heat only to the air- and fuel feed. In order *to move away* from the pinch, part of the flue gas must be cooled down by supplying heat to part of the HP sCO_2. As a consequence, the mass flow of the cold side of what would normally be the recuperator in the sCO_2 Brayton cycle decreases.

The flue gas flow has to be split into three in order to supply heat to the fuel- and air feed and the HP sCO_2. The choice has been made to split this at its highest temperature, avoiding unnecessary additional heat exchangers and flow splits. The hot mass flow of the fuel preheater, flue gas, is determined so that the heat duty of the fuel feed above the pinch is matched with the supplied heat by the

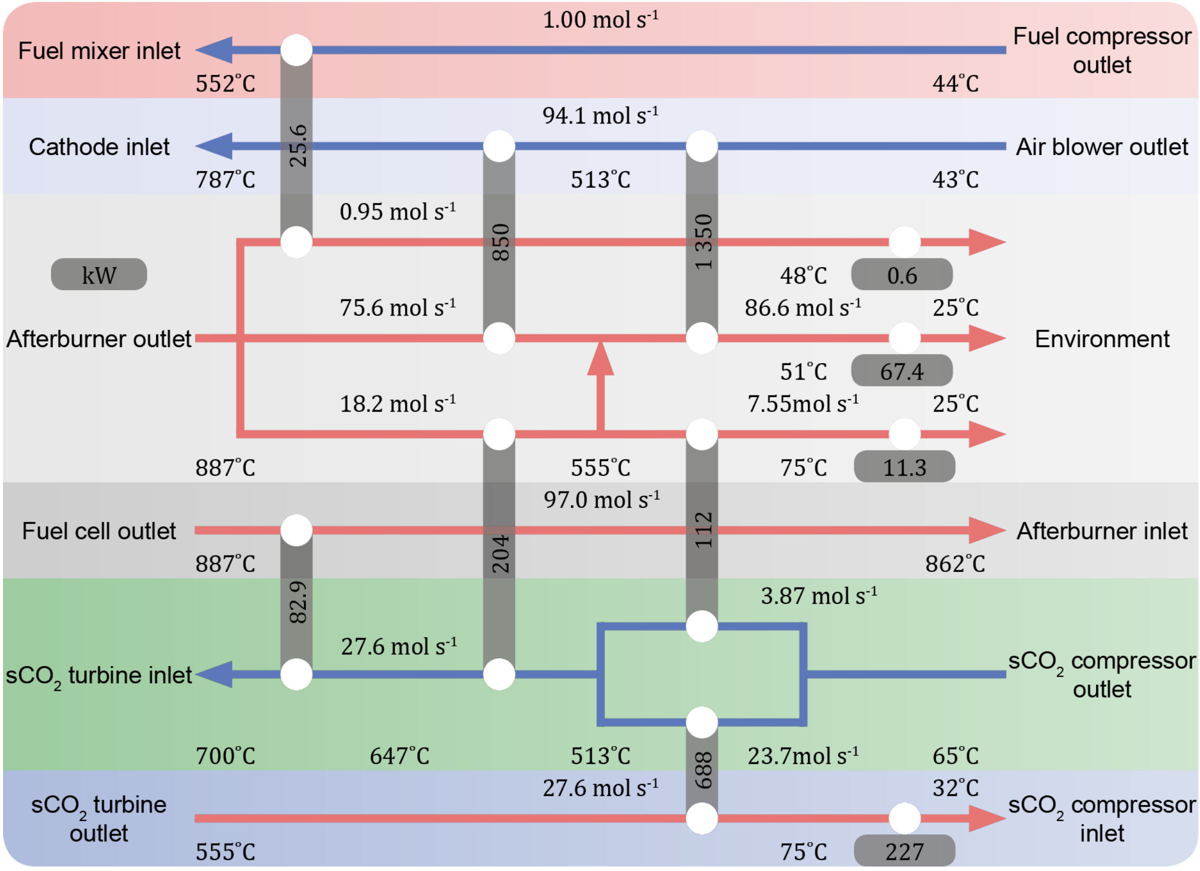

Figure 4.6: *Heat exchanger network (case I: Basic setup, ΔT_{hex} = 10 °C)*

flue gas above the pinch. Below the pinch, the same mass flow of flue gas is maintained. This does mean there is not enough flue gas is in the preheater to maintain a minimum temperature difference of 10 °C at the low temperature (LT) end. It is chosen to relax this constraint in favor of adding another heat exchanger.

The remaining flue gas, the vast majority, and the LP sCO_2 must supply heat to the air feed and HP sCO_2. The flue gas supplies heat to the air and part of the HP sCO_2. The LP sCO_2 supplies heat to the remaining HP sCO_2. This situation changes when the turbine outlet temperature (TOT) (555 °C) is reached, the inlet temperature of the LP sCO_2 flow. The mass flows are split in such a way that the inlet temperature of the hot flows of these heat exchangers, the LT heater and recuperator, is the TOT and that the outlet temperatures of the cold flows are equal (513 °C in this case). Similar to the fuel preheater, the choice has been made to preheat the air below the pinch with the same mass flow of flue gas to avoid an additional heat exchanger.

With the flue gas at TOT and the HP sCO_2 and air at the same temperature, a new mass flow division of flue gas is determined. The mass flow of flue gas through the high temperature air preheater is chosen to match the remaining heat duty of the air feed. The complete HP sCO_2 flow is first heated by the remaining flue gas, the high temperature (HT) heater, and then used to cool down the exhaust of the fuel cell before it enters the afterburner, the precooler for the afterburner.

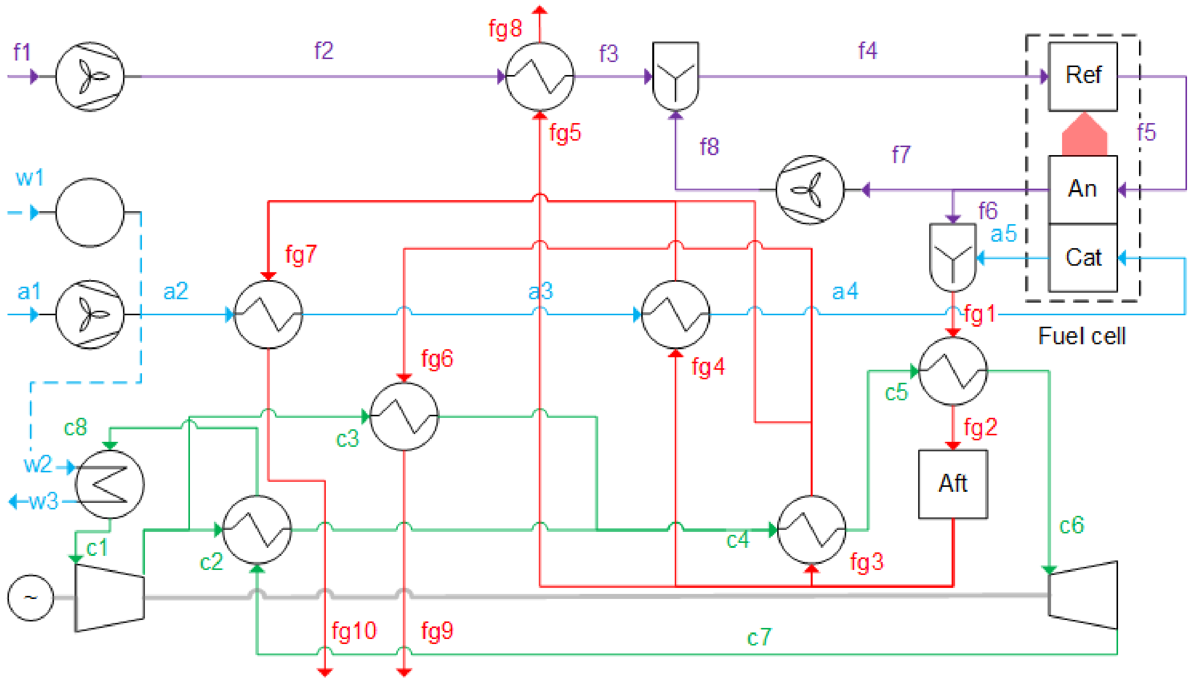

Figure 4.7: *Process flow diagram (case I: Basic setup)*

4.1.5. Performance analysis

Table 4.3 and figure 4.8a show the key performance data of this case.

Fuel cell power	380 kW
Generator power	164 kW
Auxiliary power consumption	53 kW
Net AC system power	491 kW
LHV AC efficiency	61.13 %
Thermodynamic efficiency	70.22 %
Second law efficiency	60.03 %
Thermodynamic cycle efficiency	43.16 %
sCO_2 cycle flow	27.6 mol s^{-1}
Total PCHE area	44 m^2
Total STHE area	3778 m^2
Number of heat exchangers	8

Table 4.3: *Key performance data (case I: Basic setup, ΔT_{hex} = 10 °C)*

The majority of the power is produced by the SOFC system. The sCO_2 Brayton cycle significantly adds to this power, producing over 40% of the power produced by the SOFC system. The auxiliary power consumption significantly reduces the performance. The air blower, responsible for the majority of the auxiliary power consumption, figure 4.8b, significantly reduces the overall performance of the system.

The thermodynamic efficiency of the system, excluding losses in the DC/AC converter, generator and auxiliary power consumption, is significantly higher (70.22%) than the net LHV efficiency (60.22%). This illustrates the energy lost in the BoP components. Heat is also produced in the sCO_2 cooler as hot water. However, the outlet temperature of the water (50 °C) is limited by the high specific heat capacity of the sCO_2 near the critical point (figure 4.10b).

The biggest contributor to exergy loss is the heat exchanger network. Figure 4.9a shows that almost half of this loss is in the two air preheaters. The air feed is the largest heat duty in the system, in combination with the low overall heat transfer coefficient of the STHE (20 W m^{-2} °C) compared to the

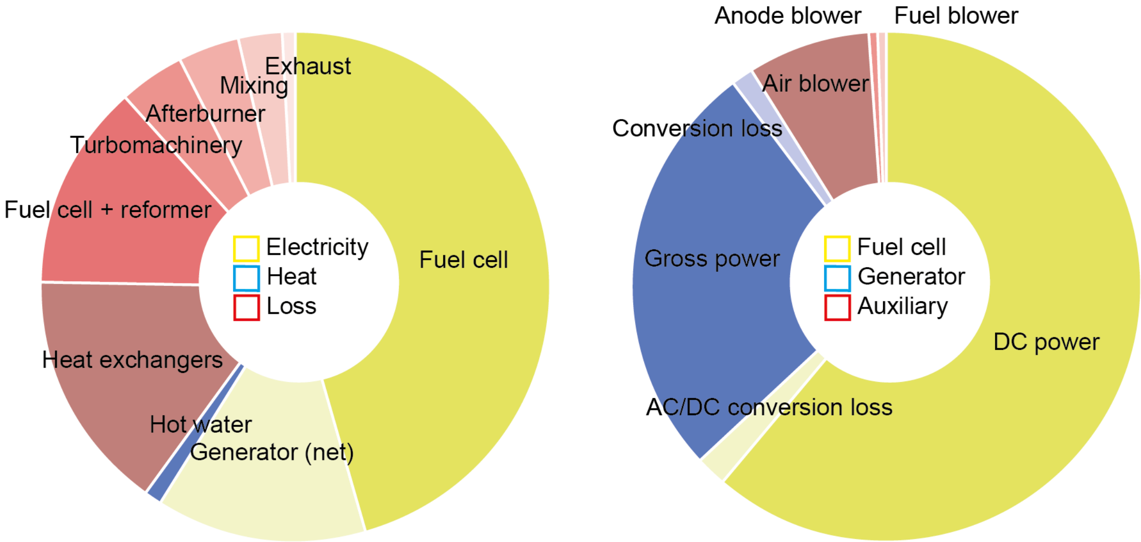

(a) *Overall exergy analysis* (b) *Electric power consumption and losses*

Figure 4.8: *Exergy analysis (case I: Basic setup, ΔT_{hex} = 10 °C)*

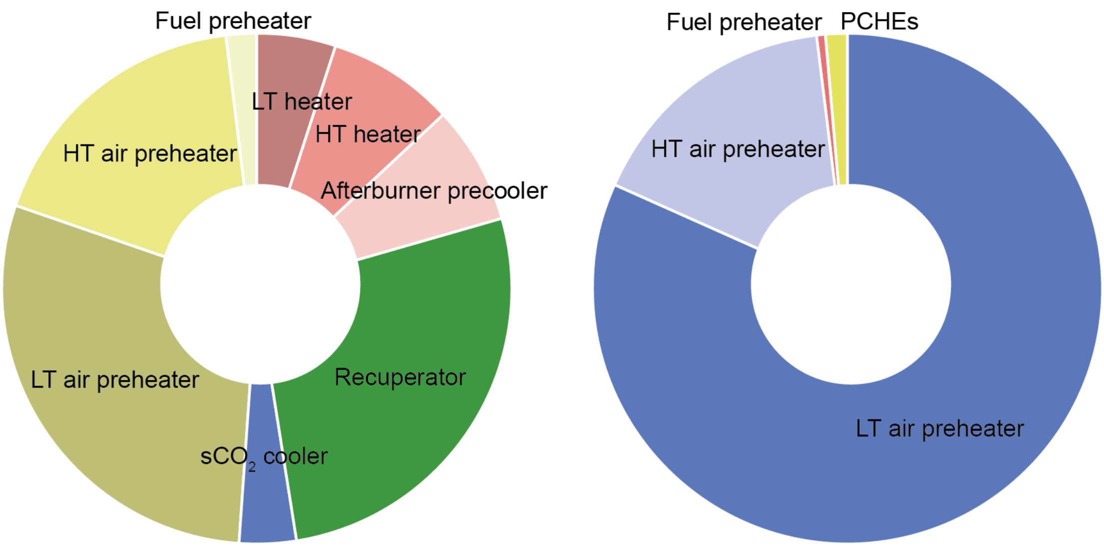

(a) *Exergy loss* (b) *Size*

Figure 4.9: *Heat exchanger analysis (case I: Basic setup, ΔT_{hex} = 10 °C)*

PCHE (500-7000 W m^{-2} °C), makes the the size of the air preheaters by far the largest heat exchangers, figure 4.9b.

The largest PCHE is the recuperator, figure 4.10a. It has a large heat duty and the driving force, temperature difference, is not as big as in the heaters. The cooler, even if it has a very high heat transfer coefficient (7000 W m^{-2} °C) still has a quite significant size. This is because of the very limited temperature difference near the critical point. This also limits the outlet temperature of the water. As mentioned before, see figure 4.10b.

The sizes of the two types of heat exchangers, PCHE and STHE, are considered separately because the cost of both types probably differs significantly.

Changing the minimal temperature difference does not change the pinch point. Regardless of this

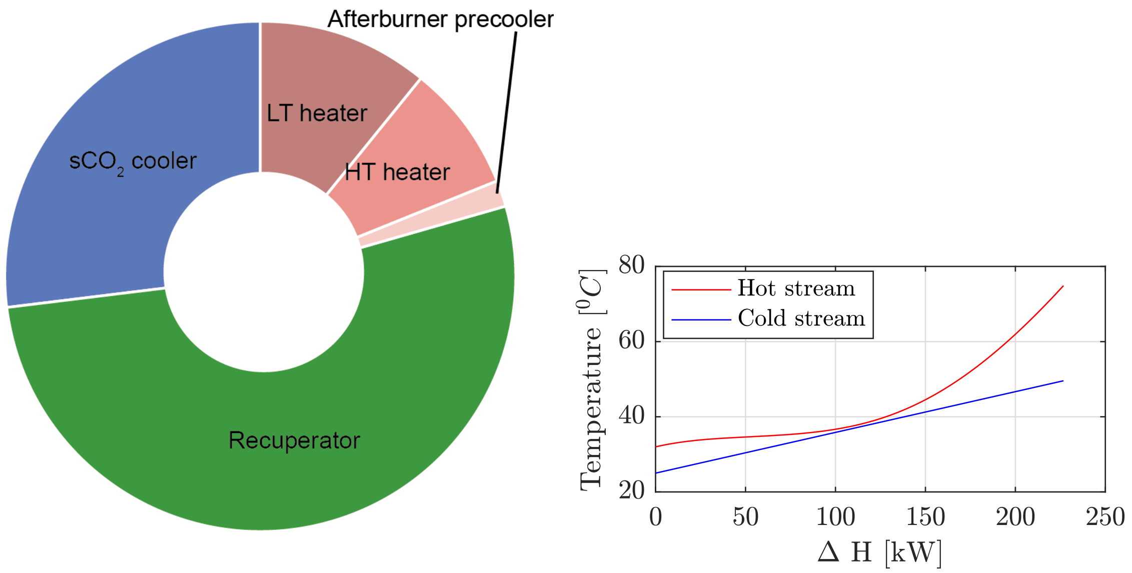

(a) *PCHE size* (b) *Temperature-enthalpy diagram of the sCO_2 cooler*

Figure 4.10: *Size of the PCHEs and temperature-enthalpy diagram of the sCO_2 cooler (case I: Basic setup, ΔT_{hex} = 10 °C)*

difference, the pinch point is the interval temperature of the outlet of the sCO_2 compressor.

$$T_{pinch} = T_{com,L} + \frac{\Delta T_{hex}}{2} \tag{4.4}$$

Therefore the same design of the heat exchanger network can be applied when changing the minimal temperature difference [8]. Decreasing the minimal temperature difference of the system increases the efficiency but also the size of the heat exchangers and vice versa. Figure 4.11 confirms this.

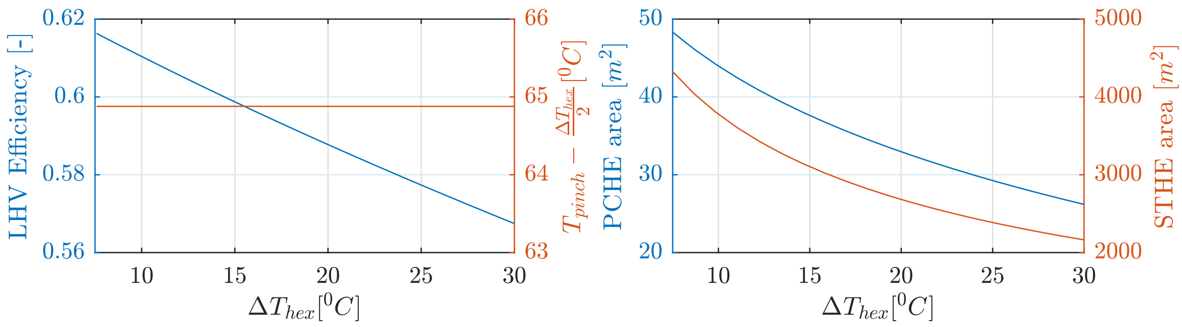

(a) *LHV AC efficiency and pinch temperature* (b) *Heat exchanger area*

Figure 4.11: *Effect of the minimal temperature difference (case I: Basic setup, ΔT_{hex} = 10 °C)*

4.2. Case II: Recompression cycle

4.2.1. The SOFC system

The operation of the SOFC system is not changed in this case compared to case I. See section 4.1.1.

4.2.2. The sCO_2 Brayton cycle

In this case, the more advanced and efficient recompression cycle is employed, see figure 1.1b and 4.12. In the recompression cycle, the flow is split (8) before entering the cooler. Part of the flow is cooled down to minimum temperature (8-1) and is compressed at the lowest temperature and pressure, as in

[8] Keeping in mind that the temperature difference at the LT end of the fuel- and LT air preheater is maintained

the simple recuperative cycle. The other part of the flow is not cooled down and is compressed in the HTC (8-3). The outlet of the LTC is heated in the LTR up to the outlet of the HTC (2-3). The two flows join and are heated in the HTC before entering the heater (3-4). As in the simple recuperative cycle, the flow is heated up to a TIT of 700 °C. The flow is expanded in the turbine (5-6) and supplies heat to the HTC (6-7) and LTC (7-8) before it is split.

Less heat is rejected by the cycle but the compression work increases because the HTC operates in a region where the density of the gas is lower than near the critical point. The net result is an increase in efficiency.

The TIT and minimum temperature of the cycle are the same as in the simple recuperative cycle. Two variables remain to be determined: The inlet temperature of the HTC (8) and the mass flow ratio between the two compressors. The inlet temperature of the HTC (8) is chosen in such a way that the

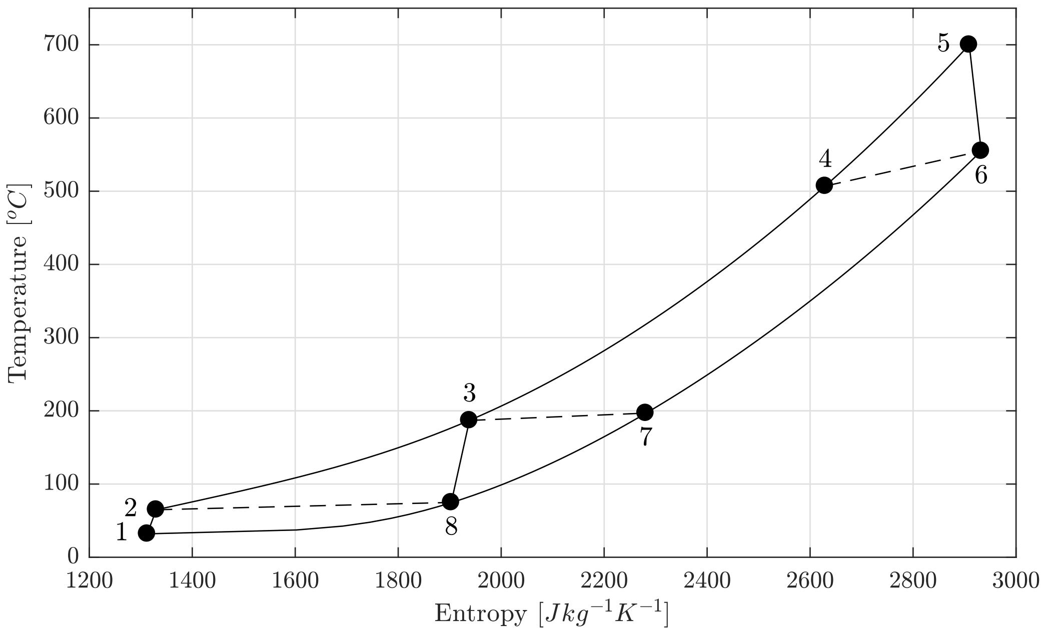

Figure 4.12: *T-s diagram (recompression cycle, the numbers refer to the PFD, figure 1.1b)*

temperature difference at the LT end of the LTC is the imposed minimal temperature difference:

$$T_8 = T_2 + \Delta T_{hex} \tag{4.5}$$

The mass flow is split in such a way that the heat flows in the LTC are balanced.

$$\dot{n}_{CO_2}(h_7 - h_8) = x_I \dot{n}_{CO_2}(h_3 - h_2) \tag{4.6}$$

For a minimum temperature difference of 10 °C the thermodynamic efficiency of the cycle is 50.79 %.

4.2.3. Pinch analysis

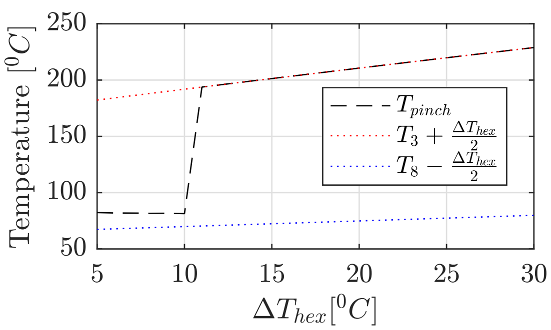

Figure 4.13: *Relation between the minimum temperature difference and pinch temperature(case II: Recompression cycle, numbered temperatures refer to figure 1.1b and 4.12)*

Contrary to case I, the minimal temperature difference has a qualitative effect on the pinch temperature. Figure 4.13 shows the pinch temperature and the interval temperatures of in- and outlet of the HTC (3 and 8).

For lower minimum temperature differences, the pinch temperature does not correspond to an interval temperature related to either the in- or outlet temperature of HTC (3/8). Neither to the in- or outlet temperature of one of the other hot or cold streams in the system. The pinch temperature *floats* between the interval temperatures of the in- and outlets of hot and cold streams. This is only possible if the streams do not have constant specific heat capacities, as is the case.

At some point the pinch temperatures *jumps* to the interval temperature of the outlet of the HTC (3). With a pinch temperature at two qualitatively different points, two designs for a heat exchangers network are necessary. The choice has been made to design networks for a minimum temperature

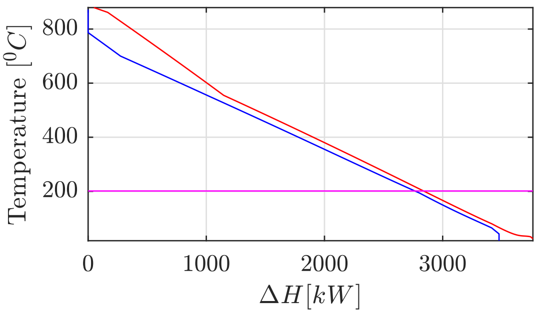

(a) *Case II.A: Recompression cycle,* ΔT_{hex} =15 °C

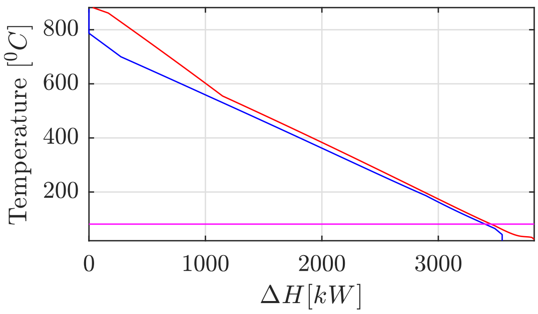

(b) *Case II.B: Recompression cycle,* ΔT_{hex} =10 °C

Figure 4.14: *Pinch diagrams (Hot stream = red, cold streams = blue, pinch temperature = magenta)*

difference of 15 °C, referred to as case II.A, and 10 °C, case II.B. Case II.A is considered the better case, this will become clear in section 4.2.4 and 4.2.5. The heat flows resulting from the pinch analysis for both cases can be found in figure C.4 and C.6 respectively.

4.2.4. Heat exchanger network

Case II.A, makes for a simpler heat exchanger network design. Above the pinch the problem is almost identical to that of case I, except for the higher pinch temperature.

Therefore, as a starting point, the same design principles as in case I are applied. At the pinch, moving to higher temperatures, the flue gas is split into three, heating the fuel- and air feed and part of the HP sCO_2. The LP sCO_2 will supply heat to the remaining HP sCO_2.

Contrary to case I, the pinch temperature is much higher, since it corresponds to the outlet temperature of the HTC. The temperature differences at both ends of the fuel- and air preheater remain unchanged. At the HT end this is the difference between the outlet temperature of the afterburner and the inlet of fuel mixer and cathode respectively. At the LT end, which is at the pinch, this still is the minimal temperature difference, 15 °C. This increases the temperature gradient of the flue gas in fuel- and air preheater, thus decreasing the mass flow of flue gas in these heat exchangers.

Therefore, more flue gas is supplied to the heat exchanger supplying heat to the HP sCO_2. This also increases the mass flow of HP sCO_2 in this heater. Consequently, the mass flow of HP sCO_2 in the HTR decreases to such an extent that a temperature crossover occurs, making this design impossible.

This problem can be avoided by decreasing the inlet temperature of the flue gas in the fuel- and air preheater. This can be done by cooling down the flue gas first before splitting it, adding a heat exchanger in the process. Another way to bring down the inlet temperature is by decreasing the outlet temperature of the afterburner by cooling the exhaust of the fuel cell more. The latter option is chosen because this design approach has one less heat exchanger.

The complete LP sCO_2 supplies heat to the HTR. The cold stream in the HTR is determined so that the temperature difference at the HT end is the imposed minimal temperature difference. The remaining HP sCO_2 is heated by the flue gas. The flue gas also supply heat to the fuel- and air feed and the full HP sCO_2 stream from the outlet of the HTR up to inlet of the precooler of the afterburner. The outlet temperature of the afterburner is determined so that the energy in the flue gas flow is balanced with the heat duties it has to supply.

Below the pinch the LTR is operated as it is designed by equation 4.6. Contrary to case I, flue gas must be added to the fuel- and air preheater below the pinch to avoid a temperature crossover. This is because of the higher pinch temperature.

In case of a lower minimum temperature difference, case II.B, an additional problem arises. The sCO_2 flows present at the pinch are those designed for the LTR, equation 4.6. This means that taking some

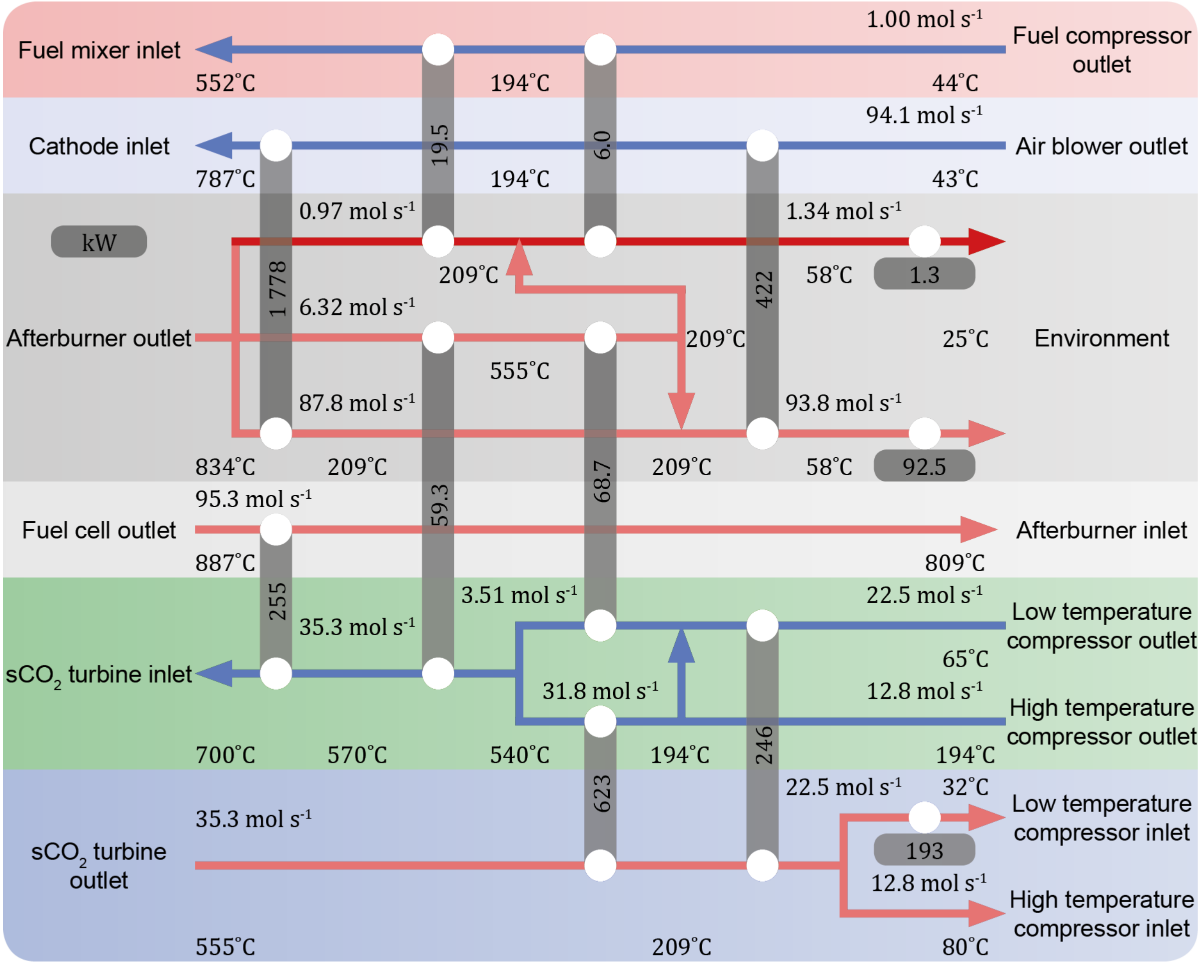

Figure 4.15: *Heat exchanger network (case II.A: Recompression cycle, ΔT_{hex} = 15 °C)*

of HP sCO_2 to cool down the flue gas will inevitably cause a temperature difference violation in the LTR as this changes the energy balance of equation 4.6. This makes the solution to move away from the pinch used before in case II.A impossible.

In order to move away from the pinch, the flue gas heats the HP sCO_2 and fuel. The air is preheated by the LP sCO_2. Moving away from the pinch, to higher temperatures, this situation changes when at the outlet temperature of the HTC. From here on, the same design principle as in the case of a higher minimal temperature difference, case II.A, figure 4.15, is applied.

Below the pinch, flue gas does not have to be added to the fuel preheater to avoid a temperature crossover, this is similar to case I. The heat exchanger that transfers heat from the LP sCO_2 to the air feed does not supply heat to the air from the outlet of the air blower. An additional LT air preheater is necesarrry. The resulting heat exchanger network, figure C.8, is even more complex. This shows that below a certain threshold the complexity of the system increases significantly.

In both designs the in- and outlet temperature of the afterburner is adjusted. This means that the heat flows determined in section 4.2.3 change slightly. This is not displayed in figures, 4.14, C.6 and C.4. This has not been adjusted in these figures since they are the result of the pinch analysis and form the basis for the design of the heat exchanger network.

A PFD of case II.A and II.B can be found in figure C.5 and C.7 respectively.

4.2.5. Performance analysis

Looking at table 4.4, it stands out that the two qualitatively different cases corresponding to the different pinch temperatures show similar efficiencies but a very large difference in total the area of the PCHEs.

	Case II.A (ΔT_{hex} =15 °C)	**Case II.B** (ΔT_{hex} =10 °C)
Fuel cell power (kW)	380	380
Generator power (kW)	181	192
Auxiliary power consumption (kW)	53	53
Net AC system power (kW)	508	519
LHV AC efficiency (%)	63.26	64.64
Thermodynamic efficiency (%)	72.47	73.92
Second law efficiency (%)	61.97	63.27
Thermodynamic cycle efficiency (%)	49.68	50.79
sCO_2 cycle flow (mol s^{-1})	35.3	37.1
Total PCHE area (m^2)	79	180
Total STHE area (m^2)	4 467	4 440
Number of heat exchangers	10	11

Table 4.4: *Key performance data (case II: Recompression cycle)*

As expected, the efficiency decreases if the minimal temperature difference increases. Not only does the efficiency of the sCO_2 Brayton cycle decrease with an increasing minimal temperature difference, it also means that less heat can be transfered to the sCO_2 Brayton cycle.

In the case of a minimal temperature difference of 10 °C, case II.B, the size of the PCHE is more

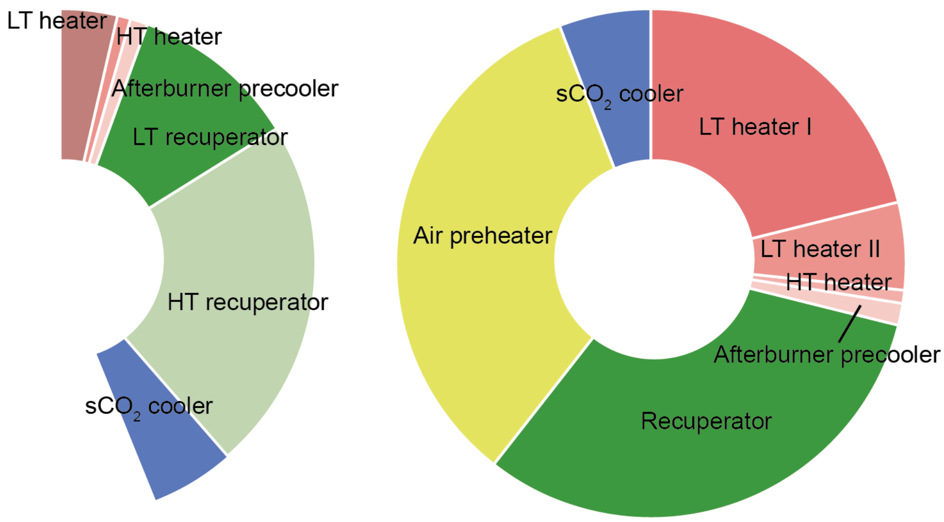

(a) *Case II.A (ΔT_{hex} =15 °C)* (b) *Case II.B (ΔT_{hex} =10 °C)*

Figure 4.16: *PCHE size (case II: Recompression cycle, 100% =* 180 m^2*)*

than doubled compared to the case of a minimal temperature difference of 15 °C, case II.A. This is because in case II.A, all the heat supplied to the air feed is by the flue gas. This heat transfer can occur in a STHE. In case II.B, part of the air is preheated by the sCO_2, in order to move away from the pinch. This requires a PCHE and significantly increases the total area of this type of heat exchanger. Figure 4.16 clearly shows the difference.

Furthermore, case II.B requires more heat exchangers. The *floating pinch temperature* complicates the design of the heat exchanger network. So besides increasing the area of the PCHEs, it also complicates the design.

Figure 4.17 shows the effect of the minimal temperature difference on the performance of the system. The two qualitatively different cases are clearly separated by a *jump* in the heat exchanger area. This

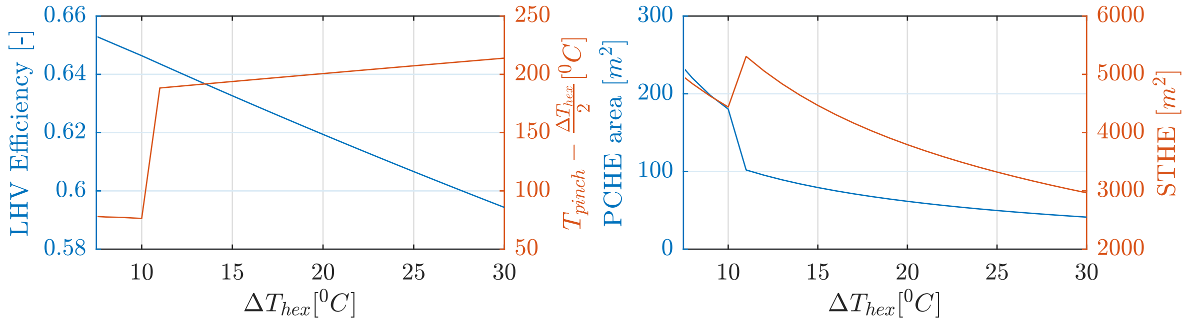

Figure 4.17: *Effect of the minimal temperature difference (case II: Recompression cycle)*

threshold is important to keep in my mind, although in practical designs this problem might be avoided.

4.3. Case III: Cathode recirculation

4.3.1. The SOFC system

Since the equivalence ratio of air supply, recirculation of the cathodic air is possible. A fraction of the outlet of the cathode is recirculated and mixed with the outlet of the air feed.

Not all air can be recirculated, enough oxygen must be supplied to enable the electrochemical reaction and combustion in the afterburner. Another restriction is that if too much air is recirculated, the temperature of the recirculated air does not cool down the required 100 °C. The latter restriction turns out to be the limiting factor in this case. The maximum recirculation ratio is found to be 87.30%.

The oxygen concentration in the cathode is not a limiting factor, but as more cathodic air is recirculated, its concentration does obviously decrease and this decreases the Nernst voltage. Because of the large equivalence ratio it does not decrease by much though. Furthermore, the Nernst voltage is not very sensitive to the oxygen concentration. Figure 4.18a shows that the recirculation of cathodic air does not have a significant effect on the fuel cells electrochemical performance.

The main reason to recirculate cathodic air is to reduce the duty of the air preheater. Clearly the mass flow of the air feed as the recirculation ratio increases. Furthermore, the outlet temperature decreases as more hot cathodic air is mixed with the outlet of the air feed. Figure 4.18b shows the effect on the outlet temperature of the air feed and the heat required to preheat the air.

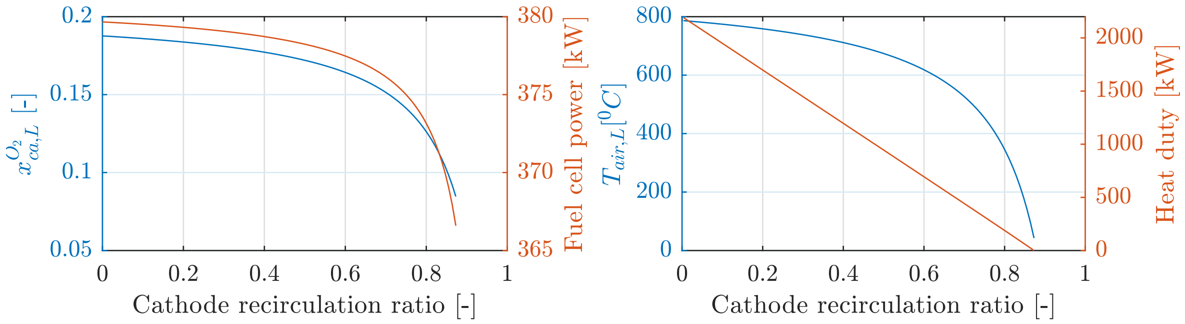

(a) *Oxygen concentration en fuel cell power*

(b) *Air feed*

Figure 4.18: *Effect of the cathode recirculation ratio on the SOFC system*

Two other temperatures are affected by the cathode recirculation ratio, the inlet temperature of the afterburner and the dew temperature of the flue gas. The former changes because the amount of fuel in the fuel cells exhaust remains the same while the total mass flow of the exhaust decreases and the outlet temperature of the afterburner is fixed. The latter because the amount of water in the flue gas remains the same while the total mass flow decreases.

4.3.2. The sCO_2 Brayton cycle

A simple recuperative cycle as in case I is used, see section 4.1.2.

4.3.3. Pinch analysis

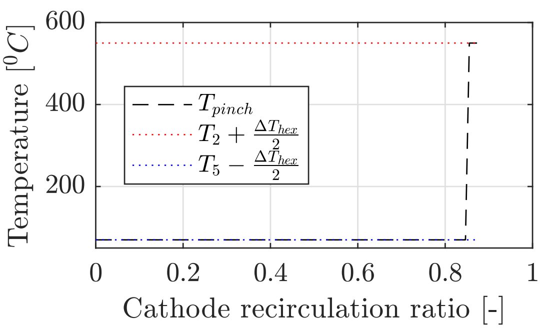

Figure 4.19: *Relation between the cathode recirculation ratio and pinch temperature (case III: Cathode recirculation, numbered temperatures refer to figure 4.3)*

Figure 4.19 shows that the pinch temperature the pinch temperature either corresponds to the interval temperature of the outlet of the compressor or to the TOT. It is only at a high recirculation ratio, near the maximum, that the pinch *jumps* from the one to the other.

This behavior is not affected by the minimal temperature difference of the system imposed in the pinch analysis. From the pinch analysis two qualitatively different cases can be identified, however, the shifting temperatures and heat duties as a result of changing the cathode recirculation ratio change the design of the heat exchanger network in more ways. This will be discussed in the next section.

4.3.4. Heat exchanger network

The analysis in this section is for a minimal temperature difference of 10 °C. As mentioned in section 4.3.1, several streams are affected by the recirculating cathodic air. This has some effect on the design of the heat exchanger network.

Case III is split into four qualitatively different cases depending on the cathode recirculation ratio. These are defined by changes to the heat exchanger network caused by the shifting temperatures and mass flows of several stream affected by recirculation cathodic air. Table 4.5 shows which considers the design for a certain recirculation ratios. Case III.A is considered the best case, which will be explained in section 4.3.5. This section very briefly discusses case III.B to III.D and III.A in more detail. All cases are discussed in more detail in section C.4.

Case III	**Cathode recirculation ratio**(%)
B (section C.4.2)	0 - 73.49
A (section C.4.1)	73.50 - 74.86
C (section C.4.3)	74.87 - 85.04
D (section C.4.4)	85.04 - 87.30

Table 4.5: *Division of heat exchanger network designs (case III: Cathode recirculation, ΔT_{hex} =10 °C)*

Case III.B applies the same design principles as case I. This is possible up to the point where the outlet temperature of the air feed has decreased to such an extent that it is no longer required to use a LT- and HT air preheater. Adjusting for this is what is discussed in case III.A. Case III.C discusses the problems that arise when the dew temperature has increases to such an extent that it causes problems for the design approach of case III.A. Case IV.D discusses the approach for the higher pinch temperature, the TOT.

The range of cathode recirculation for which the design approach of case III.A can be applied also depends on the minimum temperature difference. For a low minimal temperature difference, the upper limit of the recirculation ratio of case III.A fall below the lower limit. This obviously means that the design approach of case III.A cannot be applied. Since case III.A performs better than other cases, the choice has been made not to consider cases with a lower minimal temperature difference than 10 °C.

The design of the network, figure 4.20, is very similar to that of case I. The only difference is that there is only one air preheater instead of there being two. The outlet temperature of the air feed has decreased to a temperature below the outlet temperature of the cold streams of the recuperator and LT heater. These temperatures are still designed to be the equal and the flue gas is divided among these heaters accordingly.

The outlet temperature of the flue gas of the air preheater equals the dew temperature of the flue gas. After all, the recirculation ratio is at the upper limit of case III.A. Case III.C, a higher recirculation ratio, considers the design when this dew temperature is higher than the outlet temperature of these preheaters. Another difference in the design compared to case I is the addition of a blower and air mixer to make the recirculation of cathodic air possible, see figure 4.21. Other differences with case I are reflected in the performance and size of the heat exchangers.

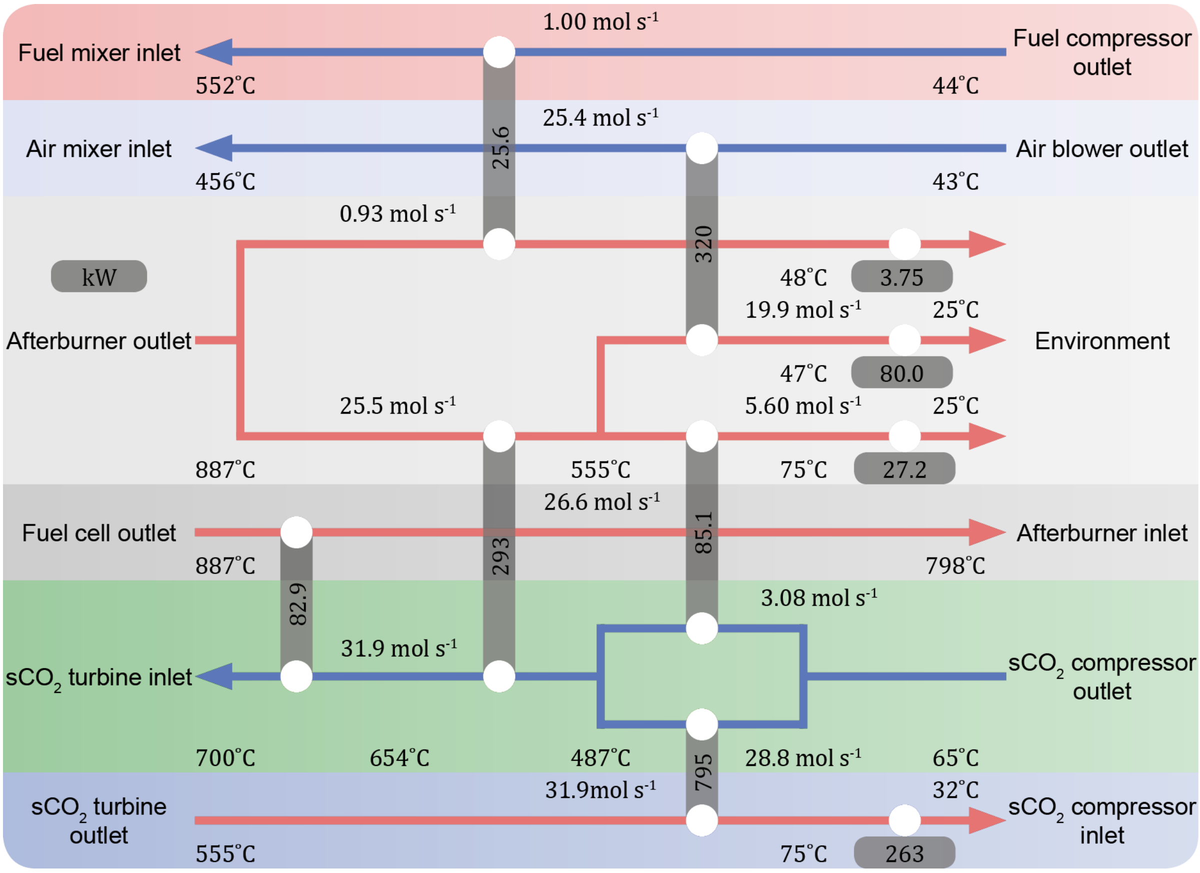

Figure 4.20: *Heat exchanger network (case III.A: Cathode recirculation, r_{ca} = 74.86%,ΔT_{hex} = 10 °C)*

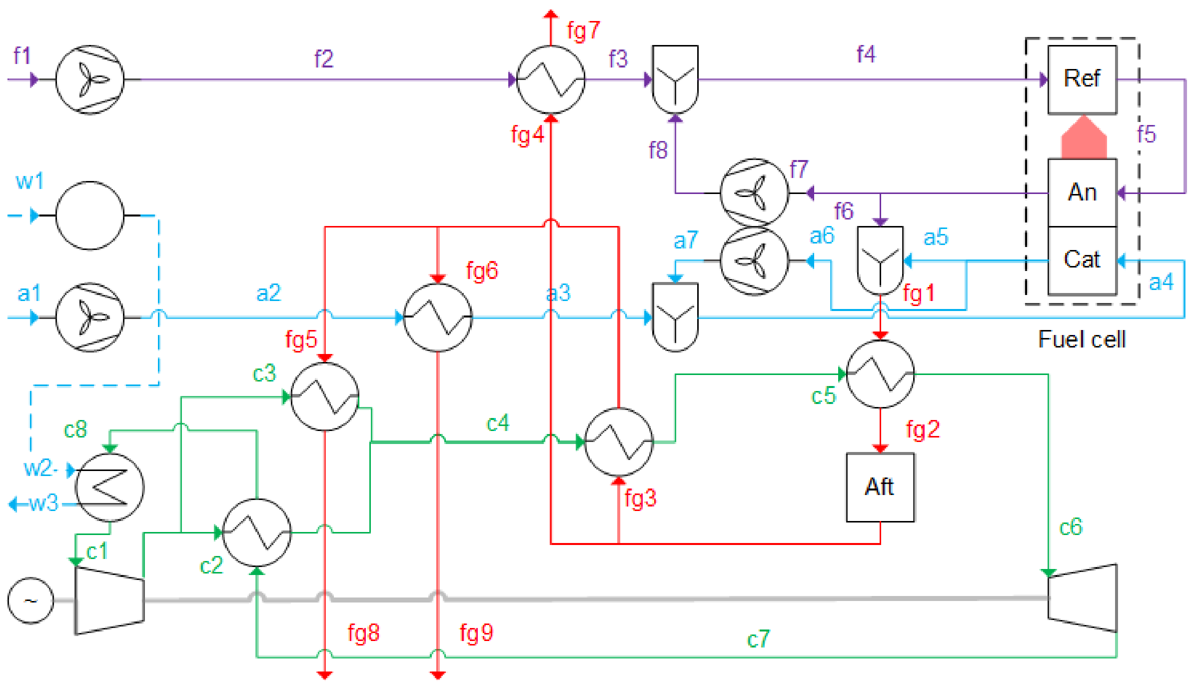

Figure 4.21: *PFD (case III.A: Cathode recirculation, r_{ca} = 74.86%,ΔT_{hex} = 10 °C)*

4.3.5. Performance analysis

This section will first analyze the performance of the system for the complete range of cathode recirculation ratios. From this analysis it will become clear why the recirculation ratios that case III.A operates in is selected as the best option. The second part of this section will discuss this specific case in more detail.

Figure 4.22a shows that the efficiency of the system slightly increases as the cathode recirculation ra-

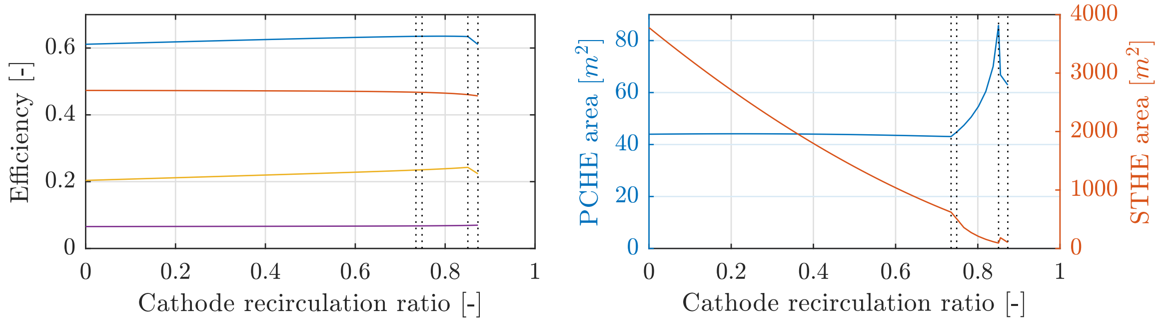

(a) *Power production/consumption as fraction of LHV of methane (From top to bottom: Net system AC, SOFC, generator and auxiliary)*

(b) *Heat exchanger area*

Figure 4.22: *Effect of the cathode recirculation ratio (case III: Cathode recirculation,* ΔT_{hex} = 10 °C*))*

tio increases up to the point where the pinch temperature *jumps*(85.05%). The efficiency of the SOFC slightly decreases as cathode recirculation ratio increases and thus the oxygen concentration in the cathode decreases. The auxiliary power consumption remains more or less constant. Work is shifted from the LT air blower to the HT air blower recirculating the cathodic air. Compression requires more work at a higher temperature, but the pressure difference is smaller for the HT air blower because the pressure drop in the preheaters does not have to be taken into account anymore. The power produced by the generator increases significantly, increasing the performance of the system.

This is because mass flow in the sCO_2 Brayton cycle is increased by recirculating cathodic air and by transferring more heat to the cycle. This has two reasons. Firstly, since the power production of the SOFC decreases, more heat is produced. But more importantly, the air mixer *acts* as a heat exchanger where the outlet has a temperature difference of 0 °C. This means more heat is available to be transfered to the sCO_2 Brayton cycle.

Looking at figure 4.22b, a few things can be observed. The total size of the STHEs, dominated by the air preheater(s), decreases since the heat required by the air feed decreases and the temperature difference at the HT end increases.

The size of the PCHE remains more or less the same in case III.B (r_{ca} =0-73.49%). Both the mass flow and heat duty of the flue gas and air feed change but the balance determining the outlet temperature of the cold streams of the LT air preheater, LT heater and recuperator is not affected much by this change. Therefore the temperature difference and heat duty of the LT heater and recuperator does not change significantly, as does the size of the PCHEs. However, in case III.A (r_{ca} =73.50-74.86%) this balance changes. The outlet temperature of the air preheater, which there is only one of in this case, fall below the outlet temperature of the cold streams of the recuperator and LT heater. These temperature increase but the temperatures of the hot streams at this end of the heat exchangers remain unchanged. This decreases the temperature difference and thus increases the area of the PCHEs. Figure 4.23 shows that the temperature difference in this temperature range, 75 to 555 °C, decreases between case III.A and III.D. This is also reflected in the increasing area of the PCHEs, figure 4.22b.

Besides the total size, the number of heat exchanger changes in each case. Case III.A and III.D have the least heat exchangers, 7. Case III.B has 8 and III.C 9.

Taking this analysis into account, case III.A is deemed to be the best option because compared to the other cases: It has a relatively high efficiency, the increase of the total area of PCHEs is limited, the

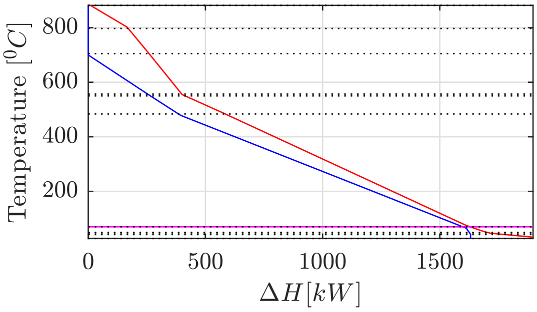

(a) *Critical point 1: r_{ca} = 73.49%*

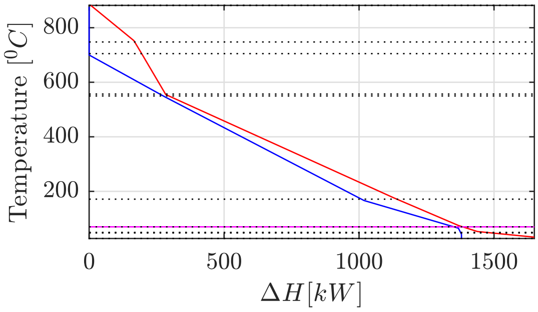

(b) *Critical point 3: r_{ca} = 85.04%*

Figure 4.23: *Pinch diagrams (Hot stream = red, cold streams = blue, pinch temperature = magenta) (case III: Cathode recirculation, ΔT_{hex} = 10 °C))*

Fuel cell power	375 kW
Generator power	189 kW
Auxiliary power consumption	54 kW
Net AC system power	510 kW
LHV AC efficiency	63.52 %
Thermodynamic efficiency	72.97 %
Second law efficiency	62.50 %
Thermodynamic cycle efficiency	43.16 %
sCO_2 cycle flow	31.8 mol s^{-1}
Total PCHE area	45 m^2
Total STHE area	508 m^2
Number of heat exchangers	7

Table 4.6: *Key performance data (case III.A: Cathode recirculation ratio, r_{ca} = 74.86%,ΔT_{hex} = 10 °C)*

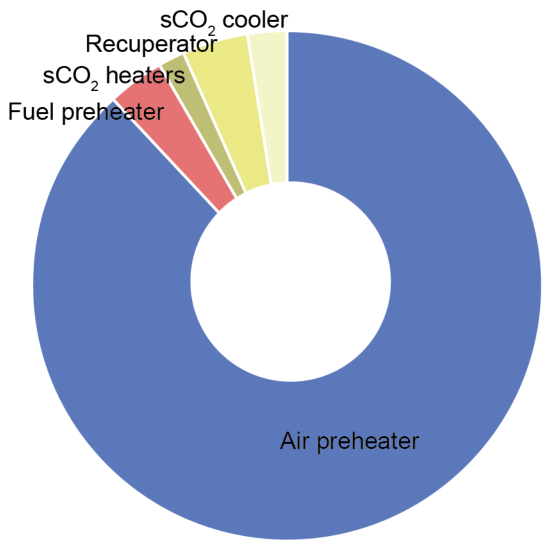

Figure 4.24: *Heat exchangers size (case III.A: Cathode recirculation ratio, r_{ca} = 74.86%,ΔT_{hex} = 10 °C)*

area of the STHE is relatively small and the number of heat exchangers is the lowest. More specifically, case III.A is evaluated at its upper limit, 74.86%.

Table shows 4.6 shows the key characteristics of case III.A. The total area of the PCHEs has slightly increased, from 44 to 45 m^2, while the total area of the STHEs has decreases drastically, from 3778 to 508 m^2, when compared to case I. Figure 4.24 illustrates this as well, the PCHEs, the sCO_2 heaters, cooler and recuperator, make up a relatively much larger part of the total size of the heat exchangers. So while the efficiency increases slightly, the main advantage of recirculating cathodic air is the fact that the size of the air preheater decreases drastically and only one air preheater, instead of two, is required.

Figure 4.25 shows the effect of the minimal temperature difference on the performance of the system. The recirculation ratio is adjusted accordingly so that the system operates on the same design principle for each minimal temperature difference. As mentioned before, section 4.3.4, the minimal temperature difference should not be too low because this makes case III.A impossible.

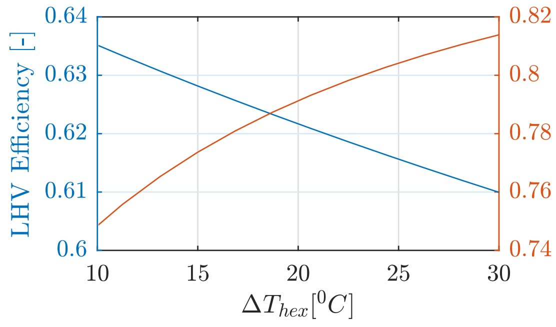

(a) *Efficiency and cathode recirculation ratio*

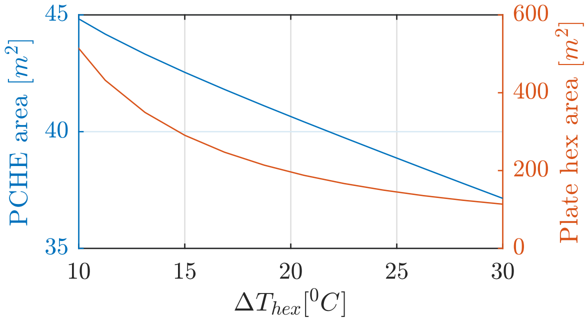

(b) *Heat exchanger area*

Figure 4.25: *Effect of the minimal temperature difference (case III.A: Cathode recirculation)*

4.4. Case IV: Recompression cycle + cathode recirculation

4.4.1. The SOFC system

Cathode recirculation is applied as in case III, see section 4.3.1.

4.4.2. The sCO_2 Brayton cycle

A recompression cycle as in case II is used, see section 4.2.2.

4.4.3. Pinch analysis

Combining the recompression cycle with recirculating cathodic air shows characteristics of both cases separately.

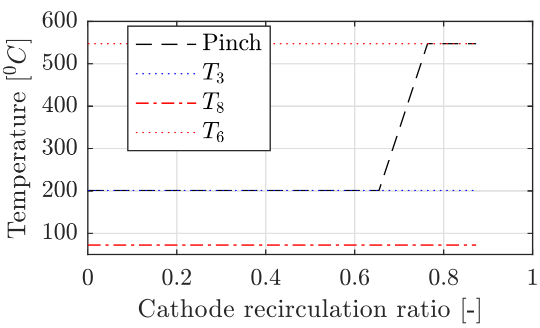

(a) $\Delta T_{hex} = 15\,°C$

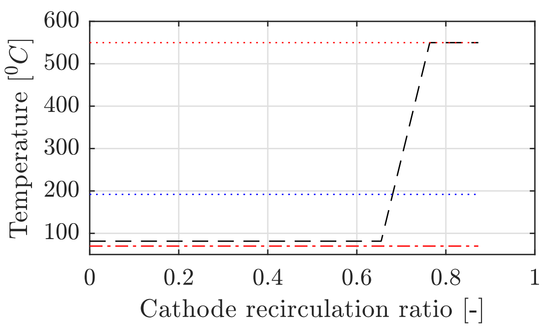

(b) $\Delta T_{hex} = 10\,°C$

Figure 4.26: *Pinch analysis (case IV: Recompression cycle + cathode recirculation, numbered temperatures refer to figure 4.12)*

The behavior of the pinch temperature as a function of the minimal temperature difference is similar to that of case II, section 4.2.3. At lower minimal temperatures, the pinch temperature *floats*, case II.B. At higher minimal temperature differences the pinch temperature *jumps* to the interval of outlet temperature of the HTC, case II.A.

These two cases respond similarly to cathode recirculation as case III, section 4.3.3. The pinch temperature *jumps* to the interval temperature related to the TOT at high recirculation ratios, see figure 4.26.

Section 4.2 showed that the *floating pinch temperature*, case II.B, considerably complicates the design and size of the PCHEs. It is therefore chosen not to consider this case in combination with recirculating cathodic air. The other case, II.A, considered the better option, is further explored in combination with recirculating cathodic air in this section.

4.4.4. Heat exchanger network

Similar to case III, case IV can be divided into several designs dependent on the cathode recirculation ratio. Specifically, five cases, IV.A to IV.E are defined, see table 4.7. As mentioned before, these cases are for a minimal temperature difference of 15 °C.

Case III	**Cathode recirculation ratio**(%)
B (section C.5.2)	0 - 63.76
A (section C.5.1)	63.77 - 69.63
C (section C.5.3)	69.64 - 75.93
D (section C.5.4)	73.94 - 82.41
E (section C.5.5)	82.42 - 87.30

Table 4.7: *Division of heat exchanger network designs (case IV: Recompression cycle + cathode recirculation,* ΔT_{hex} =15 °C*)*

Case IV.B applies the same design principle as case II.A. This is possible up to a recirculation ratio of 63.77%, at this point the temperatures in the heat exchangers have changed in such a way that it is possible to cut out the LT fuel preheater from the design and just use one fuel preheater, case IV.A. The temperature difference at the LT end of this one fuel preheater at the lower limit of case IV.A is only 5 °C. This is less than the imposed 15 °C but deemed to be favorable over the use of two fuel preheaters.

The upper limit of case IV.A (69.63%) is characterized by the temperature difference of the LT end of the precooler of the afterburner. This is the difference between the inlet temperature of the afterburner and the outlet temperature of the HP sCO_2 of the HT heater, which is 15 °C at this recirculation ratio. It would be possible to still apply the approach of case IV.A for a higher recirculation ratio, decreasing this temperature difference below the imposed 15 °C, but at a certain recirculation ratio a temperature crossover would occur, making this approach impossible. The choice has been made to switch to a different design approach when this temperature difference reaches the imposed 15 °C.

Case IV.C is a more efficient but also significantly more complex design than case IV.A. Therefore case IV.A is deemed to be the better option. Case IV.C is possible up to the point where the pinch *jumps*.

Case IV.D and IV.E design a heat exchanger network for this high pinch, the only difference between the two is the use of either two (case IV.D) or one (case IV.E) air preheater.

Case IV.A is considered the best of these options. More specifically, case IV.A is evaluated at its upper limit, 69.63%. Section 4.4.5 discusses the performance of case IV and from this it will become clear why case IV.A is considered the best option. Figure 4.27 shows the design of the heat exchanger network, figure 4.28 a PFD.

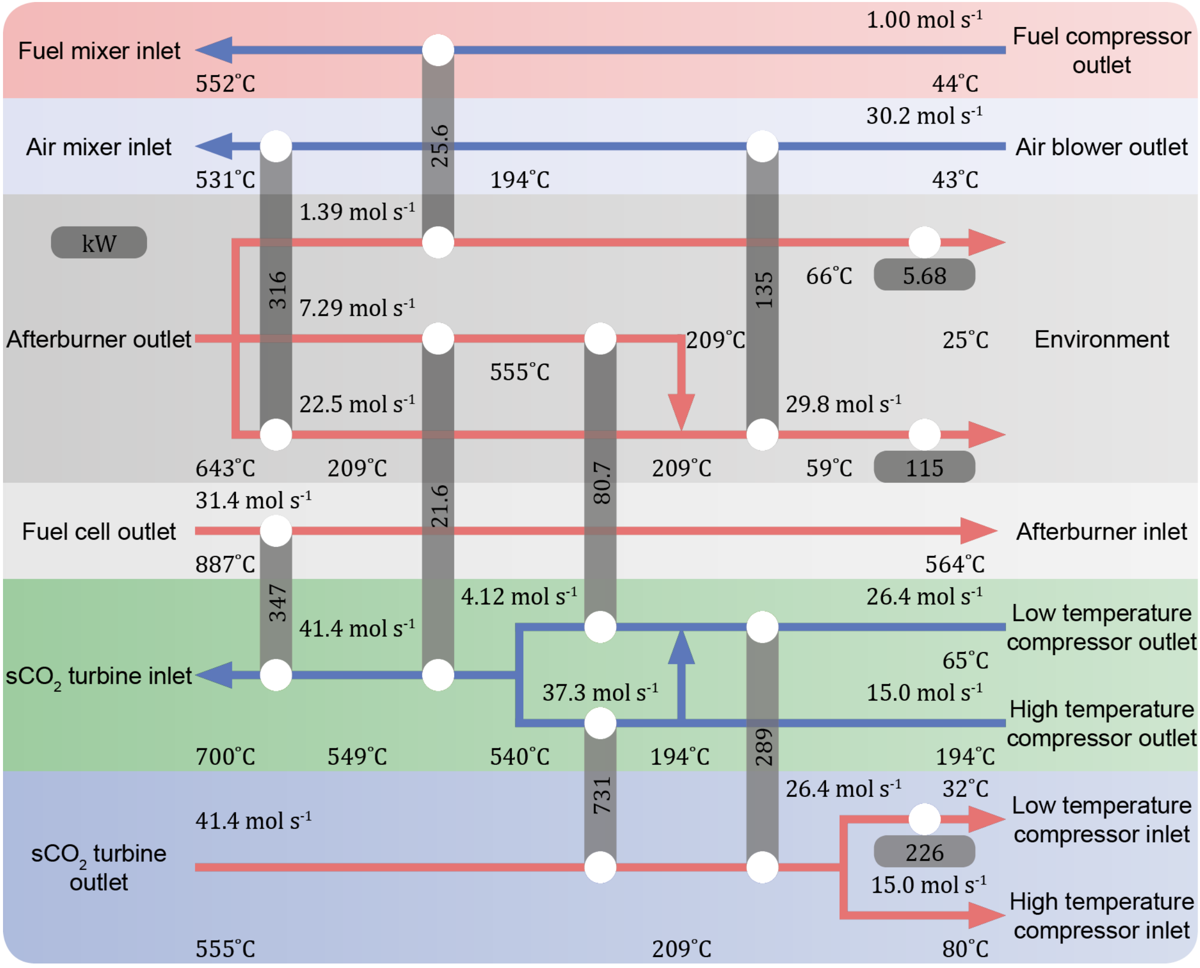

Figure 4.27: *Heat exchanger network (case IV.A: Recompression cycle + cathode recirculation,* r_{ca} *= 69.63%,*ΔT_{hex} = 15 °C)

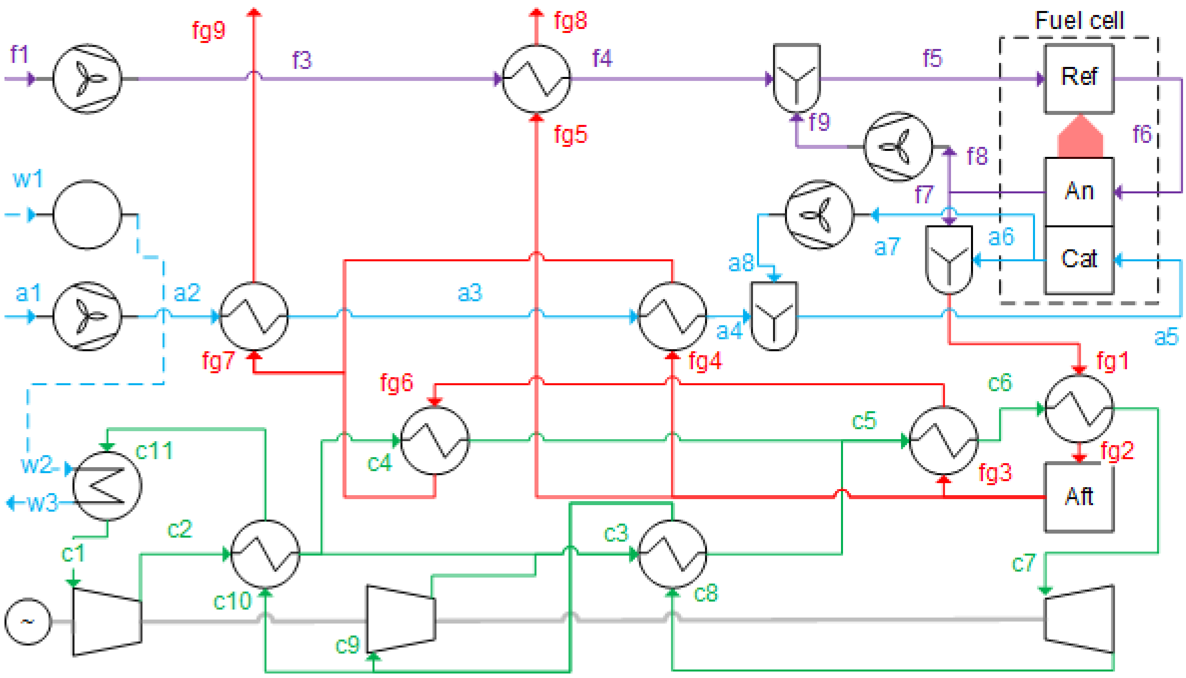

Figure 4.28: *PFD (case IV.A: Recompression cycle + cathode recirculation ,* $0.6378 \leq r_{ca} \leq 0.6963$ *,*ΔT_{hex} = 15 °C)

4.4.5. Performance analysis

This section will first analyze the performance of the system for the complete range of cathode recirculation ratios. From this analysis it will become clear why case IV.A is selected as the best option. The second part of this section will discuss this specific case in more detail.

Figure 4.29 shows that the efficiency of the system increases up to the point where the pinch *jumps*,

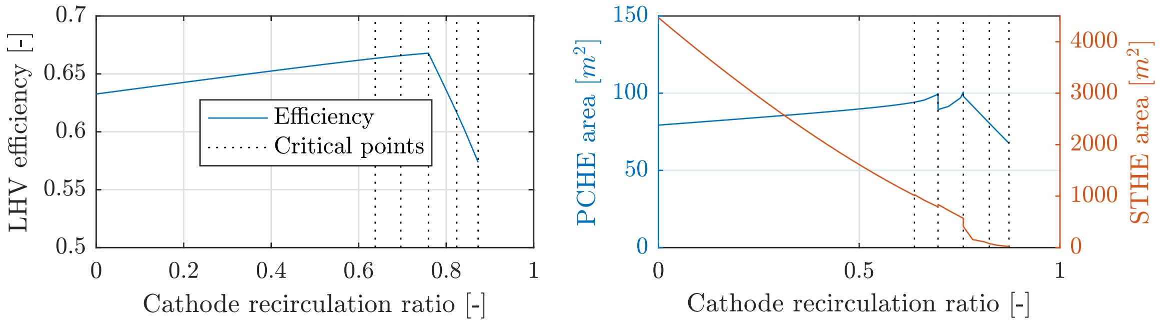

(a) *Efficiency* (b) *Heat exchanger area*

Figure 4.29: *Effect of the cathode recirculation ratio (case IV: Recompression cycle + cathode recirculation,* ΔT_{hex} = 15 °C*))*

75.93%. The total area of the PCHEs also increases, which can be explained by the fact that simply more heat is transfered from the SOFC system to the sCO_2. A *jump* can be in the area of the PCHE can be observed between case IV.A and IV.C at 69.63%.

Up to the point where the pinch *jumps*, the systems efficiency improves and the area of the STHEs drastically decreases. The total area of the PCHE increases but not very significantly. From this it can be concluded that a higher cathode recirculation ratio is beneficial up to the point where the pinch temperature *jumps*. The number of heat exchanger and complexity is also important. For this reason, case IV.A, the upper limit of that, is considered the best case. Case IV.A has the 9 heat exchangers where IV.B and IV.C have 10. Case IV.D also has 9 and IV.E even one less, but these cases have a lower efficiency.

As can be seen in table 4.8, case IV.A shows a very high efficiency. The size of the PCHEs is

Fuel cell power	376 kW
Generator power	212 kW
Auxiliary power consumption	54 kW
Net AC system power	534 kW
LHV AC efficiency	66.58 %
Thermodynamic efficiency	76.15 %
Second law efficiency	65.33 %
Thermodynamic cycle efficiency	49.68 %
sCO_2 cycle flow	41.4 mol s^{-1}
Total PCHE area	100 m^2
Total STHE area	792 m^2
Number of heat exchangers	9

Table 4.8: *Key performance data (case IV.A: Cathode recirculation ratio + recompression cycle,* r_{ca} = *69.63%,*ΔT_{hex} = 15 °C*)*

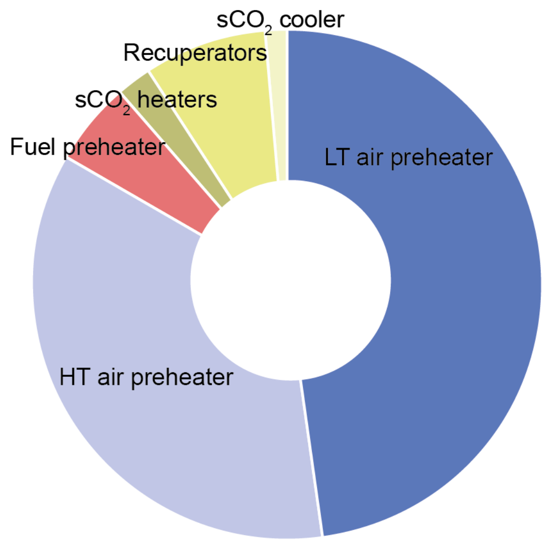

Figure 4.30: *Heat exchangers size (case IV.A: Cathode recirculation ratio + recompression cycle,* r_{ca} = *69.63%,*ΔT_{hex} = 15 °C*)*

relatively large compared to the relatively small size of the STHEs, figure 4.30. Compared to case II.A, the recirculation of cathodic air has improved the system by more than 3% in efficiency, drastically decreases the size of the STHEs and it has one less heat exchanger. The size of the PCHEs has increased as a consequence of the increased heat transfered to the sCO_2 cycle.

Figure 4.31 shows that the system is affected by the minimal temperature difference as expected.

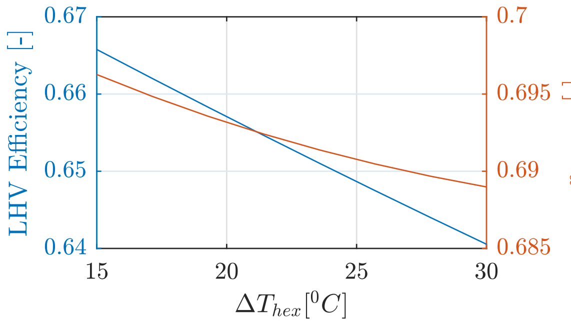

(a) *Efficiency and cathode recirculation ratio*

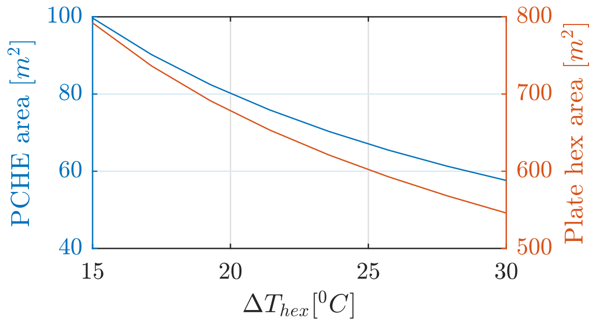

(b) *Heat exchanger area*

Figure 4.31: *Effect of the minimal temperature difference (case IV.A: Recompression cycle + cathode recirculation)*

The critical recirculation ratio at which case IV.A is operated slightly decreases, as does the efficiency. The area of the PCHEs decreases significantly more than the efficiency does.

4.5. Case V: Heat recovery steam generator

4.5.1. The SOFC system

As mentioned before, steam needed for the reforming reaction can either be supplied by recirculating anodic exhaust gas and/or by a HRSG. Figure 2.2 shows these options.

Supplying steam through a HRSG has some effects on the reforming process and performance of the SOFC. A direct effect is that by increasing the steam supply through a HRSG, less anodic exhaust is recirculated. This means less hot exhaust enters the fuel mixer and the outlet temperature of the fuel and HRSG feed increases. See figure 4.32a.

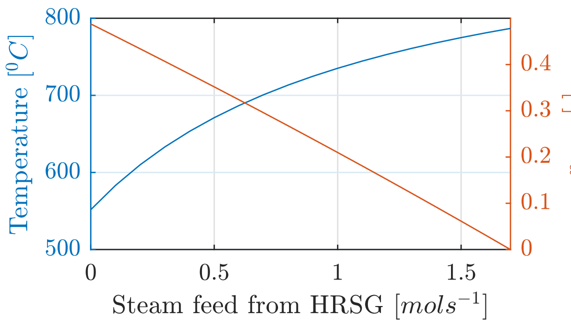

(a) *Outlet temperature of the fuel and HRSG feed and anode recirculation ratio*

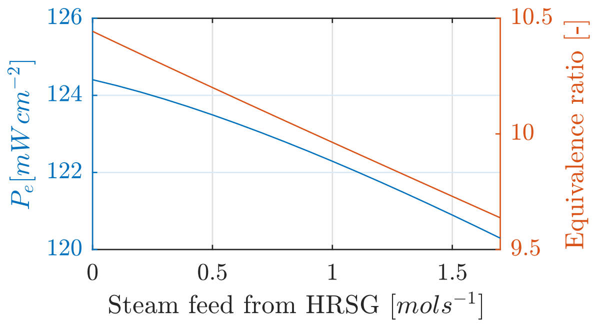

(b) *SOFC power density and equivalence ratio*

Figure 4.32: *Effect of supplying steam by through a HRSG (case V: HRSG)*

The electrochemical performance is also effected, most notably in the total current that is produced. This can be explained by the definition of the fuel utilization ratio, equation 2.17. It is defined as the ratio of the current in the fuel cell over the maximum current that would be possible if all combustible products entering the anode would be oxidized. Because supplying steam through a HRSG reduces the anode recirculation ratio, thereby decreasing the amount of combustible products entering the anode, the current reduces as well; if the fuel utilization ratio is kept constant, which it is.

So for the same number of cells, the current density decreases, which decreases the ohmic resistance. So the operating voltage increases and the current density decreases. Overall, the power density decreases, figure 4.32b , decreasing the performance of the fuel cell. Since the total current decreases and the ohmic resistance decreases, the heat produced in the SOFC also decreases, reflected in a lower equivalence ratio, figure 4.32b.

The composition of the flows entering and leaving the reformer and anode also change, these different compositions do not have a significant effect on the overall performance.

Besides these effects, the composition of the flue gas is effected. The mass flow through the cathode decreases and more anodic exhaust is mixed into the flue gas. This increases the water concentration and thus the dew temperature. The dew temperature increases to a maximum temperature of 40.3 °C, which is lower than the outlet temperature of the fuel and air blower.

4.5.2. The sCO_2 Brayton cycle

A simple recuperative cycle as in case I is used, see section 4.1.2.

4.5.3. Pinch analysis

As in case I, the pinch temperature is the interval temperature of the outlet of the sCO_2 compressor regardless of the minimal temperature difference or mass flow through the HRSG. Figure 4.33 shows

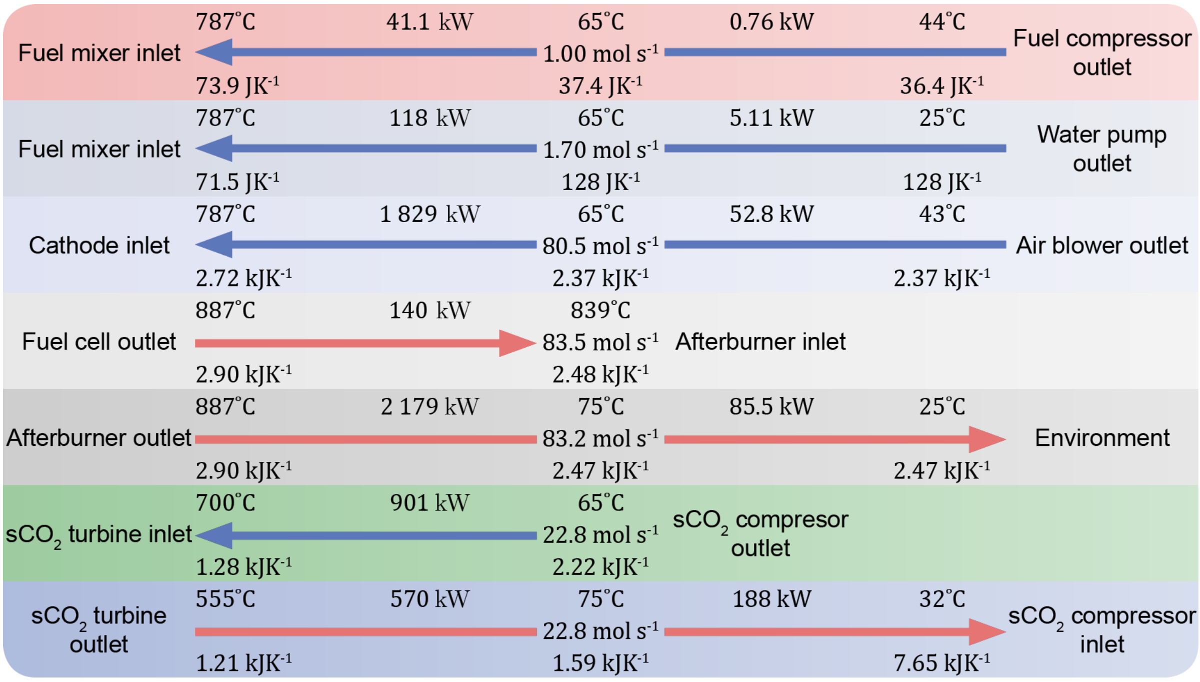

Figure 4.33: *Heat flows (case V: HRSG,* $\dot{n}_{fd}^{H_2O}$ *=1.7 mol s*$^{-1}$*,* ΔT_{hex} *=10 °C)*

the heat flows if all the steam is supplied by the HRSG and consequently the anode exhaust gas is not recirculated.

4.5.4. Heat exchanger network

The design of the heat exchanger network requires three additional heaters for the HRSG system. An economizer, boiler and superheater. A fraction of the cooling water for the sCO_2 Brayton cycle is used to feed the HRSG.

Besides the additions of the HRSG, the design differs in that an additional fuel preheater is necessary to avoid temperature crossovers. This is due to the fact that the outlet temperature and thus the heat required by the fuel feed is increased. This is only the case if a certain amount of steam is supplied by the HRSG and thus the outlet temperature of the fuel feed increases. If less than 0.5256 mol s^{-1} of steam is supplied by the HRSG, only one fuel preheater is required as in case I. Figure 4.34 shows the heat exchanger network if all the steam is supplied through a HRSG at a minimal temperature difference of 10 °C.

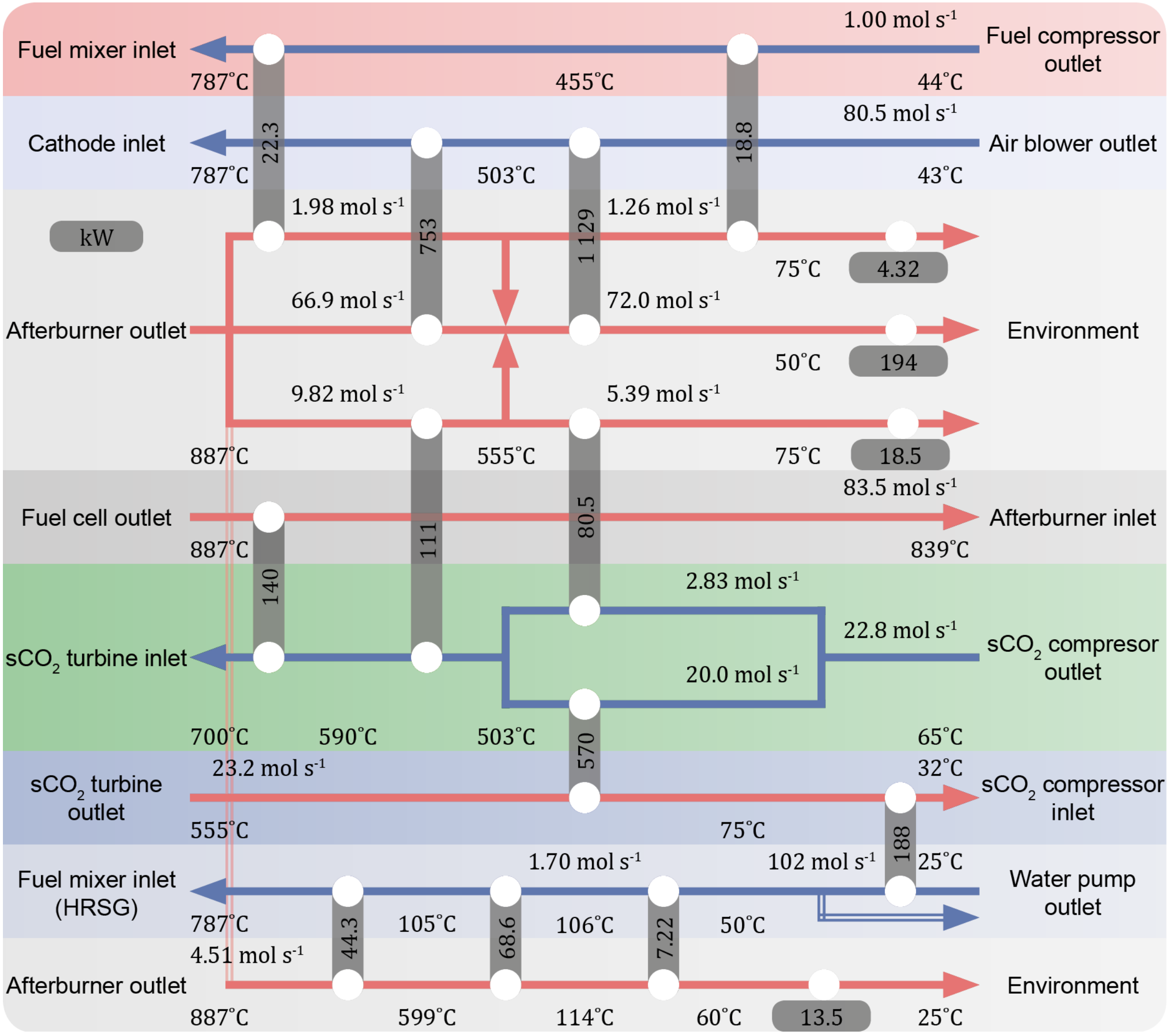

Figure 4.34: *Heat exchanger network (case V: HRSG, $\dot{n}_{fd}^{H_2O}$ =1.7 mol s^{-1}, ΔT_{hex} =10 °C)*

A PFD and all the details of this case can be found in section C.6.

4.5.5. Performance analysis

Supplying steam externally significantly decreases the efficiency of the system, figure 4.35a. The fuel cells performance decreases and less heat can be transfered to the sCO_2 cycle, resulting in a lower mass flow. More heat of the flue gas becomes *trapped* in the latent heat of water due to the increasing dew temperature and heat must be supplied to the HRSG. Because of this, the area of the PCHEs

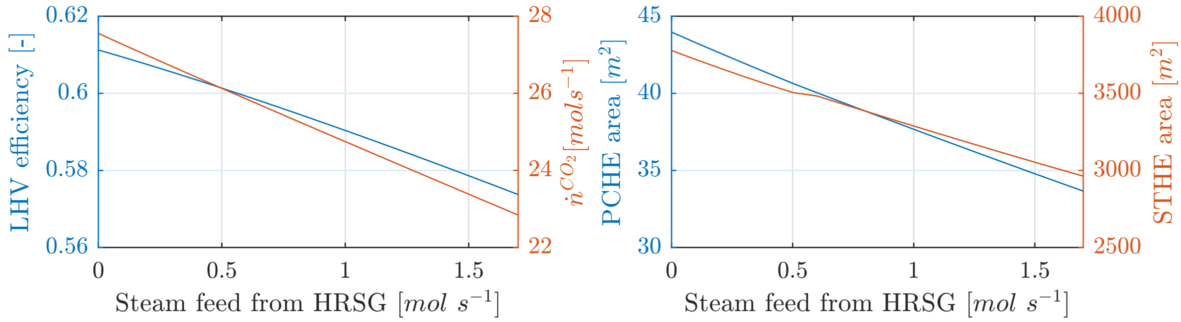

(a) *Efficiency and cycle mass flow* (b) *Heat exchanger area*

Figure 4.35: *Effect of external steam supply (case V: HRSG, $\dot{n}_{fd}^{H_2O}$ =1.7 mol s^{-1}, ΔT_{hex} =10 °C)*

decreases as well, figure 4.35a. As mentioned before, the air flow decreases, resulting in a smaller STHE area. The small *bump* in the area of the STHE is at the point where the design switches between one and two fuel preheaters.

Table 4.9 shows the operating characteristic of case V, when all steam is supplied by a HRSG.

Fuel cell power	367 kW
Generator power	136 kW
Auxiliary power consumption	42 kW
Net AC system power	460 kW
LHV AC efficiency	57.37 %
Thermodynamic efficiency	64.94 %
Second law efficiency	56.22 %
Thermodynamic cycle efficiency	43.16 %
sCO_2 cycle flow	22.8 mol s^{-1}
Total PCHE area	34 m^2
Total STHE area	2963 m^2
Number of heat exchangers	12

Table 4.9: *Key performance data case V: HRSG, $\dot{n}_{fd}^{H_2O}$ =1.7 mol s^{-1}, ΔT_{hex} =10 °C)*

4.6. Case VI: Simplified heat exchanger networks

4.6.1. Case VI.I: Simplified basic setup

Though maximizing the mass flow through the sCO_2 Brayton cycle might be beneficial for the efficiency, it does complicate the heat exchanger network. For a closer look at the available heat from the SOFC system at relevant temperature intervals, table 4.10.

Interval	**Interval temperature** (°C)	**Availbe heat** (kW)
Afterburner outlet/fuel cell outlet	883	
Afterburner inlet	857	166
Air feed outlet	792	212
sCO_2 compressor outlet	70	21
Environment	30	78

Table 4.10: *Available heat from the SOFC system (base case, ΔT_{hex} =10 °C)*

Integrating both systems by a pinch analysis means that all heat available above the pinch temperature, the sCO_2 compressors outlet temperature, is transfered to the sCO_2 Brayton cycle. However, the vast majority of the heat is available at temperatures above the TIT (700 °C). Determining the mass flow through the sCO_2 not by a pinch analysis but simply by the heat available at intervals above the air feed outlet temperature could decrease the number of heat exchangers and flow splits considerably while only slightly less heat is transfered to the sCO_2 Brayton cycle. This is done by considering a simpler design approach. In this approach, the exhaust flow from the fuel cell is cooled down to such a degree that the outlet temperature of the afterburner is the minimal temperature difference above the air feed outlet temperature.

$$T_{aft,L} = T_{ca,E} + \Delta T_{hex,min} \tag{4.7}$$

Figure 4.36 shows the resulting heat exchanger network if this approach is applied to case I. A PFD and all the details can be found in section C.7.1

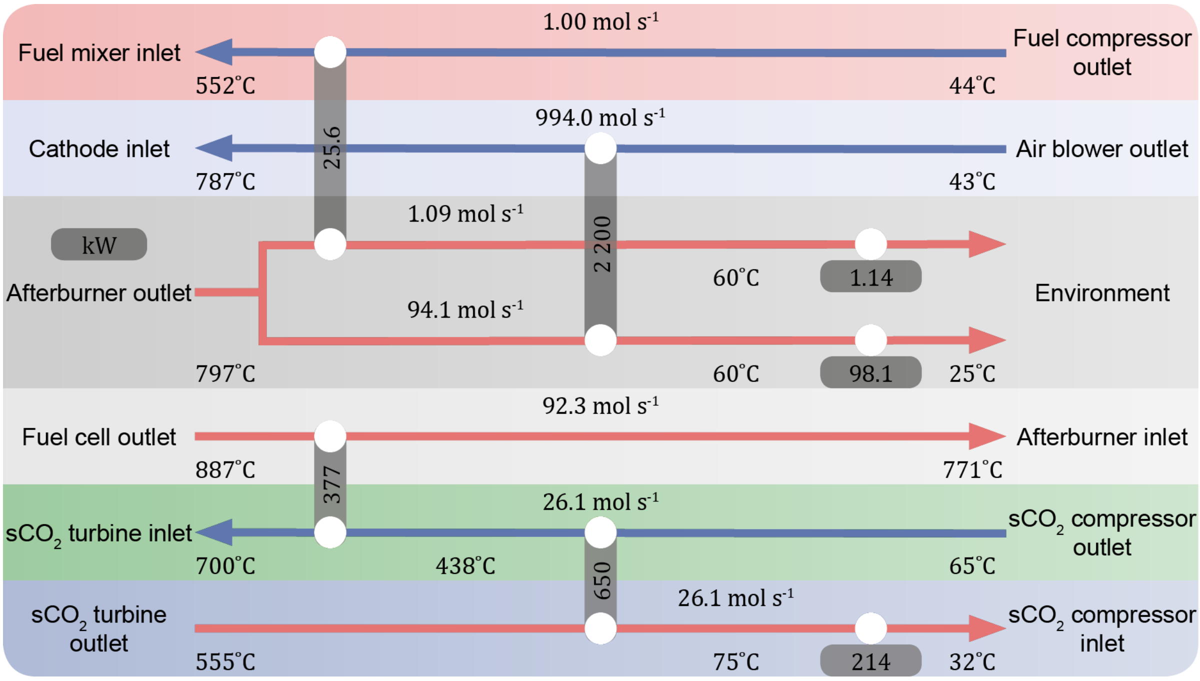

Figure 4.36: *Heat exchanger network (case VI.I: Case I simplified, ΔT_{hex} = 10 °C)*

The efficiency of the SSHS is not effected much compared to the former design approach, case I.

Fuel cell power	380 kW
Generator power	155 kW
Auxiliary power consumption	53 kW
Net AC system power	482 kW
LHV AC efficiency	60.01 %
Thermodynamic efficiency	69.05 %
Second law efficiency	58.90 %
Thermodynamic cycle efficiency	43.16 %
sCO_2 cycle flow	26.1 mol s^{-1}
Total PCHE area	29 m^2
Total STHE area	8109 m^2
Number of heat exchangers	5

Table 4.11: *Key performance data (case VI.I: Case I simplified, ΔT_{hex} = 10 °C)*

However, the size of the STHEs, is. This is because the temperature difference in the air preheater has become smaller, resulting in a significantly larger air preheater. A full comparison of all simplified cases is made in section 4.8.

4.6.2. Case VI.II: Simplified recompression cycle

The exact same approach as in case VI.I can be applied to case II. The simplified design is evaluated for a minimal temperature difference of 10 °C. See section C.7.2 for the details on case VI.II.

4.6.3. Case VI.III: Simplified Cathode recirculation

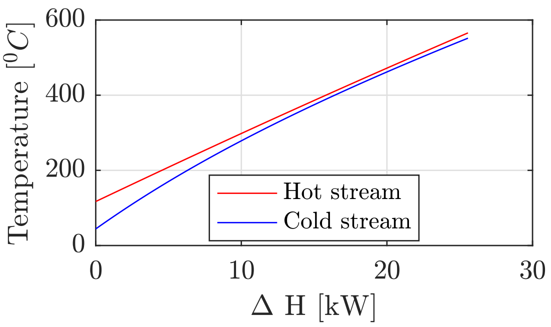

Figure 4.37: *Temperature-enthalpy diagram of the fuel preheater (case VI.III: Case III simplified, ΔT_{hex} =10 °C,$r_{cathode}$ =67.39%)*

A similar design strategy can be applied in the case of cathode recirculation. The difference is that the recirculation ratio has an effect on the outlet temperature of the air feed. Therefore, determining the outlet temperature of the afterburner is not as straightforward as in case VI.I and VI.II. An extra variable, the cathode recirculation ratio is added.

The outlet temperature of the afterburner is still determined by equation 4.7. A maximum recirculation ratio is found for the case where the minimal temperature difference (10 °C) in the fuel preheater can still be maintained. This maximum is found at a recirculation ratio of 67.39% for a minimal temperature difference of 10 °C. Figure 4.37 shows the temperature-enthalpy diagram of the fuel preheater in this case.

Increasing the cathode recirculation ratio, increases the efficiency and decreases the STHE area,

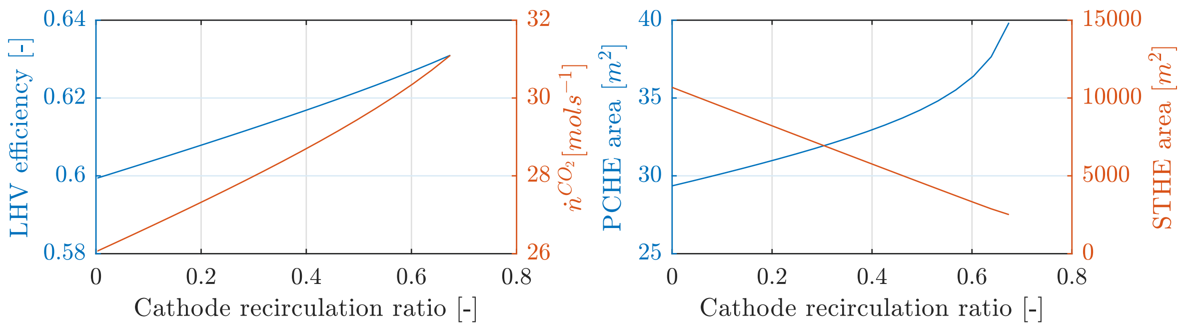

(a) *Efficiency and afterburner outlet temperature*

(b) *Heat exchanger area*

Figure 4.38: *Effect of the cathode recirculation ratio (case VI.III: Case III simplified, ΔT_{hex} =10 °C)*

see figure 4.38. The area of the PCHEs increases, but so does the the heat transferred to the sCO_2 Brayton cycle, reflected in the increasing mass flow. Therefore the choice has been made to further analyze this case for the maximum recirculation ratio, case VI.III. The heat exchanger network (figure C.22) is essentially the same as in case VI.I, except for differences in temperature and heat duties. All details on case VI.III can be found in section C.7.3.

4.6.4. Case VI.IV: Simplified recompression cycle + cathode recirculation

A very similar approach as used in case VI.III can be applied to case IV. The difference is that the maximum recirculation ratio is limited by another factor: It is limited by the temperature difference at the LT end of the heater. In the recompression cycle, the outlet temperature of the cold stream of the (HT) recuperator is higher than in the simple recuperative cycle. This limitation occurs at a lower recirculation ratio than the constraint of the temperature difference in the fuel preheater as in case VI.III, therefore the maximum recirculation ratio, at which this case is designed, is slightly lower, 65.16%, for a minimal temperature difference of 10 °C. See section C.7.4 for the details on case VI.IV.

4.6.5. Case VI.V: Simplified heat recovery steam generator

In this case all steam is supplied by a HRSG. Consequently, no anode gas is recirculated and the outlet temperature of the fuel feed is that of the reformer.

Considering this and the fact that steam has to be heated, means that if the afterburner outlet temperature was determined by equation 4.7, the flue gas would be unable to supply the heat to the fuel- air and steam feed without temperature crossovers occurring. So a higher outlet temperature of the afterburner is required to make the system feasible. This temperature difference is determined in such that the minimal temperature difference of 10 °C in the fuel- air and HRSG heaters is maintained.

This is the case if the outlet temperature of the afterburner is 822.93 °C. The details of this case, case VI.V, can be found in section C.7.5

4.7. Case VII: Directly coupled GT

In order estimate the potential of a sCO_2 Brayton cycle as a way to convert excess heat from a SOFC system, a comparison with other concepts is valuable. Table 1.2 shows the efficiencies of other concepts. These results vary considerably, as do the assumptions behind them. In order to make a fair comparison, a directly coupled GT hybrid system is developed to operate in the same conditions and with the same assumptions the sCO_2 Brayton cycle.

4.7.1. System setup

GT pressure ratio	3.5
Compressor isentropic efficiency	78%
Turbine isentropic efficiency	85%

Table 4.12: *Additional parameters case VII [25]*

The setup is based on the system by Yang *et al.* [25]. The fuel cell is pressurized and the exhaust gas is directly expanded through a turbine. Table 4.12 shows the additional parameters needed for this case. All the the other parameters and efficiencies used before are applied in this case to make a good comparison possible. Part of the cathodic air has to be recirculated. Without this, the TOT is lower than the outlet temperature of the air feed. The cathode recirculation ratio is chosen in such a way that the temperature difference at HT end of the air preheater is the imposed minimal temperature difference of 10 °C.

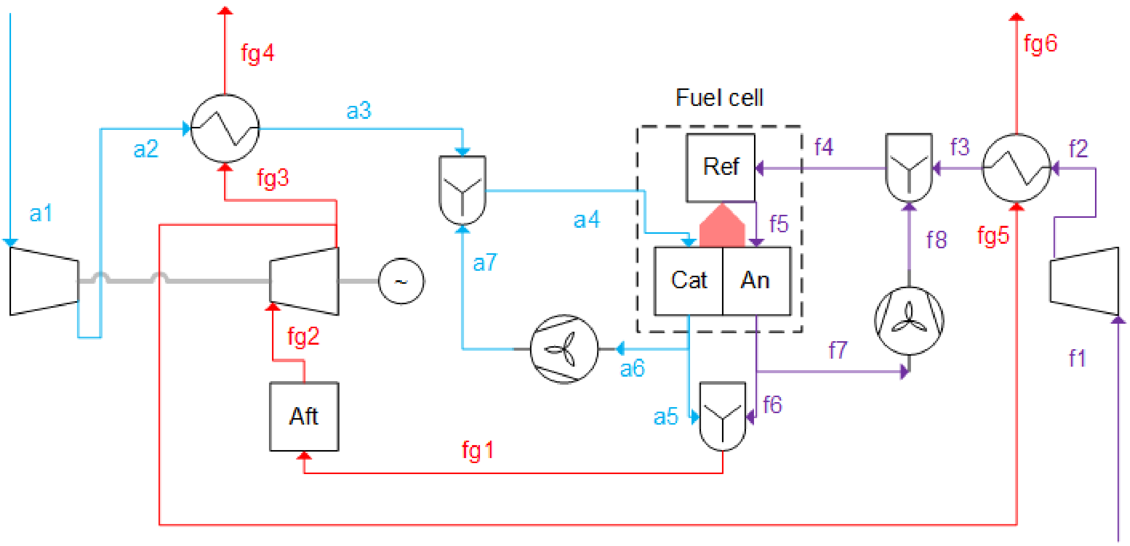

Figure 4.39: *Process flow diagram (Case VII: directly coupled GT)*

4.7.2. Performance analysis

The net power produced by this system is very similar to that of the basic setup. The exergy loss is mostly shifted from the heat exchanger network to the turbomachinery and exhaust. The PCHEs are not necessary in this system and the STHEs are smaller.

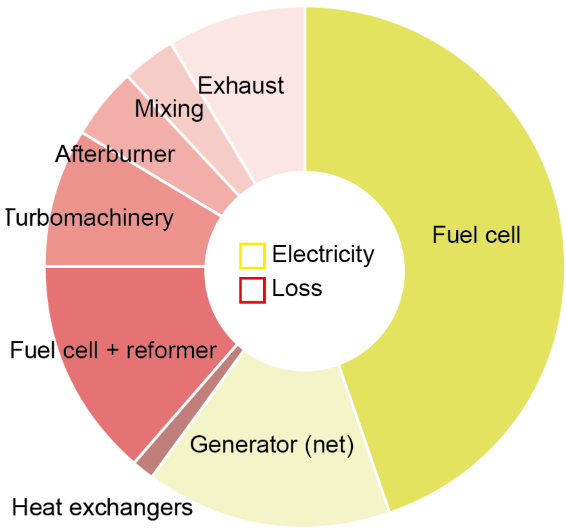

Figure 4.40: *Overall exergy analysis (directly coupled GT)*

Fuel cell power	373 kW
Turbine power	428 kW
Air compressor power	250 kW
Auxiliary power consumption	37 kW
Net system power	501 kW
LHV AC efficiency	62.38%
Thermodynamic efficiency	69.55%
Second law efficiency	60.17 %
Turbine pressure ratio	3.5
TIT	920 °C
Cathode recirculation ratio	55.27%
Total STHE area	2961 m^2

Table 4.13: *Key performance data (Case VII: Directly coupled GT)*

Further analysis of this setup is outside of the scope of this study. It only serves as a reference case to compare the different SOFC-sCO_2 Brayton cycle hybrid system setups.

4.8. Comparison

All cases are compared on their efficiency, number of heat exchangers and heat exchanger area of both types, PCHE and STHE. Three effects are compared. First, the two design approaches of the heat exchanger network are compared, comparing the simplified approach to the pinch analysis. Secondly, the effects of changes to the SOFC system are compared, recirculation of cathodic air and steam supply by a HRSG. Thirdly, the performance of the simple recuperative cycle is compared to the recompression cycle. Finally, the best cases are compared to the reference case, case VII: Directly coupled GT. An overview of all cases can be found in table C.56.

Only cases where configuration A applies are evaluated in this section because A has come out as being the best configuration. This means that case II.B, case III.B to III.D and case IV.B to IV.E are not considered in this section.

Figure 4.41 compares the design approaches of the basic setup, case I and VI.I. The efficiency

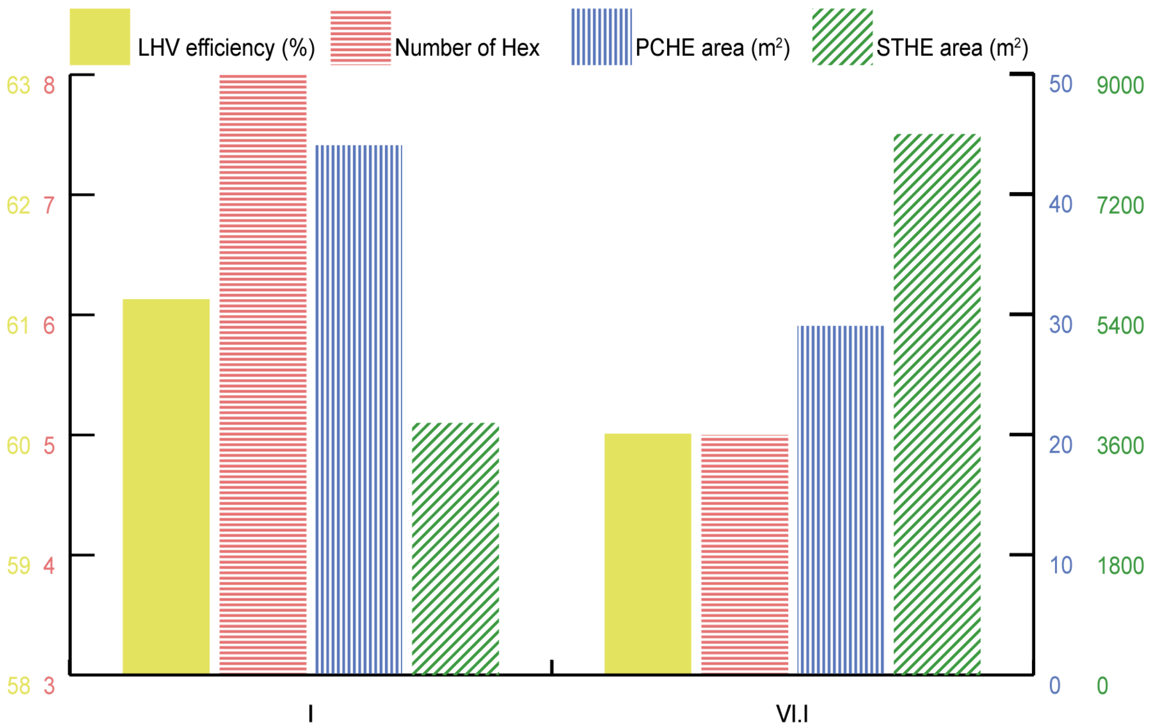

Figure 4.41: *Comparison of design approaches of the heat exchanger network (case I and case VI.I)*

decreases slightly when a simpler design approach (case VI.I) is applied, since less heat is transfered to the sCO_2 Brayton cycle. In the simplified approach, two less heaters for the supplying heat to the sCO_2 are used and one less air preheater. This results in a considerably simpler design and three heat exchangers less. The total area of the PCHEs is smaller in the simpler approach because less heat is transfered to the sCO_2 and the driving force in the heaters is also larger. The total size of the STHEs more than doubles. In the simpler approach, the temperature difference at the HT end of the air preheater is only 10 °C, compared to 100 °C in the design of case I. This much smaller driving force, combined with the large heat required to preheat the air, leads to much larger total area of STHE.

This shows that designing a heat exchanger network along a pinch analysis instead of a *simple* approach does not only improve efficiency, albeit slightly, but it also greatly reduces the size of the heat exchangers. The increased complexity of the system seems to be worth it, considering the general improvement of the system.

All other cases show a similar trend when compared to their simplified counterparts. The efficiency decreases slightly, the design is simpler but the size of the STHE increases drastically. These increases in the STHE area are less significant in the cases where cathode recirculation is applied. In these cases, the heat duty of the air feed has significantly decreased. So while the relative change in the size of the STHE is the same, the actual impact on the system is less significant.

Figure 4.42 compares the performance of the simple recuperative cycle, case I, to the recompression

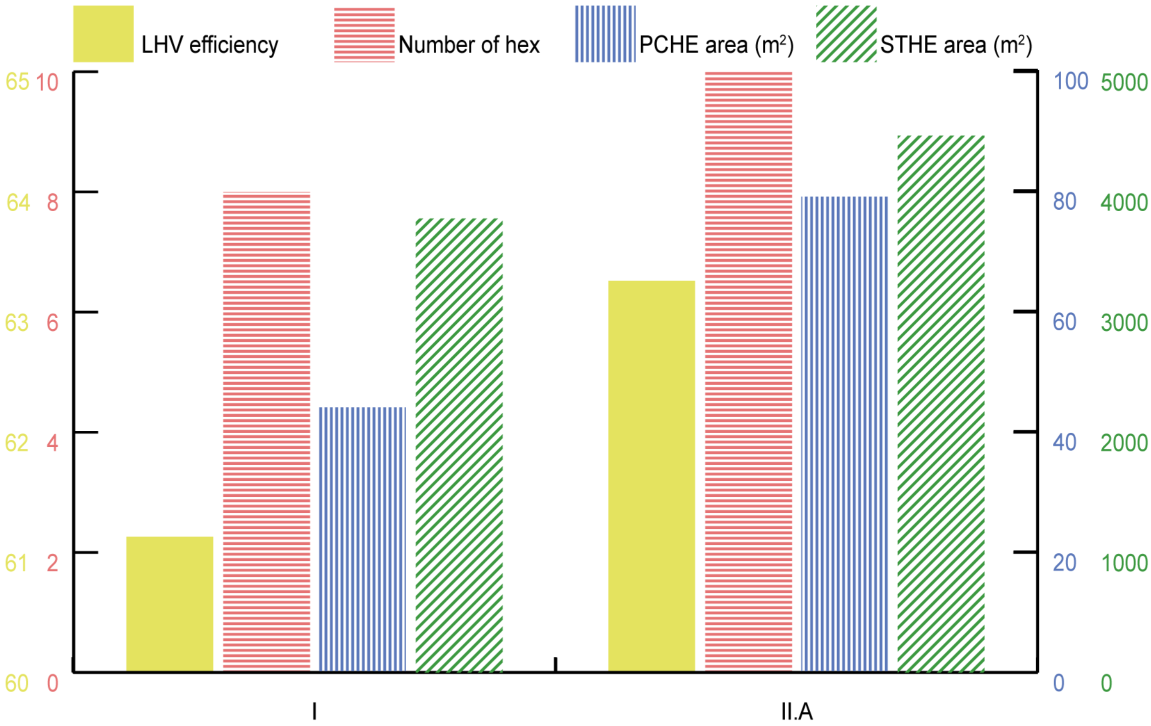

Figure 4.42: *Comparison of sCO_2 Brayton cycle setups (case I and II.A)*

cycle, case II.A, as part of the hybrid system. The recompression cycle converts heat more efficiently into work, therefore the efficiency of the system also increases. This is still the case even though the minimal temperature difference in case II.A (15 °C) is higher than in case I (10 °C) [9]. An additional recuperator is necessary in the recompression cycle, increasing the area of the PCHEs. Furthermore, the higher pinch temperature associated with the outlet of HTC makes it that an additional fuel preheater is required. Overall, this increases the total number of heat exchangers by two. The higher pinch temperature also reduces the driving force in the air preheaters, resulting in a larger area of STHEs.

So, a recompression cycle does not only have an effect on the equipment of the sCO_2 Brayton cycle itself, it also complicates and increases the size of the heat exchangers of the SOFC system. Efficiency is increased, but not by as much as when the sCO_2 operates as a standalone system. After all, most power is still produced by the SOFC system and the efficiency of the sCO_2 Brayton cycle only has an effect on the conversion of the excess heat.

Similar differences are observed when comparing the recompression cycle to the simple recuperative cycle in combination with cathode recirculation. In the simplified design approach, the number of heat exchangers required is only increased by one and the size of the fuel- and air preheaters is not affected.

Figure 4.43 compares two adjustments of the SOFC system to the basic setup.

Cathode recirculation, case III.A, increases the performance of the system. More heat can be transferred to the sCO_2 Brayton cycle. The reduction of the oxygen pressure in the fuel cell is limited and the performance of the fuel cell is only very slightly affected. Therefore cathode recirculation increases the efficiency of the hybrid system quite significantly. Furthermore, one instead of two air preheaters are necessary, making the heater exchanger network simpler. However, recirculating cathodic air does require the outlet flow of the cathode to be split,a high temperature blower and large mixer, complicating

[9]Case II is evaluated at a higher minimal temperature difference in order to avoid the complications associated with a lower minimal temperature difference, see section 4.2

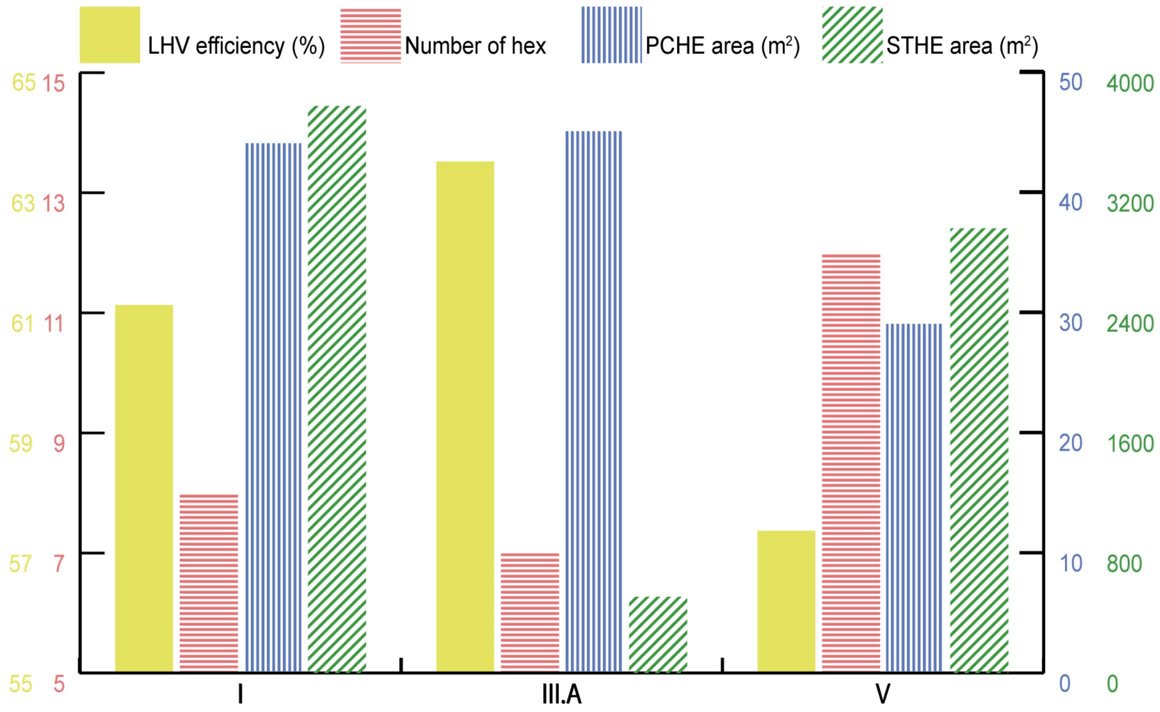

Figure 4.43: *Comparison of changes to the SOFC system (case I, III.A and V)*

the system. The smaller air flow does not only decrease the number of air preheaters, it also drastically decreases its size, which is reflected in a much smaller area of STHE. The total area of PCHE is barely affected.

In case of cathodic recirculation in combination with the recompression cycle, similar changes are observed. A difference is that the heat exchanger that *cut out* when comparing case IV.A to case II, is the LT fuel preheater. A much smaller and therefore less significant heat exchanger than the large air preheaters.

Feeding steam through a HRSG does not only complicate the system, it also drastically decreases its efficiency. Anode recirculation is no longer applied, decreasing the fuel consumption in the fuel cell, decreasing its power output and heat production. This does mean that less air is needed to cool the fuel cell, reflected in smaller STHEs. Furthermore, less heat is available for the sCO_2 cycle since heat must be supplied to the HRSG. Also, the water concentration in the flue gas increases, *trapping* heat in the steam, only making it available at temperatures below the dew temperature. Therefore less heat can be transferred to the sCO_2 Brayton cycle, decreasing the performance of the hybrid system even more. As a result, the area of the PCHE also decreases.

Three cases are considered to perform the best and are compared with the directly coupled GT. Firstly, the case with highest efficiency, case IV.A. It combines two favorable effects, cathode recirculation and the recompression cycle. It should be noted that case VI.IV, table C.56, shows an even higher efficiency. This case, VI.IV, is the simplified version of case IV, evaluated at a lower minimal temperature difference (10 °C) than case IV.A (15 °C) and it therefore has a slightly higher efficiency. If evaluated at a minimal temperature difference of 15 °C however, the efficiency of case VI.IV would be lower than that of case IV.A. Furthermore, the area of the STHEs is significantly higher in case VI.IV.

Secondly, case III.A: Cathode recirculation. This case shows a relatively high efficiency and the smallest area of STHEs and a relatively small area of PCHEs.

Thirdly, the case with the least heat exchangers, case VI.III, is chosen. It has the same amount of heat exchangers as case VI.I but a higher efficiency and a much smaller area of STHEs.

Figure 4.44 shows that the different setups of the SSHS have a higher efficiency compared to the directly coupled GT. This comes at a price though. The total number of heat exchangers increases

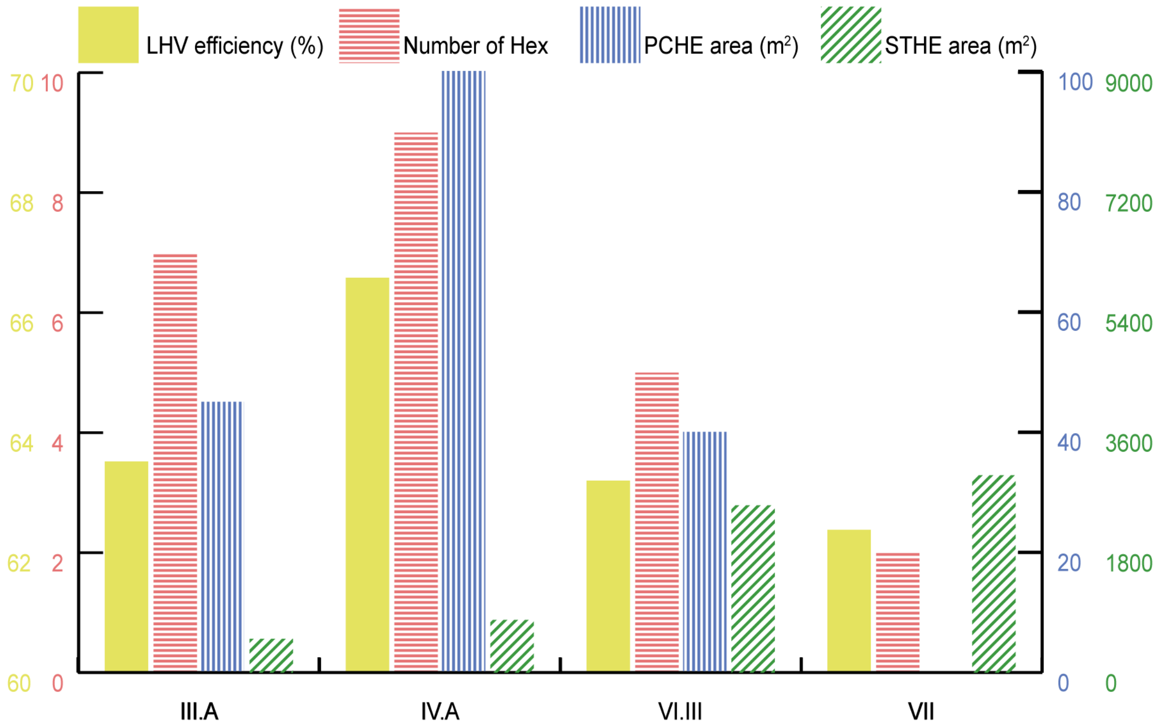

Figure 4.44: *Comparison of selected cases (case III.A, IV.A and VI.III) with a directly coupled GT (case VII)*

significantly and a PCHE is necessary. The size of the STHE mainly depends on the cathode recirculation ratio, since this has a significant effect on the air feed. It should be noted that case VII is not optimized like the the other cases since it only serves as a reference.

5 Conclusion and recommendations

5.1. Conclusion

This study has explored several design concepts of a SOFC- sCO_2 Brayton cycle hybrid system. All concepts show efficiencies in the same range, but differ quite significantly in the design and total size of the heat exchanger network. Designing a SSHS is not simply a matter of picking the setup with the highest efficiency. It is a trade off between system complexity, size of the heat exchangers and system efficiency.

Designing a SSHS along the line of a pinch analysis or a simpler approach illustrates this trade off. With more knowledge of practical operation and components cost and optimized design can be found.

The differences between the cases are mainly in the design and size of the heat exchangers, less in their efficiency. The recompression cycle clearly demonstrates this. Applying it does not only add a recuperator and compressor to the system, it complicates the SSHS as a whole.

Adding a HRSG makes the system less efficient and more complex. It is clearly more attractive to supply steam by anode recirculation.

Cathode recirculation clearly is preferable from a thermodynamic point of view as well from the point of view of the number and size of heat exchangers. However, it does require a blower at high temperatures and large mixer.

The best setups, case III.A, IV.A and VI.III, all involve cathode recirculation. Depending on which design criteria are most important, one of these setups should be considered. For the highest efficiency, case IV.A: Recompression cycle + cathode recirculation, is the best option. For the smallest heat exchangers, case III.A: Simple recuperative cycle + cathode recirculation, is the best. For a relatively simple system, a simplified design approach to this case, case VI.III, is the best option.

Compared to a more simple, directly coupled GT, the best setups of the SSHS show better efficiencies. Keeping in mind that the case for the directly coupled GT is not optimized, it can be concluded that the efficiency of the SSHS is at least comparable to that of a directly coupled SOFC-GT hybrid system and potentially better. But, as mentioned, this comes at a cost in the form of a complex system of heat exchangers.

For an indirectly coupled system, such as the SSHS, this is remarkable since these systems are generally less efficient than directly coupled systems. The advantage of indirectly coupled systems is that in general these are easier to operate [19]. If this is the case for the sCO_2 Brayton cycle is not clear yet. The high operating pressures of the sCO_2 Brayton cycle, the not so straightforward design of the heat exchanger network, the required mixers and necessary high temperature blowers involved make it hard to judge if a sCO_2 Brayton cycle would indeed be easier to operate than a directly coupled GT.

Furthermore, all components in this system, the SOFC, the sCO_2 turbomachinery and the PCHE, are all relatively undeveloped and expensive technologies. The potential advantages of this system might not outweigh the probably high costs.

Taking everything into account, the SSHSs high efficiency comes at a cost. A consideration one will have to make carefully. Its potential lies in the fact that it is an indirectly coupled system with the high efficiencies of a directly coupled system. It therefore benefits from a SOFC system operating at atmospheric pressure and a potentially easier system to operate.

5.2. Recommendations

Since the main potential of this system is in its potential ease of operation compared to a directly coupled system, this is what future research and practice should be focused on. Practical feasibility of cathode recirculation and off-design operation should be investigated in order to determine if a SSHS has a future.

Off-design operation is especially important when taking into consideration that increased production by renewable energy sources requires more flexibility from other sources. It is important to analyze the turbomachinery in part-load operations, thermal management of the fuel cell and the possibility to easily start and stop the system completely.

As in any scientific model, assumptions are of key importance. Conclusions drawn in this study might not be valid with different assumptions. It is therefore recommended to analyze the sensitivity of the system to the basic assumptions.

Bibliography

[1] M. J. Moran, *Principles of engineering thermodynamics*, 7th ed. (Wiley, Hoboken, N.J :, 2012).

[2] P. Breeze, *Pushing the steam cycle boundaries,* Power Engineering International (2012).

[3] R. K. Bhargava, M. Bianchi, A. De Pascale, G. Negri di Montenegro, and A. Peretto, *Gas turbine based power cycles - a state-of-the-art review,* in *Challenges of Power Engineering and Environment: Proceedings of the International Conference on Power Engineering 2007*, edited by K. Cen, Y. Chi, and F. Wang (Springer Berlin Heidelberg, Berlin, Heidelberg, 2007) pp. 309–319.

[4] J. Harinck, G. J. Witkamp, and P. Colonna, *Super- and Transcritical Fluid Expansions for Next-Generation Energy Conversion Systems*, Thesis, Delft University of Technology (2010).

[5] V. Dostal, M. Driscoll, and P. Hejzlar, *A Supercritical Crabon Dioxide Cycle for Next Generation Nuclear Reactors*, Thesis, Massachusetts Institute of Technology (2004).

[6] Y. Ahn, S. J. Bae, M. Kim, S. K. Cho, S. Baik, J. I. Lee, and J. E. Cha, *Review of supercritical co2 power cycle technology and current status of research and development,* Nuclear Engineering and Technology **47**, 647 (2015).

[7] J. S. Bahamonde Noriega, P. Colonna, and B. J. Boersma, *Design method for s-CO2 gas turbine power plants: Integration of thermodynamic analysis and components design for advanced applications*, Thesis, Delft University of Technology (2012).

[8] F. A. Al-Sulaiman and M. Atif, *Performance comparison of different supercritical carbon dioxide brayton cycles integrated with a solar power tower,* Energy **82**, 61 (2015).

[9] T. Neises and C. Turchi, *A comparison of supercritical carbon dioxide power cycle configurations with an emphasis on csp applications,* Energy Procedia **49**, 1187 (2014).

[10] M. Kulhanek and V. Dostal, *Supercritical carbon dioxide cycles thermodynamic analysis and comparison,* in *Supercritical CO2 Power Cycle Symposium, Boulder, CO, May* (2011) pp. 24–25.

[11] C. Turchi, *10 MW Supercritical CO2 Turbine Test*, Report DE-EE0002589 United States 10.2172/1117025 NREL English (; National Renewable Energy Laboratory (NREL), Golden, CO (United States), 2014).

[12] J. Larminie and A. Dicks, *Fuel cell systems explained*, 2nd ed. (J. Wiley, Chichester, West Sussex :, 2003).

[13] S. Sui and G. H. Xiu, *Fuels and fuel processing,* in *High-Temperature Solid Oxide Fuel Cells for the 21st Century*, edited by M. Kendall (Academic Press, Boston, 2016) Book section 14, pp. 461–495, 2nd ed.

[14] EG& G Technical Services, Inc., *Fuel cell handbook*, 7th ed. (BusinessTechnology Books, 2004).

[15] N. Q. Minh, *Cell and stack design, fabrication and performance,* in *High-Temperature Solid Oxide Fuel Cells for the 21st Century*, edited by M. Kendall (Academic Press, Boston, 2016) Book section 8, pp. 255–282, 2nd ed.

[16] K. Hassmann, *SOFC Power Plants, the Siemens-Westinghouse Approach,* Fuel Cells **1**, 78 (2001).

[17] Bloom Energy, *Bloom Energy,* (2016).

[18] F. Calise, M. Dentice d' Accadia, L. Vanoli, and M. R. von Spakovsky, *Full load synthesis/design optimization of a hybrid sofc–gt power plant,* Energy **32**, 446 (2007).

[19] A. Buonomano, F. Calise, M. D. d'Accadia, A. Palombo, and M. Vicidomini, *Hybrid solid oxide fuel cells–gas turbine systems for combined heat and power: A review,* Applied Energy **156**, 32 (2015).

[20] X. Zhang, S. H. Chan, G. Li, H. K. Ho, J. Li, and Z. Feng, *A review of integration strategies for solid oxide fuel cells,* Journal of Power Sources **195**, 685 (2010).

[21] S. H. Chan, H. K. Ho, and Y. Tian, *Modelling of simple hybrid solid oxide fuel cell and gas turbine power plant,* Journal of Power Sources **109**, 111 (2002).

[22] S. H. Chan, H. K. Ho, and Y. Tian, *Multi-level modeling of sofc–gas turbine hybrid system,* International Journal of Hydrogen Energy **28**, 889 (2003).

[23] T. W. Song, J. L. Sohn, J. H. Kim, T. S. Kim, S. T. Ro, and K. Suzuki, *Performance analysis of a tubular solid oxide fuel cell/micro gas turbine hybrid power system based on a quasi-two dimensional model,* Journal of Power Sources **142**, 30 (2005).

[24] J. Jia, A. Abudula, L. Wei, and Y. Shi, *Performance comparison of three solid oxide fuel cell power systems,* International Journal of Energy Research **37**, 1821 (2013).

[25] W. J. Yang, S. K. Park, T. S. Kim, J. H. Kim, J. L. Sohn, and S. T. Ro, *Design performance analysis of pressurized solid oxide fuel cell/gas turbine hybrid systems considering temperature constraints,* Journal of Power Sources **160**, 462 (2006).

[26] A. Arsalis, *Thermoeconomic modeling and parametric study of hybrid sofc–gas turbine–steam turbine power plants ranging from 1.5 to 10 mwe,* Journal of Power Sources **181**, 313 (2008).

[27] S. K. Park and T. S. Kim, *Comparison between pressurized design and ambient pressure design of hybrid solid oxide fuel cell–gas turbine systems,* Journal of Power Sources **163**, 490 (2006).

[28] E. Facchinetti, D. Favrat, and F. Marechal, *Design and optimization of an innovative solid oxide fuel cell–gas turbine hybrid cycle for small scale distributed generation,* Fuel Cells **14**, 595 (2014).

[29] J. Leeper, *220 kWe solid oxide fuel cell/microturbine generator hybrid proof of concept demonstration report*, 3rd ed., Consultant report (California Energy Commission) (California Energy Commission, [Sacramento, Calif.] :, 2001).

[30] T. Gengo, Y. Kobayashi, Y. Ando, N. Hisatome, T. Kabata, and K. Kosaka, *Development of 200kW class SOFC combined cycle system and future view,* Mitsubishi Heavi Industrie, Ltd. Technical Review **45** (2008).

[31] T.-H. Lim, R.-H. Song, D.-R. Shin, J.-I. Yang, H. Jung, I. C. Vinke, and S.-S. Yang, *Operating characteristics of a 5 kw class anode-supported planar sofc stack for a fuel cell/gas turbine hybrid system,* International Journal of Hydrogen Energy **33**, 1076 (2008).

[32] S. J. Bae, Y. Ahn, J. Lee, and J. I. Lee, *Various supercritical carbon dioxide cycle layouts study for molten carbonate fuel cell application,* Journal of Power Sources **270**, 608 (2014).

[33] E. Lemmon, M. Huber, and M. McLinden, *NIST Standard Reference Database 23, Version 9.0,* (2010).

[34] M. W. Chase, S. National Institute of, and Technology, *NIST-JANAF thermochemical tables* (American Chemical Society ; American Institute of Physics for the National Institute of Standards and Technology, [Washington, D.C.]; Woodbury, N.Y., 1998) (U.S.).

[35] K. Ahmed and K. Föger, *Fuel processing for high-temperature high-efficiency fuel cells,* Industrial & Engineering Chemistry Research **49**, 7239 (2010).

[36] P. V. Aravind, T. Woudstra, N. Woudstra, and H. Spliethoff, *Thermodynamic evaluation of small-scale systems with biomass gasifiers, solid oxide fuel cells with ni/gdc anodes and gas turbines,* Journal of Power Sources **190**, 461 (2009).

[37] U. Bossel and L. Dubal, *Facts & figures : final report on SOFC data* (Swiss Federal Office of Energy, Operating Agent Task II, Berne, 1992).

[38] N. F. Bessette II, W. J. Wepfer, and J. Winnick, *A mathematical model of a solid oxide fuel cell,* Journal of Electrochemical society **142**, 3792 (1995).

[39] R. Holyst and A. Poniewierski, *Thermodynamics for chemists, physicists and engineers,* (2012).

[40] S. Campanari and P. Iora, *Definition and sensitivity analysis of a finite volume sofc model for a tubular cell geometry,* Journal of Power Sources **132**, 113 (2004).

[41] A. O. Omosun, A. Bauen, N. P. Brandon, C. S. Adjiman, and D. Hart, *Modelling system efficiencies and costs of two biomass-fuelled sofc systems,* Journal of Power Sources **131**, 96 (2004).

[42] R. A. Bidkar, A. Mann, R. Singh, D. Sevincer, S. Cich, M. Day, C. D. Kulhanek, A. M. Thatte, A. M. Peter, D. Hofer, and J. Moore, *Conceptual Designs of 50MW_e and 450MW_e Supercritical CO_2 Turbomachinery Trains for Power Generation from Coal. Part 1: Cycle and Turbine,* (2016).

[43] R. A. Bidkar, G. Musgrove, M. Day, C. D. Kulhanek, T. Allison, A. M. Peter, D. Hofer, and J. Moore, *Conceptual Designs of 50MW_e and 450MW_e Supercritical CO_2 Turbomachinery Trains for Power Generation from Coal. Part 2: Compressors,* (2016).

[44] Y. Haseli, I. Dincer, and G. F. Naterer, *Thermodynamic modeling of a gas turbine cycle combined with a solid oxide fuel cell,* International Journal of Hydrogen Energy **33**, 5811 (2008).

[45] I. C. Kemp, *Pinch analysis and process integration : a user guide on process integration for the efficient use of energy*, 2nd ed. (Butterworth-Heinemann, Oxford :, 2007).

[46] G. Towler and R. K. Sinnott, *Chemical engineering design - principles, practice and economics of plant and process design,* (2013).

[47] Heatric, *Typical characteristics of diffusion-bonded heat exchangers,* (2017).

[48] J. E. Hesselgreaves, R. Law, and D. A. Reay, *Compact Heat Exchangers - Selection, Design and Operation*, 2nd ed. (Elsevier, 2017).

[49] T. Bowdery, *LNG applications of diffusion bonded heat exchangers,* (2006).

[50] K. Oyakawa, T. Shinzato, and I. Mabuchi, *The effects of the channel width on heat-transfer augmentation in a sinusoidal wave channel,* JSME international journal. Ser. 2, Fluids engineering, heat transfer, power, combustion, thermophysical properties **32**, 403 (1989).

[51] H. Song, *Investigation of a printed circuit heat exchanger for supercritical CO2 and water*, Thesis, Kansas State University (2007).

[52] A. F. Mills, *Heat transfer*, 2nd ed. (Prentice Hall, Upper Saddle River, N.J. :, 1999).

[53] Mathworks, *MATLAB,* (2016).

[54] P. Aguiar, D. Chadwick, and L. Kershenbaum, *Modelling of an indirect internal reforming solid oxide fuel cell,* Chemical Engineering Science **57**, 1665 (2002).

[55] P. Aguiar, C. S. Adjiman, and N. P. Brandon, *Anode-supported intermediate temperature direct internal reforming solid oxide fuel cell. i: model-based steady-state performance,* Journal of Power Sources **138**, 120 (2004).

[56] Asimptote, *Cycle-Tempo,* (2011).

[57] S. C. Singhal, *Advances in solid oxide fuel cell technology,* Solid State Ionics **135**, 305 (2000).

A

Examples

A.1. Pinch analysis

The example in this section is taken from Kemp [45].

This example considers four stream, two hot and two cold, with a constant heat capacity are considered. A minimal temperature difference of 10 °C is imposed. Table A.1 shows the streams and their specifics. Besides the actual temperature of the streams, an interval temperature of each stream is defined. For hot stream this is the actual temperature minus half of the minimum temperature difference, for cold stream half of the minimum temperature difference is added to the actual temperature. This is done to define intervals in which stream are able to exchange heat with one another.

Stream	CP(kW °C^{-1})	Actual temperature (°C)		Interval temperature (°C)	
		Inlet	Outlet	Inlet	Outlet
1 (hot)	3	170	60	165	55
2 (hot)	1.5	150	30	145	25
3 (cold)	2	20	135	25	140
4 (cold)	4	80	140	85	145

Table A.1: *Stream data (pinch analysis example)*

Next, the problem is split into intervals based on the interval temperatures of each stream. For each interval a net enthalpy change is determined. This is positive in the case that the heat supplied by cooling down the hot streams is greater than the heat required by the cold stream in that specific interval. Excess heat from higher temperature intervals can be transfered to lower temperature intervals.

Interval temperature (°C)	Streams	ΔH^{int} (kW)	$\Sigma\Delta H^{int}$ (kJ)	Shifted $\Sigma\Delta H^{int}$ (kJ)
165				+20
145	1	+60	+60	+80
140	1+2-4	+2.5	+62.5	+82.5
85	1+2-3-4	-82.5	-20	0
55	1+2-3	+75	+55	+75
25	2-3	-15	+40	+60

Table A.2: *Interval data (pinch analysis example)*

Adding this excess heat produces the fourth column in table A.2. The interval from 140 to 85 °C still has a deficit of 20 kW, making the system infeasible. In order to make the system feasible, a hot utility of 20 kW must be added to the system, column 5. This produces a surplus of energy in every interval except one, which is where the pinch is, 85 °C in this case. The surplus in the lowest interval represents cooling that must be supplied by an external source.

The resulting pinch diagram of the system, figure A.1, illustrates the changing heat capacities at the interval temperatures and the pinch temperature, where the imposed minimal temperature difference of 10 °C applies. The cold and hot utility are the horizontal difference between the hot and cold temperature-enthalpy curves.

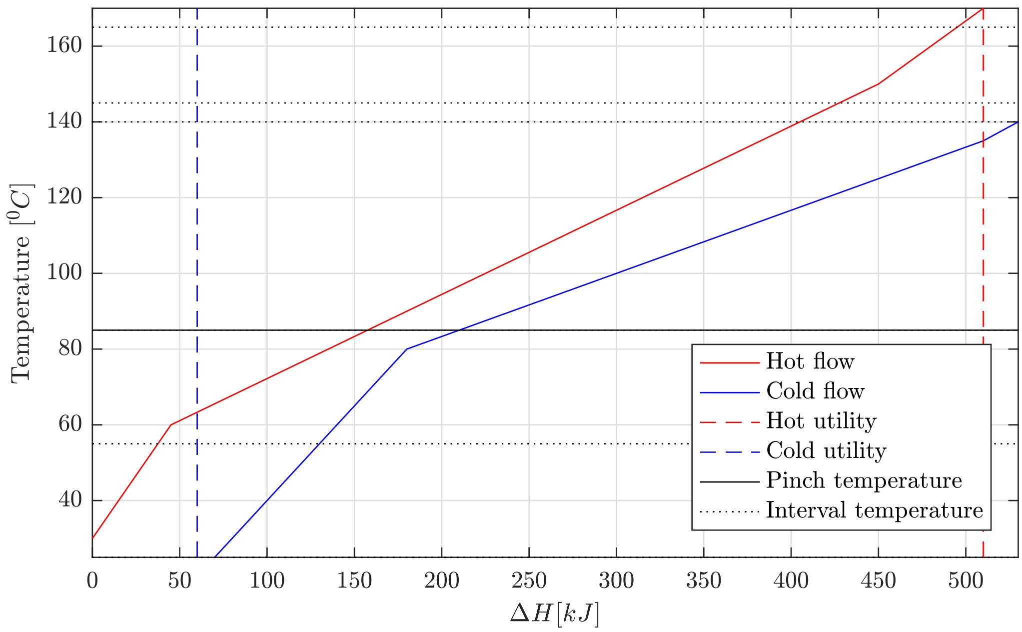

Figure A.1: *Pinch diagram (pinch analysis example)*

The system can now split in two, one subsystem above the pinch and one below, figure A.2. From this picture the hot need for a hot and cold utility can be confirmed as well. A pinch analysis does not

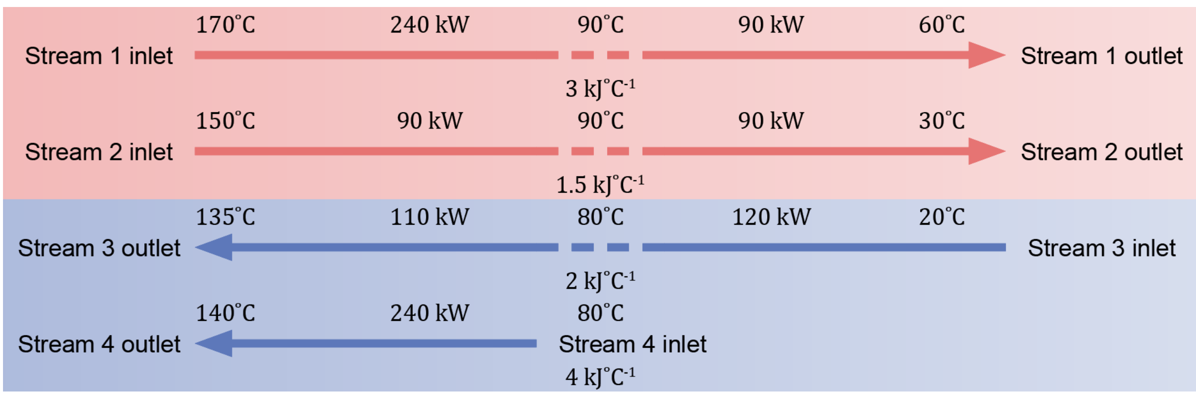

Figure A.2: *Heat flows (pinch analysis example)*

lead to a design of a heat exchanger network. It does however provide a very useful starting point for a design. It minimizes the need for hot and cold utilities, thus maximizing thermodynamic efficiency. The choice of the minimal temperature difference is a trade off between thermodynamic efficiency and size of the heat exchangers/cost.

Contrary to this example, the problems analyzed in this work differ on a few points. Firstly, the streams do not have constant heat capacities. As a consequence, the pinch temperature does not always coincide with an interval where a flow is begins or ends as is the case for constant heat capacities. Therefore, the problem should be evaluated at a more regular temperature interval than only the shifted in- and outlet temperature of each stream.

Secondly, the mass flow through the sCO_2 Brayton is an unknown variable in the problem that is to be solved by the pinch analysis. The same principles apply, but the analysis must be done in a different order of steps.

Finally, in order to solve the problem with this unknown variable, an additional constraint must be imposed. No external heat utility is possible.

B
Numerical discretization

B.1. Ohmic resistance

Consider figure 2.5, representing the equivalent electrical circuit of a tubular fuel cell. In this figure, 6 cells, are depicted. Since the tubular cell is symmetrical, the complete tube has 12 cells. In order to estimate the ohmic resistance correctly however, the grid needs to be refined.

Figure B.1 shows the effect of the number of cells on the resistance on the left axis. On the right axis, the relative change compared to a the previous step in number of cells. From this figure it becomes clear

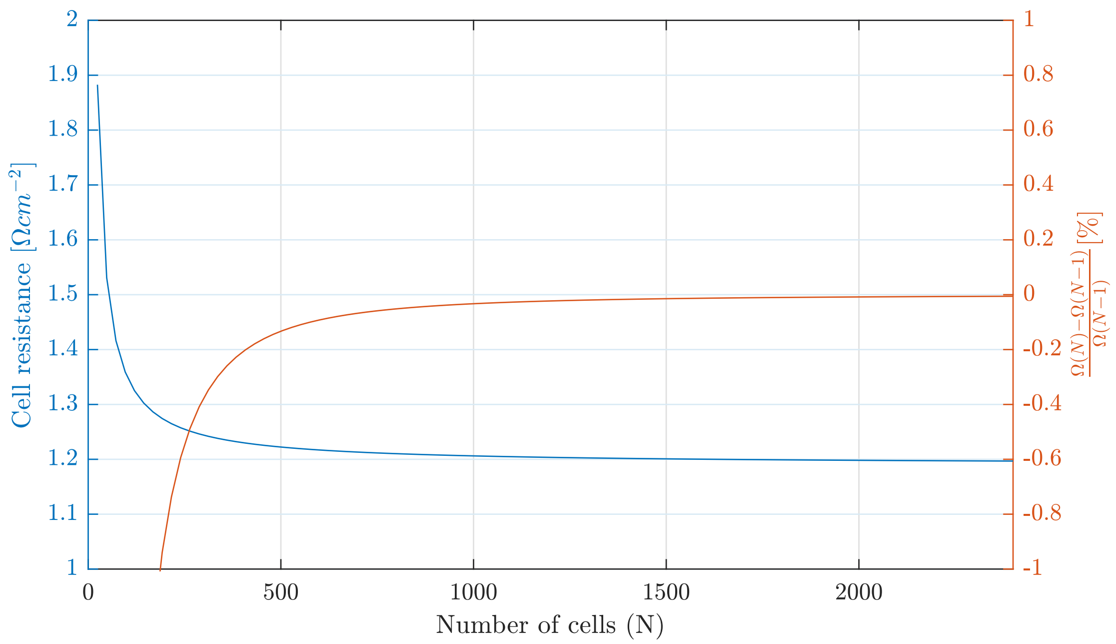

Figure B.1: *Numerical discretization of the equivalent electrical circuit (T_{FC} =836.85 °C)*

that the ohmic resistance converges for a certain number of cells in the discretization. This number of cells, 2400, will be used in all calculations in this work.

B.2. Heat exchanger area

Consider figure 2.7, representing the numerical discretization of a heat exchanger. The more cells are used in the discretization, the more accurate the calculation will be. Especially near the critical this is important, since this is the point where thermodynamic properties change the most.

The effect of the number of cells on the area of the heat exchanger will be evaluated for the cooler of the sCO_2, because the hot flow in this heat exchanger is near the critical point. A temperature-enthalpy diagram of this heat exchanger can be found in figure 4.10b.

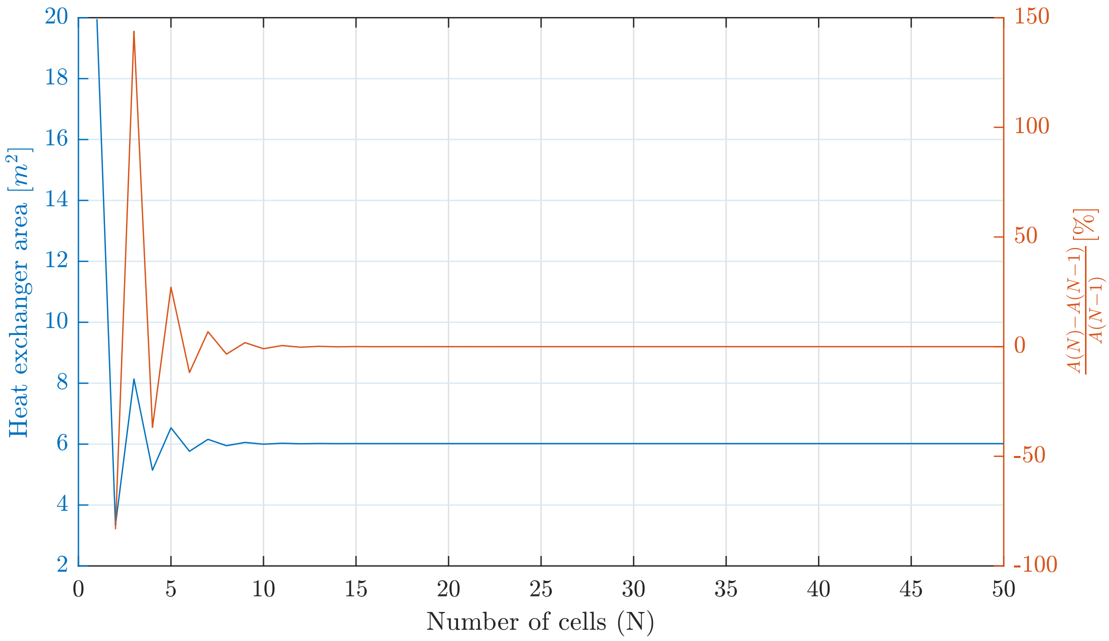

Figure B.2: *Numerical discretization of the heat exchanger area ($\dot{n}^{CO_2}$ =1 mol s^{-1})*

Figure B.2 clearly shows that the area of the heat exchangers converges from about a number of cells of 10. To be on the safe side, 20 cells is chosen as an appropriate number of cells to achieve an accurate result.

C

Additional figures and tables

C.1. General additional tables and figures

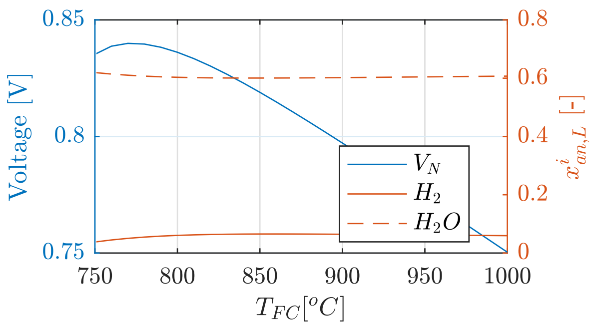

(a) *Nernst voltage and concentrations*

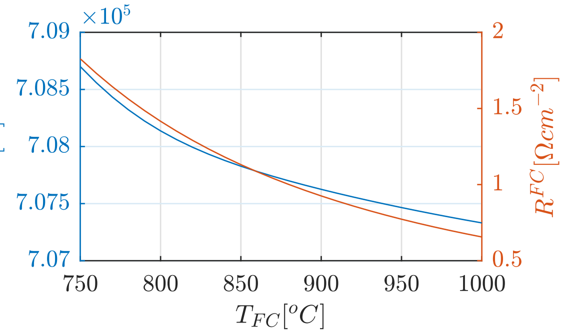

(b) *Total current and ohmic resistance*

Figure C.1: *Effect of the operating fuel cells operating temperature*

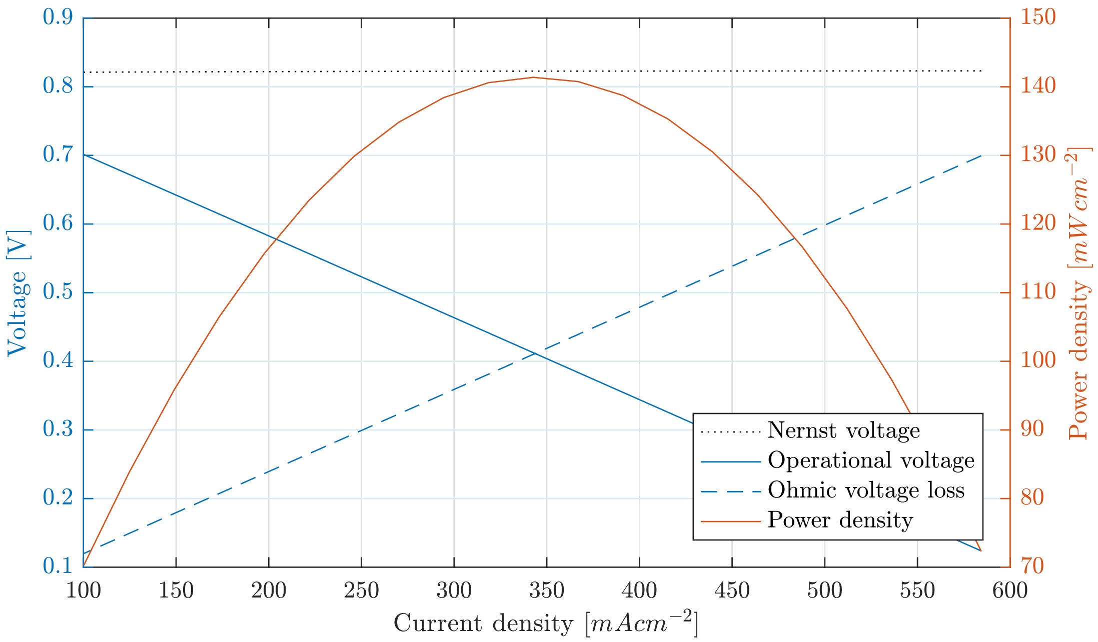

Figure C.2: *IV-plot (T_{FC} =836.85 °C)*

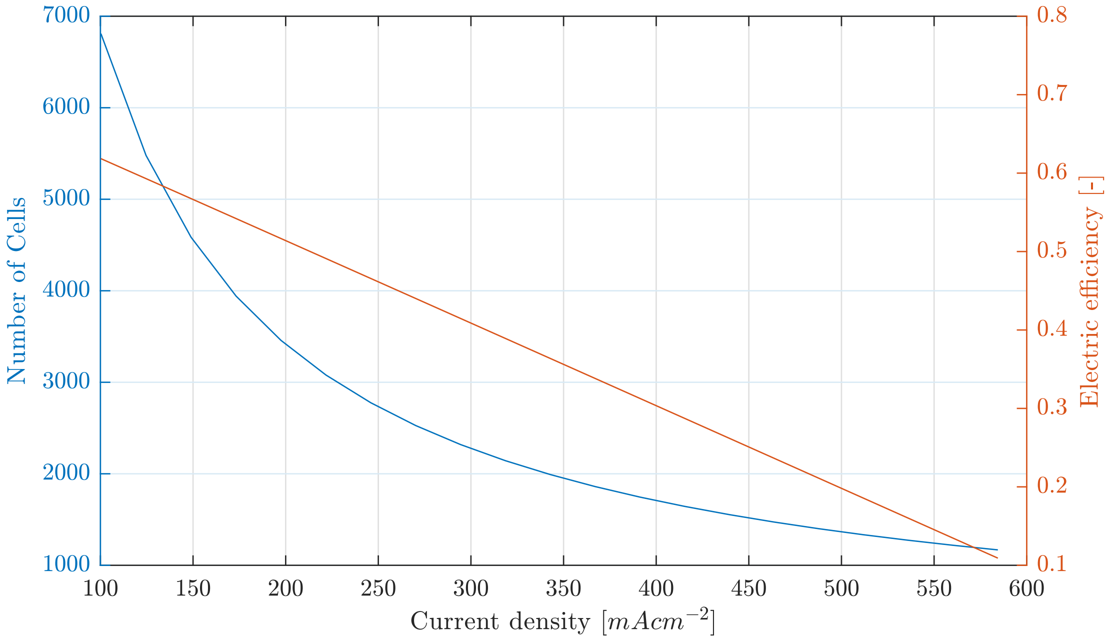

Figure C.3: *Number of cells and fuel cell efficiency (T_{FC} =836.85 °C)*

C.2. Case I: Basic setup (4.1)

The points referred to in table C.1 to C.4 refer to the PFD in figure 4.7.

Point	$\dot{n}$ (mol s^{-1})	P (bar)	T (°C)	**Exergy**(kW)		
				Thermo mechanical	Chemical	Total
f1	1.00	1.01325	25.00	0	832	832
f2	1.00	1.2426	44.19	0.53	832	832.53
f3	1.00	1.2177	551.68	12.33	832	844.33
f4	3.85	1.2177	786.85	69.45	923.33	993.78
f5	5.8348	1.1568	786.85	77.07	1 141.3	1 218.3
f6	2.99	1.1106	886.85	57.52	100.21	157.73
f7	2.85	1.1106	886.85	54.77	95.43	150.20
f8	2.85	1.2177	912.82	57.96	95.43	153.39
a1	94.1	1.01325	25.00	0	0	0
a2	94.1	1.1804	42.59	37.00	0	37.00
a3	94.1	1.1659	512.78	608.55	0	608.55
a4	94.1	1.1568	786.85	1 180.4	0	1 180.4
a5	923	1.1106	886.85	1 376.5	0.04	1 376.5
fg1	95.3	1.1106	886.85	1 433.2	83.26	1 516.4
fg2	95.1	1.0883	861.63	1 367.1	83.26	1 450.3
fg3	18.21	1.0339	886.85	271.14	0.41	271.55
fg4	75.96	1.0339	886.85	1 131.1	1.71	1 132.8
fg5	0.95	1.0339	886.85	14.17	0.02	13.19
fg6	7.55	1.0255	554.89	53.31	0.17	53.48
fg7	86.62	1.0255	554.89	611.79	1.95	613.74
fg8	0.95	1.0138	47.79	0.02	0.02	0.05
fg9	7.66	1.0144	74.88	0.86	0.17	1.03
fg10	88.27	1.0138	50.82	2.83	1.95	4.78
c1	27.55	80.0000	32.00	260.98	554.09	815.07
c2	23.69	250.0000	64.88	249.52	476.33	725.84
c3	3.87	250.0000	64.88	40.73	77.76	118.49
c4	27.55	246.3185	512.71	617.11	554.09	1 171.2
c5	27.55	245.3762	646.27	749.20	554.09	1 303.3

c6	27.55	245.0000	700.00	805.85	554.09	1 359.9
c7	27.55	81.6327	554.89	589.72	554.09	1 143.8
c8	27.55	80.4048	74.88	274.20	554.09	828.28
w1	122.50	1.01325	25.00	0	0	0
w2	122.50	1.0339	25.00	0	0	0
w3	122.50	1.01325	49.58	8.86	0	8.86

Table C.1: *State points (case I: Base case)*

	Point	**Concentration**						
		CH_4	H_2	H_2O	CO	CO_2	O_2	N_2
Methane	f1-3	1	0	0	0	0	0	0
Fuel mix	f4	0.2614	0.0480	0.4444	0.0285	0.2177	0	0
Syngas	f5	0.0019	0.4941	0.1713	02380	0.0947	0	0
Anode outlet	f6-8	0.0019	0.0649	0.6005	0.0385	0.2942	0	0
Air	a1-4	0	0	0.0313	0	0.0003	0.2035	0.7649
Cathode outlet	a5	0	0.0319	0	0.0003	0	0.7801	0.1877
Fuel cell exhaust	fg1-2	0.0001	0.0020	0.0497	0.0012	0.0095	0.1818	0.7556
Flue gas	fg3-10	0	0	0.0519	0	0.0108	0.18084	0.7570
Carbon dioxide	c1-8	0	0	0	0	1	0	0
Water	w1-3	0	0	1	0	0	0	0

Table C.2: *Gas compositions (case I: Base case)*

	Inlet	**Outlet**	$\dot{W}/\dot{Q}$ (kW)	**Exergy destruction** (kW)	η_{ex} (%)
			SOFC		
Reformer	f4	f5	234.77		
Fuel cell	f5/a4	f6/a5	379.66		
Total	f4/a4	f6/a5		109.08	94.98
			sCO$_2$ Brayton cycle		
Turbine	c6	c7	207.74	8.39	96.12
Compressor	c1	c2	35.57	6.30	82.29
Generator			165.10	8.61	95.00
			BoP		
Air blower	a1	a2	48.54	11.54	76.23
Fuel blower	f1	f2	0.69	0.16	76.33
Water pump	w1	w2	0.006	0.002	75.00
Anode blower	f7	f8	3.40	0.21	93.70
Fuel mixer	f3/f8	f4	0	4.94	99.50
Exhaust mixer	f6/a5	fg1	0	17.80	98.85

Table C.3: *System components (case I: Base case)*

	Hot stream		**Cold stream**		$\dot{Q}$	$\dot{Ex}_D$	η_{ex}	$\dot{U}$	A
	Inlet	**Outlet**	**Inlet**	**Outlet**	(kW)	(kW)	(%)	(W m^{-2} °C^{-1})	(m^2)
					STHE				
Fuel preheater	fg5	fg8	f2	ff3	25.57	2.34	83.45	20	20.37
LT air preheater	fg7	fg10	a2	a3	1 349.9	37.41	93.86	20	3 127.4
HT air preheater	fg4	fg7-fg6	a3	a4	849.97	22.72	96.18	20	630.00
					PCHE				
LT heater	fg6	fg9	c3	c4	85.00	6.58	87.45	500	4.80
HT heater	fg3	fg6+fg7	c4	c5	203.75	10.43	92.68	500	3.53

Aft precooler	fg1	fg2	c5	c6	82.88	9.47	85.68	500	0.8257
Recuperator	c7	c8	c2	c4	687.65	34.54	89.05	754	23.97
Cooler	c8	c1	w2	w3	226.72	4.36	67.02	7 000	11.84

Table C.4: *Heat exchangers (case I: Base case)*

C.3. Case II: Recompression cycle(4.2)

C.3.1. Case II.A ($\Delta T_{hex} = 15\,^{\circ}\mathrm{C}$)

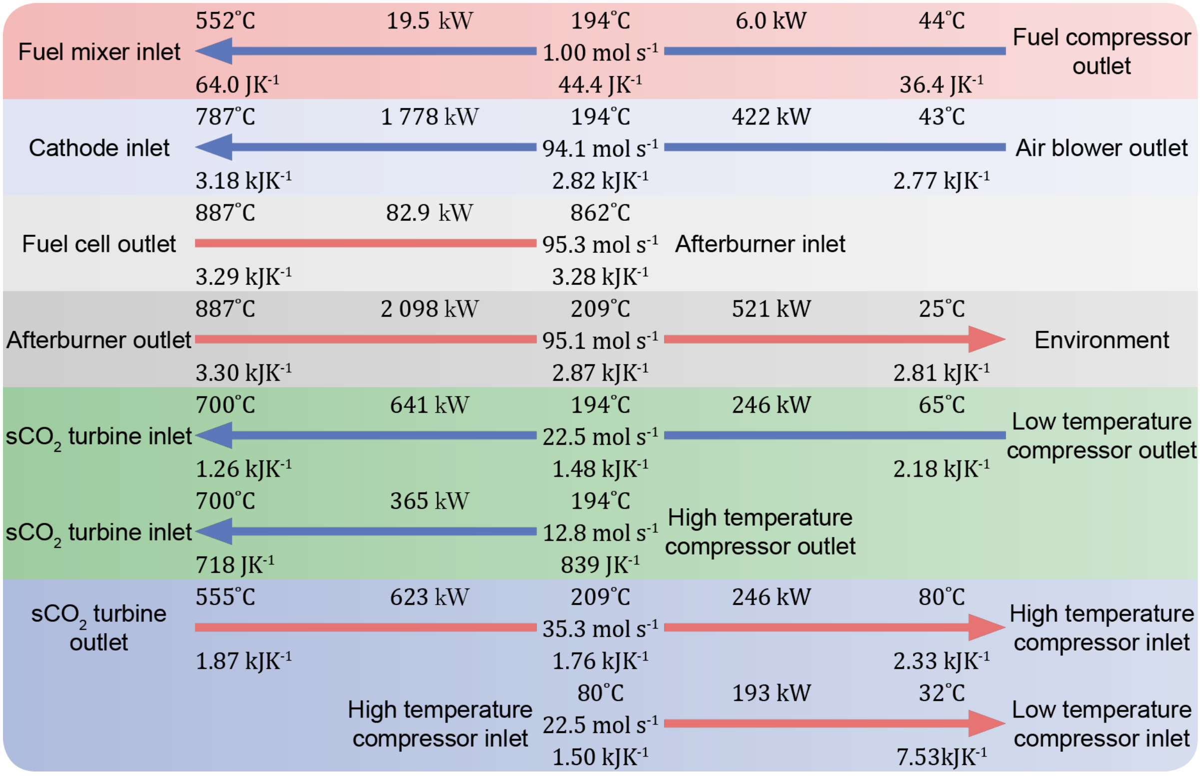

Figure C.4: *Heat flows (case II.A: Recompression cycle, $\Delta T_{hex} = 15\,^{\circ}\mathrm{C}$)*

The points referred to in table C.5 to C.8 refer to the PFD in figure C.5.

Point	$\dot{n}$ (mol s^{-1})	P (bar)	T (°C)	**Exergy**(kW) Thermo mechanical	Chemical	Total
f1	1.00	1.01325	25.00	0.00	832.00	832.00
f2	1.00	1.24257	44.19	0.53	832.00	832.53
f3	1.00	1.23671	193.84	1.93	832.00	833.93
f4	1.00	1.21772	551.68	12.33	832.00	844.33
f5	3.85	1.21772	786.85	69.45	923.33	992.78
f6	5.83	1.15683	786.85	77.07	1141.28	1218.34
f7	2.99	1.11056	886.85	57.52	100.21	157.73
f8	2.85	1.11056	886.85	54.77	95.43	150.20
f9	2.85	1.21772	912.82	57.96	95.43	153.39
a1	94.13	1.01325	25.00	0.00	0.00	0.00
a2	94.13	1.18044	42.59	37.00	0.00	37.00
a3	94.13	1.17592	193.84	132.60	0.00	132.60
a4	94.13	1.15683	786.85	1180.42	0.00	1180.42
a5	92.30	1.11056	886.85	1376.48	0.04	1376.52
fg1	95.29	1.11056	886.85	1433.19	83.26	1516.45

fg2	95.29	1.08835	809.05	1241.51	83.26	1324.77
fg3	6.32	1.03393	834.45	85.73	0.14	85.87
fg4	87.83	1.03393	834.45	1190.79	1.97	1192.76
fg5	0.96	1.03393	834.45	13.08	0.02	13.10
fg6	6.32	1.02639	554.89	44.67	0.14	44.82
fg7	93.78	1.01766	208.84	114.98	2.11	117.09
fg8	1.34	1.01766	208.84	1.64	0.03	1.67
fg9	93.78	1.01325	58.36	4.82	2.11	6.93
fg10	1.34	1.01325	58.36	0.07	0.03	0.10
c1	22.49	80.00	32.00	213.05	452.32	665.37
c2	22.49	250.00	64.88	236.94	452.32	689.26
c3	31.78	248.61	193.84	419.00	639.04	1058.05
c4	3.51	248.61	193.84	46.23	70.51	116.74
c5	35.29	246.13	539.89	823.30	709.55	1532.85
c6	35.29	245.92	570.34	861.18	709.55	1570.73
c7	35.29	245.00	700.00	1031.96	709.55	1741.51
c8	35.29	81.63	554.89	755.19	709.55	1464.74
c9	12.79	80.42	79.88	127.95	257.23	385.18
c10	35.29	80.76	208.84	420.95	709.55	1130.51
c11	22.49	80.42	79.88	224.99	452.32	677.31
w1	100.00	1.01325	25.00	0.00	0.00	0.00
w2	100.00	1.03393	25.00	0.00	0.00	0.00
w3	100.00	1.01325	50.59	7.83	0.00	7.83

Table C.5: *State points (case II.A: Recompression cycle,* ΔT_{hex} = 15 °C*)*

	Point	**Concentration**						
		CH_4	H_2	H_2O	CO	CO_2	O_2	N_2
Methane	f1-4	1.0000	0.0000	0.0000	0.0000	0.0000	0.0000	0.0000
Fuel mix	f5	0.2614	0.0480	0.4444	0.0285	0.2177	0.0000	0.0000
Syngas	f6	0.0019	0.4941	0.1713	0.2380	0.0947	0.0000	0.0000
Anode outlet	f7-9	0.0019	0.0649	0.6005	0.0385	0.2942	0.0000	0.0000
Air	a1-4	0.0000	0.0000	0.0313	0.0000	0.0003	0.2035	0.7649
Cathode outlet	a5	0.0000	0.0000	0.0319	0.0000	0.0003	0.1877	0.7801
Fuel cell exhaust	fg1-2	0.0001	0.0020	0.0497	0.0012	0.0095	0.1818	0.7556
Flue gas	fg3-10	0.0000	0.0000	0.0519	0.0000	0.0108	0.1804	0.7570
Carbon dioxide	c1-11	0.0000	0.0000	0.0000	0.0000	1.0000	0.0000	0.0000
Water	w1-3	0.0000	0.0000	1.0000	0.0000	0.0000	0.0000	0.0000

Table C.6: *Gas compositions (case II.A: Recompression cycle,* ΔT_{hex} = 15 °C*)*

	Inlet	**Outlet**	$\dot{W}/\dot{Q}$ (kW)	**Exergy destruction** (kW)	η_{ex} (%)
			SOFC		
Reformer	f5	f6	234.77		
Fuel cell	f6/a5	f7/a5	379.66		
Total	f5/a4	f7/a5		109.08	94.98
			sCO_2 Brayton cycle		
Turbine	c7	c8	266.03	10.75	96.12
LT compressor	c1	c2	29.03	5.14	82.29
HT compressor	c9	c3	46.75	6.04	87.08
Generator			180.73	9.51	95.00
			BoP		
Air blower	a1	a2	48.54	11.54	76.23

Fuel blower	f1	f2	0.69	0.16	76.33
Anode blower	f8	f9	3.40	0.21	93.70
Water pump	w1	w2	0.01	0.00	75.00
Fuel mixer	f4/f9	f5	0.00	4.94	99.50
Exhaust mixer	f7/a5	fg1	0.00	17.80	98.84

Table C.7: *System components (case II.A: Recompression cycle,* ΔT_{hex} = 15 °C*)*

	Cold side		**Hot side**		$\dot{Q}$	$\dot{Ex}_D$	η_{ex}	$\dot{U}$	A
	Hot	**Cold**	**Hot**	**Cold**	(kW)	(kW)	(%)	(W m^{-2} °C^{-1})	(m^2)
STHE									
LT fuel preheater	fg8	fg10	f2	f3	6.03	0.17	89.26	20	24.54
HT fuel preheater	fg5	fg8	f3	f4	19.54	1.50	87.39	20	11.16
LT air preheater	fg7	fg9	a2	a3	421.54	14.56	86.78	20	1366.55
HT air preheater	fg4	fg7-fg8	a3	a4	1778.34	35.27	96.74	20	3065.10
PCHE									
LT heater	fg6	fg7+fg8	c4	c5	68.71	1.34	96.37	500	6.69
HT heater	fg3	fg6	c5	c6	59.32	3.17	92.28	500	1.34
Aft precooler	fg1	fg2	c6	c7	254.92	21.10	89.00	500	2.41
LT recuperator	c10	c11	c2	c5	245.89	8.39	87.67	754	18.92
HT recuperator	c8	c9+c10	c3	c5	622.72	11.75	96.48	754	40.35
Cooler	c11	c1	w2	w3	192.71	4.11	65.54	7000	9.63

Table C.8: *Heat exchangers (case II.A: Recompression cycle,* ΔT_{hex} = 15 °C*)*

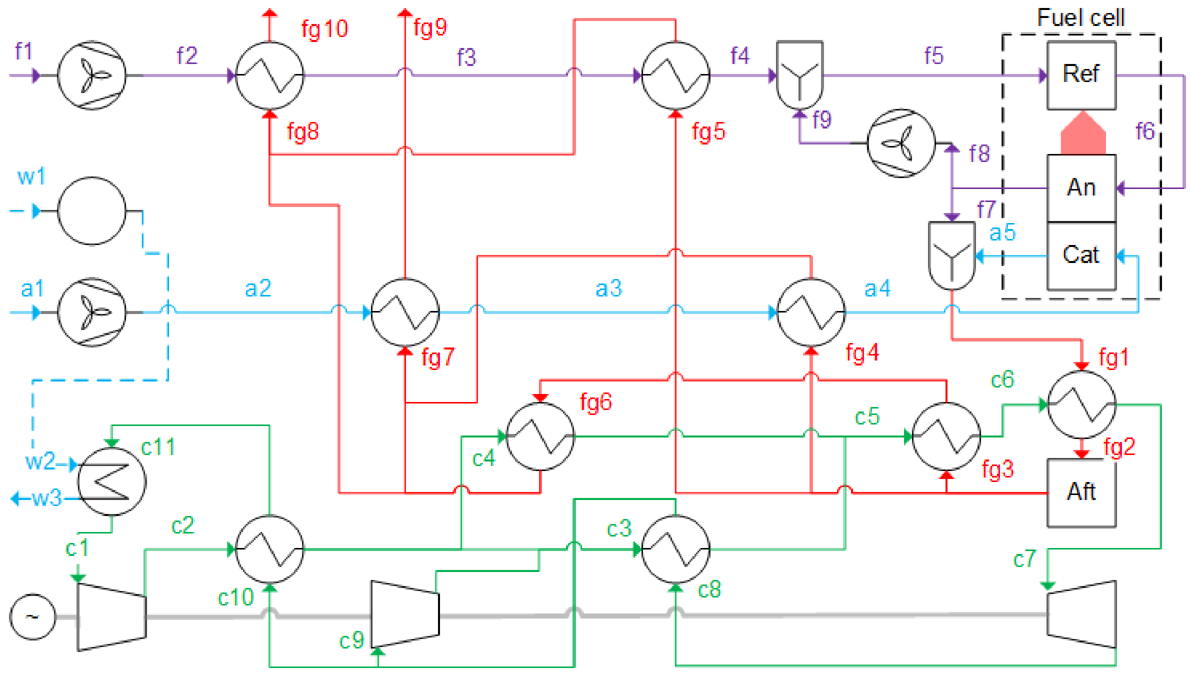

Figure C.5: *PFD (case II.A: Recompression cycle, ΔT_{hex} = 15 °C)*

C.3.2. Case II.B ($\Delta T_{hex} = 10\,°C$)

The points referred to in table C.9 to C.12 refer to the PFD in figure C.7.

Point	$\dot{n}$ (mol s^{-1})	P (bar)	T (°C)	Exergy(kW) Thermo mechanical	Chemical	Total
f1	1.00	1.01325	25.00	0.00	832.00	832.00
f2	1.00	1.24257	44.19	0.53	832.00	832.53
f3	1.00	1.21772	551.68	12.33	832.00	844.33
f4	3.85	1.21772	786.85	69.45	923.33	992.78
f5	5.83	1.15683	786.85	77.07	1141.28	1218.34
f6	2.99	1.11056	886.85	57.52	100.21	157.73
f7	2.85	1.11056	886.85	54.77	95.43	150.20
f8	2.85	1.21772	912.82	57.96	95.43	153.39
a1	94.13	1.01325	25.00	0.00	0.00	0.00
a2	67.35	1.18044	42.59	26.47	0.00	26.47
a3	67.35	1.17986	62.16	29.64	0.00	29.64
a4	26.78	1.18044	42.59	10.53	0.00	10.53
a5	94.13	1.17613	186.88	125.65	0.00	125.65
a6	94.13	1.15683	786.85	1180.42	0.00	1180.42
a7	92.30	1.11056	886.85	1376.48	0.04	1376.52
fg1	95.29	1.11056	886.85	1433.19	83.26	1516.45
fg2	95.29	1.08835	808.88	1241.10	83.26	1324.35
fg3	6.88	1.03393	834.28	93.29	0.15	93.45
fg4	87.22	1.03393	834.28	1182.07	1.96	1184.03
fg5	1.02	1.03393	834.28	13.82	0.02	13.84
fg6	6.88	1.02639	554.89	48.63	0.15	48.79
fg7	1.02	1.01377	46.75	0.02	0.02	0.05
fg8	67.44	1.01736	196.47	73.24	1.52	74.76
fg9	26.66	1.01736	196.47	28.95	0.60	29.55
fg10	67.44	1.01439	72.96	7.15	1.52	8.67
fg11	26.66	1.01391	52.67	1.00	0.60	1.60
fg12	67.44	1.01393	53.55	2.68	1.52	4.19

c1	23.77	80.00	32.00	225.10	477.90	702.99
c2	23.77	250.00	64.88	250.34	477.90	728.24
c3	33.28	248.67	186.88	433.31	669.20	1102.50
c4	3.81	248.67	186.88	49.54	76.52	126.06
c5	37.08	246.09	544.89	871.72	745.71	1617.43
c6	37.08	245.87	576.39	913.09	745.71	1658.80
c7	37.08	245.00	700.00	1084.55	745.71	1830.26
c8	37.08	81.63	554.89	793.67	745.71	1539.38
c9	13.32	80.40	74.88	132.53	267.81	400.35
c10	37.08	80.73	196.88	434.08	745.71	1179.80
c11	23.77	80.40	74.88	236.49	477.90	714.39
w1	1.00	1.01325	25.00	0.00	0.00	0.00
w2	1.00	1.03393	25.00	0.00	0.00	0.00
w3	105.66	1.01325	49.58	7.64	0.00	7.64

Table C.9: *State points (case II.B: Recompression cycle, ΔT_{hex} = 10 °C)*

	Point	Concentration						
		CH_4	H_2	H_2O	CO	CO_2	O_2	N_2
Methane	f1-3	1.0000	0.0000	0.0000	0.0000	0.0000	0.0000	0.0000
Fuel mix	f4	0.2614	0.0480	0.4444	0.0285	0.2177	0.0000	0.0000
Syngas	f5	0.0019	0.4941	0.1713	0.2380	0.0947	0.0000	0.0000
Anode outlet	f6-8	0.0019	0.0649	0.6005	0.0385	0.2942	0.0000	0.0000
Air	a1-6	0.0000	0.0000	0.0313	0.0000	0.0003	0.2035	0.7649
Cathode outlet	a7	0.0000	0.0000	0.0319	0.0000	0.0003	0.1877	0.7801
Fuel cell exhaust	fg1-2	0.0001	0.0020	0.0497	0.0012	0.0095	0.1818	0.7556
Flue gas	fg3-12	0.0000	0.0000	0.0519	0.0000	0.0108	0.1804	0.7570
Carbon dioxide	c1-11	0.0000	0.0000	0.0000	0.0000	1.0000	0.0000	0.0000
Water	w1-3	0.0000	0.0000	1.0000	0.0000	0.0000	0.0000	0.0000

Table C.10: *Gas compositions (case II.B: Recompression cycle, ΔT_{hex} = 10 °C)*

	Inlet	**Outlet**	$\dot{W}/\dot{Q}$ (kW)	**Exergy destruction** (kW)	η_{ex} (%)
			SOFC		
Turbine	c7	c8	279.58	11.29	96.12
LT compressor	c1	c2	30.68	5.43	82.29
HT compressor	c9	c3	47.05	6.17	86.89
Generator			191.76	10.09	95.00
			sCO_2 Brayton cycle		
Air blower	a1	a2	48.54	11.54	76.23
Fuel blower	f1	f2	3.40	0.21	93.70
Anode blower	f7/a5	f8	0.00	4.94	99.50
Water pump	w1	w2	0.01	0.00	75.00
Fuel mixer	f3/f8	f4	0.00	17.80	98.84
Exhaust mixer	f6/a7	fg1	0.00	17.80	98.84

Table C.11: *System components(case II.B: Recompression cycle, ΔT_{hex} = 10 °C)*

	Cold side		**Hot side**		$\dot{Q}$	$\dot{Ex}_D$	η_{ex}	$\dot{U}$	A
	Hot	**Cold**	**Hot**	**Cold**	(kW)	(kW)	(%)	(W m^{-2} °C^{-1})	(m^2)
					STHE				

Fuel preheater	fg5	fg7-fg8	f2	f3	25.57	1.99	85.60	20	27.11
LT air preheater I	fg10	fg12	a2	a3	38.77	1.31	70.77	20	178.14
LT air preheater II	fg9	fg11	a4	a5	114.37	2.73	90.24	20	579.67
HT air preheater	fg4	fg9	a5	a6	1797.92	32.58	97.00	20	3654.54
PCHE									
LT heater I	fg8	fg10	c2	c4	248.82	6.99	89.43	500	38.48
LT heater II	fg6	fg8	c4	c5	77.37	1.26	96.95	500	9.82
HT heater	fg3	fg4	c5	c6	64.53	3.29	92.63	500	1.64
Aft precooler	fg1	fg2	c6	c7	255.50	20.84	89.16	500	2.45
Recuperator	c8	c9+c10	c3	c5	676.65	10.61	97.05	754	56.81
Air preheater	c10	c11	a3	a5	248.82	4.80	92.62	500	60.85
Cooler	c11	c1	w2	w3	195.54	3.76	67.02	7000	10.21

Table C.12: *Heat exchangers (case II.B: Recompression cycle,* ΔT_{hex} = 10 °C*)*

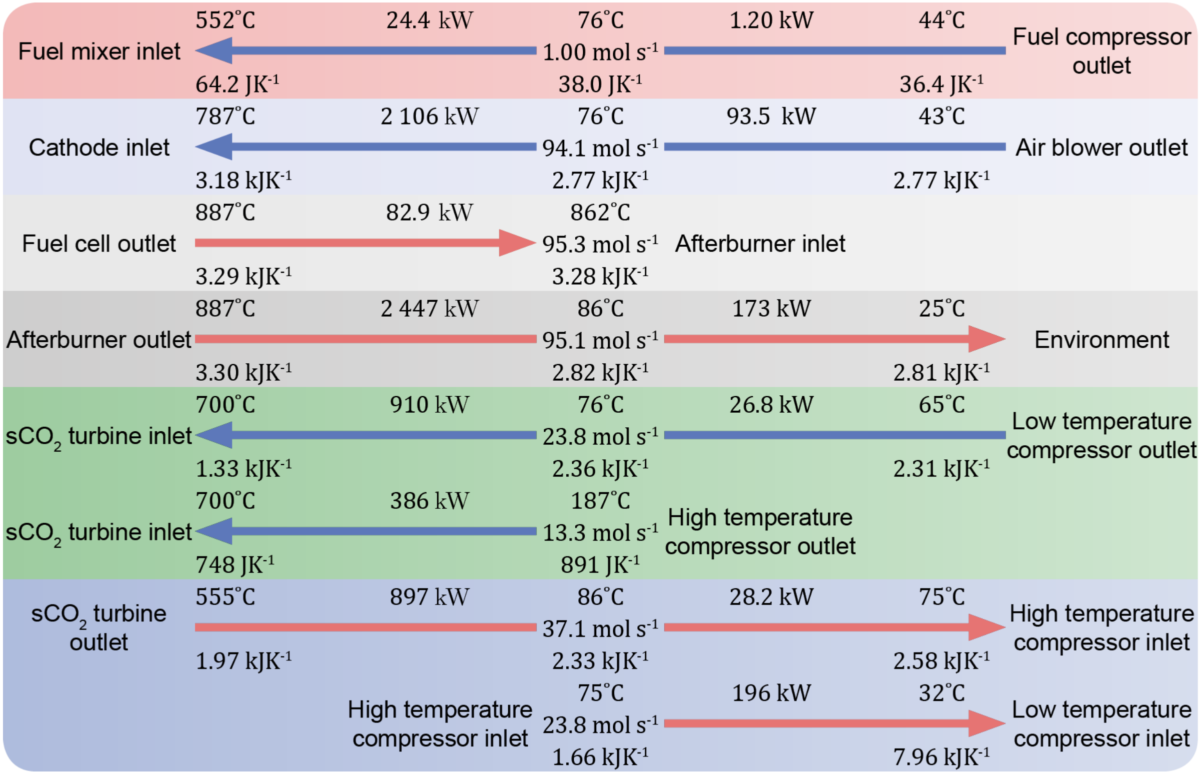

Figure C.6: *Heat flows (case II.B: Recompression cycle, ΔT_{hex} = 10 °C)*

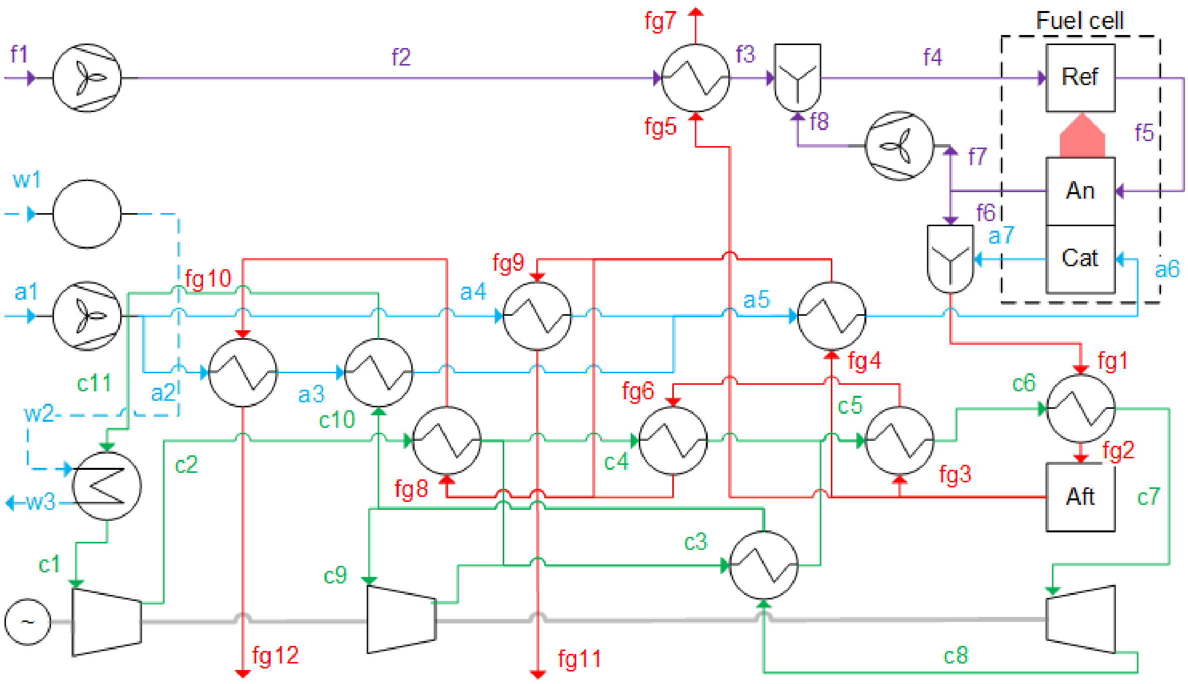

Figure C.7: *PFD (case II.B: Recompression cycle, ΔT_{hex} = 10 °C)*

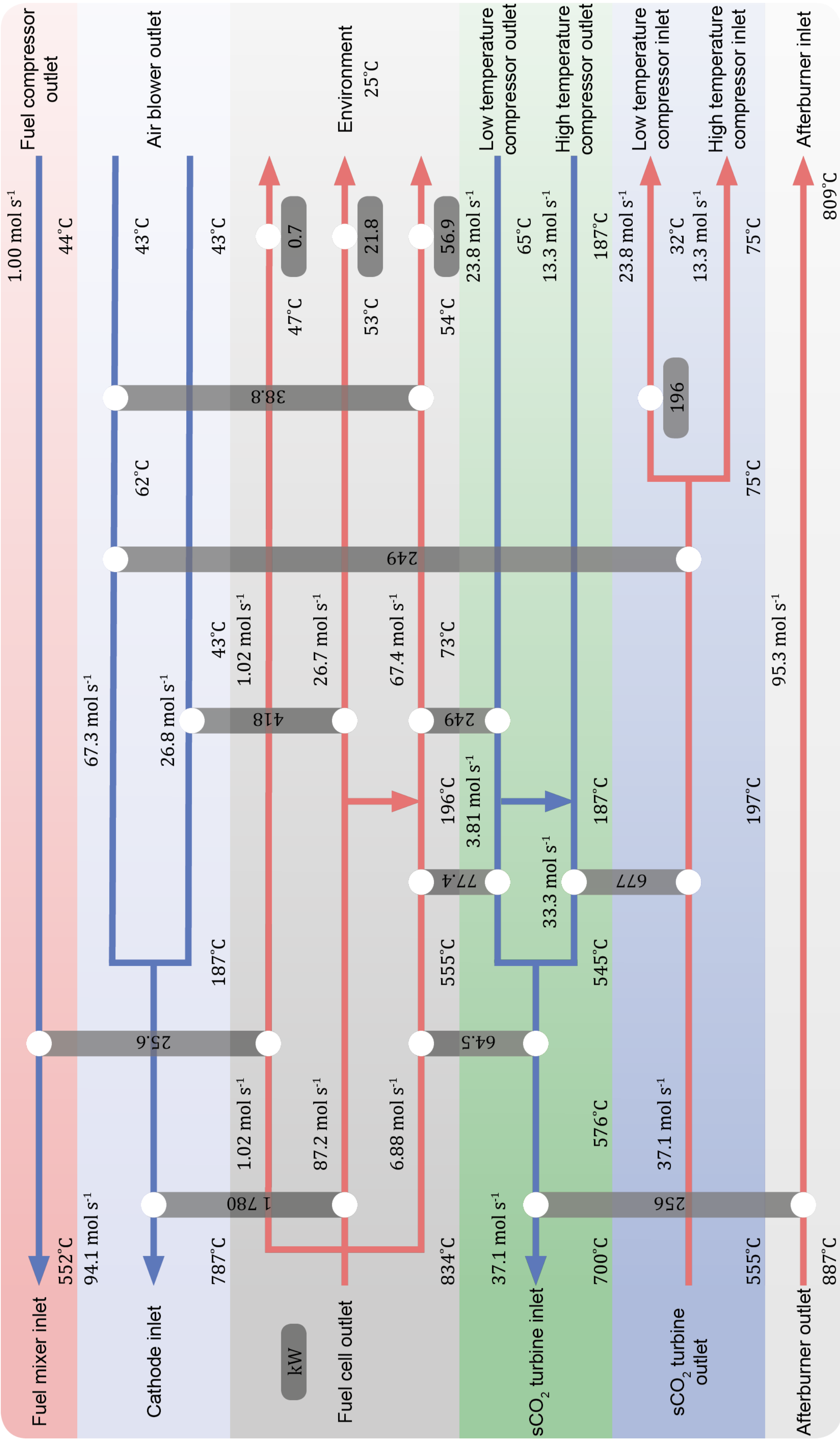

Figure C.8: *Heat exchanger network (case II.B: Recompression cycle, ΔT_{hex} =10 °C)*

C.4. Case III: Cathode recirculation (4.3)

The critical recirculation ratios mentioned in section C.4.1 to C.4.4 are valid for a minimal temperature difference of 10 °C.

C.4.1. Case III.A ($0.7350 \leq r_{ca} \leq 0.7486$)

The points referred to in table C.13 to C.16 refer to the PFD in figure 4.21.

Point	$\dot{n}$ (mol s^{-1})	P (bar)	T (°C)	**Exergy**(kW)		
				Thermo mechanical	Chemical	Total
f1	1.00	1.01325	25.00	0.00	832.00	832.00
f2	1.00	1.24257	44.19	0.53	832.00	832.53
f3	1.00	1.21772	551.68	12.33	832.00	844.33
f4	3.85	1.21772	786.85	69.45	923.33	992.78
f5	5.83	1.15683	786.85	77.07	1141.28	1218.34
f6	2.99	1.11056	886.85	57.52	100.21	157.73
f7	2.85	1.11056	886.85	54.77	95.43	150.20
f8	2.85	1.21772	912.82	57.96	95.43	153.39
a1	25.44	1.01325	25.00	0.00	0.00	0
a2	25.44	1.18044	42.59	10.00	0.00	10.00
a3	25.44	1.15683	456.25	136.26	0.00	136.26
a4	95.75	1.15683	786.85	1197.78	1.17	1198.96
a5	23.61	1.11056	886.85	351.25	0.61	351.85
a6	70.30	1.11056	886.85	1045.92	1.81	1047.73
a7	70.30	1.15683	902.28	1080.67	1.81	1082.47
fg1	26.60	1.11056	886.85	408.56	87.72	496.28
fg2	26.60	1.08835	798.29	346.51	87.72	434.22
fg3	25.50	1.03393	886.85	392.73	5.90	398.63
fg4	0.93	1.03393	886.85	14.31	0.22	14.53
fg5	5.60	1.02529	554.89	41.20	1.30	42.49
fg6	19.90	1.02529	554.89	146.47	4.61	151.08
fg7	0.93	1.01326	47.59	0.15	0.22	0.37
fg8	5.60	1.01388	74.88	1.42	1.30	2.72
fg9	19.90	1.01325	47.04	3.24	4.61	7.85
c1	31.85	80.00	32.00	301.66	640.45	942.11
c2	28.77	250.00	64.88	303.06	578.53	881.59
c3	3.08	250.00	64.88	32.43	61.92	94.35
c4	31.85	246.50	487.17	685.90	640.45	1326.35
c5	31.85	245.33	653.53	874.71	640.45	1515.16
c6	31.85	245.00	700.00	931.46	640.45	1571.91
c7	31.85	81.63	554.89	681.64	640.45	1322.09
c8	31.85	80.40	74.88	316.93	640.45	957.38
w1	141.60	1.01325	25.00	0.00	0.00	0.00
w2	141.60	1.03393	25.00	0.01	0.00	0.01
w3	141.60	1.01325	49.58	10.24	0.00	10.24

Table C.13: *State points (case III.A: Cathode recirculation ratio, r_{ca} = 74.86%,ΔT_{hex} = 10 °C)*

	Point	**Concentration**						
		CH_4	H_2	H_2O	CO	CO_2	O_2	N_2
Methane	f1-3	1.0000	0.0000	0.0000	0.0000	0.0000	0.0000	0.0000
Fuel mix	f4	0.2614	0.0480	0.4444	0.0285	0.2177	0.0000	0.0000
Syngas	f5	0.0019	0.4941	0.1713	0.2380	0.0947	0.0000	0.0000
Anode outlet	f6-8	0.0019	0.0649	0.6005	0.0385	0.2942	0.0000	0.0000
Air	a1-3	0.0000	0.0000	0.0313	0.0000	0.0003	0.2035	0.7649

Cathode inlet	a4	0.0000	0.0000	0.0331	0.0000	0.0003	0.1581	0.8085
Cathode outlet	a5-7	0.0000	0.0000	0.0337	0.0000	0.0003	0.1416	0.8243
Fuel cell exhaust	fg1-2	0.0002	0.0073	0.0974	0.0043	0.0333	0.1257	0.7317
Flue gas	fg3-9	0.0000	0.0000	0.1054	0.0000	0.0381	0.1202	0.7363
Carbon dioxide	c1-8	0.0000	0.0000	0.0000	0.0000	1.0000	0.0000	0.0000
Water	w1-3	0	0	1	0	0	0	0

Table C.14: *Gas compositions (case III.A: Cathode recirculation ratio, r_{ca} = 74.86%,ΔT_{hex} =* 10 °C*)*

	Inlet	**Outlet**	$\dot{W}/\dot{Q}$ (kW)	**Exergy destruction** (kW)	η_{ex} (%)
			SOFC		
Reformer	f4	f5	234.77		
Fuel cell	f5/a4	f6/a5	375.04		
Total	f4/a4	f6/a5		109.18	95.02
			sCO_2 Brayton cycle		
Turbine	c6	c7	240.12	9.70	96.12
Compressor	c1	c2	41.11	7.28	82.29
Generator			189.06	9.95	95.00
			BoP		
Air blower	a1	a2	13.12	3.12	76.23
Fuel blower	f1	f2	0.69	0.16	76.33
Anode blower	f7/a5	f8	3.40	0.21	93.70
Cathode blower	a6	a7	37.10	2.36	93.65
Water pump	w1	w2	0.01	0.00	75.00
Fuel mixer	f3/f8	f4	0.00	4.94	99.50
Air mixer	a3/a7	a4	0.00	19.78	98.38
Exhaust mixer	f6/a5	fg1	0.00	13.31	97.39

Table C.15: *System components (case III.A: Cathode recirculation ratio, r_{ca} = 74.86%,ΔT_{hex} =* 10 °C*)*

	Cold side		**Hot side**		$\dot{Q}$	$\dot{Ex}_D$	η_{ex}	$\dot{U}$	A
	Hot	**Cold**	**Hot**	**Cold**	(kW)	(kW)	(%)	(W m^{-2} °C^{-1})	(m^2)
					STHE				
Fuel preheater	fg4	fg7	f2	f3	25.57	2.35	83.38	20	20.26
Air preheater	fg6	fg9	a2	a3	319.14	16.97	88.15	20	487.66
					PCHE				
LT heater	fg5	fg8	c3	c4	85.07	5.90	85.18	500	3.11
HT heater	fg3	fg5+fg6	c4	c5	293.12	16.25	92.08	500	4.33
Aft precooler	fg1	fg2	c5	c6	82.88	5.30	91.45	500	1.00
Recuperator	c7	c8	c2	c4	794.83	48.17	86.79	754	22.68
Cooler	c8	c1	w2	w3	262.06	5.04	67.02	7000	13.69

Table C.16: *Heat exchangers(case III.A: Cathode recirculation ratio, r_{ca} = 74.86%,ΔT_{hex} =* 10 °C*)*

C.4.2. Case III.B ($0 \leq r_{ca} \leq 0.7349$)

For a recirculation ratio between 0% (case I) and 73.49% the same design principles for a heat exchanger network as in case I can be applied. The flue gas flow is split into three, supplying heat to the fuel, air and HP sCO_2.

The difference with case I is that the outlet temperature and mass flow of the air feed decrease. The mass flow of the flue gas also decreases, consequently the inlet temperature of the afterburner decreases since the outlet temperature remains fixed.

Figure C.9 shows the heat exchanger network for a recirculation ratio of 50%, which is essentially the same design as for case I.

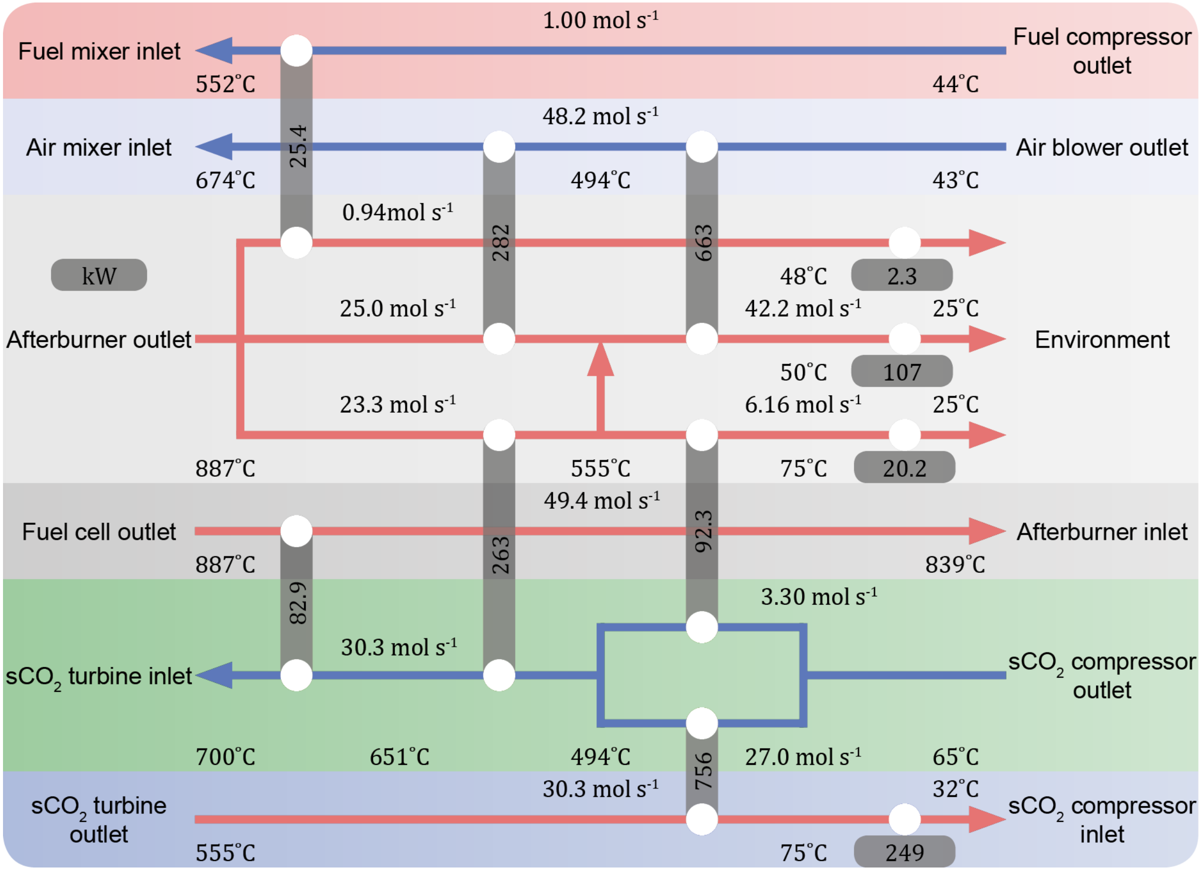

Figure C.9: *Heat exchanger network (case III.B: Cathode recirculation ratio, r_{ca} = 50%,ΔT_{hex} = 10 °C)*

Fuel cell power	378 kW
Generator power	180 kW
Auxiliary power consumption	53 kW
Net AC system power	505 kW
LHV AC efficiency	62.86 %
Thermodynamic efficiency	72.16 %
Second law efficiency	61.81 %
Thermodynamic cycle efficiency	43.16 %
sCO_2 cycle flow	30.3 mol s^{-1}
Total PCHE area	44 m^2
Total STHE area	1397 m^2
Number of heat exchangers	8

Table C.17: *Key performance data (case III.B: Cathode recirculation ratio, r_{ca} = 50%,ΔT_{hex} = 10 °C)*

Applying the same design principles for a heat exchanger network as for case I is possible up to a recirculation ratio of 73.49 %. At this point the outlet temperature of the LT air preheater and the outlet temperature of the air feed are the same. This makes the HT air preheater unnecessary. Making an adjustment for this in the design is considered in case III.A.

C.4.3. Case III.C ($0.7487 \leq r_{ca} \leq 0.8504$)

As mentioned in section 4.3.4, the difference between case III.A and III.C is that the dew temperature in case III.C has increased to such an extent that condensation could occur in the fuel- and air preheater.

The design has to be changed to either cope with the condensation by adjusting the type of heat exchanger or by supplying more flue gas to the air preheater to increase the outlet temperature and thus avoid condensation. By using the latent heat of water, the temperature difference in a heat exchanger increases. The drawback is that the condensed water needs to be dealt with, increasing the complexity and cost of the heat exchanger.

The choice has been to avoid condensation by supplying more flue gas to the air preheater. Since the outlet temperature of the flue gas in the fuel preheater is also very close to the dew temperature, additional flue gas will also be supplied to the fuel preheater. The hot stream outlet of the LT heater, exhausted in case III.A and III.B at 75 °C, will be split and added to the fuel and air preheater. Consequently the air and fuel are heated by a LT and HT preheater. This design principle works up to the

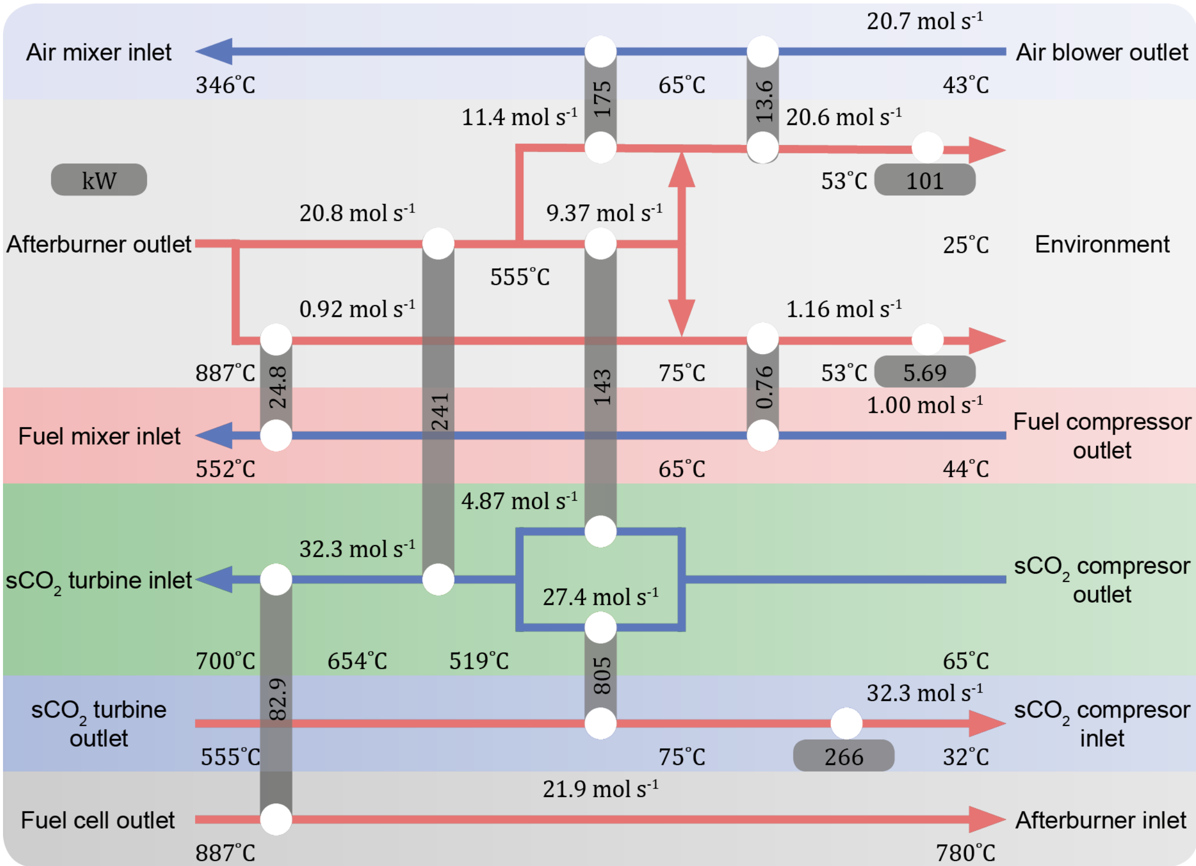

Figure C.10: *Heat exchanger network (case III.C: Cathode recirculation ratio, r_{ca} = 80%,ΔT_{hex} = 10 °C)*

point where the pinch temperature *jumps* up, at a recirculation ratio of 85.04%. Figure C.10 shows the design of the heat exchanger network for a recirculation ratio of 80%.

Fuel cell power	373 kW
Generator power	192 kW
Auxiliary power consumption	55 kW
Net AC system power	510 kW
LHV AC efficiency	63.55 %
Thermodynamic efficiency	73.06 %
Second law efficiency	62.55 %
Thermodynamic cycle efficiency	43.16 %
sCO_2 cycle flow	32.3 mol s^{-1}
Total PCHE area	54 m^2
Total STHE area	212 m^2
Number of heat exchangers	9

Table C.18: *Key performance data (case III.C: Cathode recirculation ratio, r_{ca} = 80%,ΔT_{hex} = 10 °C)*

C.4.4. Case III.D ($0.8505 \leq r_{ca} \leq 0.8730$)

For recirculation ratios near the maximum, the pinch temperature has *jumped* to the interval temperature of the TOT. Figure C.11 shows the heat flows and the pinch point at a recirculation ratio of 86%. Even though the problem is significantly different, the design of the heat exchanger network is similar to that of case I. Some heat is transferred across the pinch in order to simplify the system. The fuel is preheated with a portion of flue gas entirely below the pinch. This shows in the lower temperature difference in the fuel preheater, figure C.12. To balance this, some HP sCO_2 below the pinch is heated with flue gas above the pinch. The heat transferred across the pinch, 0.43 kW, is too small to show up in a different temperature in figure C.12.

Contrary to other cases, the air preheater operates in series with the LT heater and fuel preheater since the in- and outlet temperatures of the air feed are low enough to be able to do this.

Fuel cell power	368 kW
Generator power	188 kW
Auxiliary power consumption	56 kW
Net AC system power	500 kW
LHV AC efficiency	62.45 %
Thermodynamic efficiency	72.03 %
Second law efficiency	61.47 %
Thermodynamic cycle efficiency	43.16 %
sCO_2 cycle flow	31.7 mol s^{-1}
Total PCHE area	66 m^2
Total STHE area	125 m^2
Number of heat exchangers	7

Table C.19: *Key performance data (Case III.C: Cathode recirculation ratio, r_{ca} = 80%,ΔT_{hex} = 10 °C)*

This design is possible up to the maximum recirculation ratio of 87.30% at which point the fed air is just able to cool down the outlet of the cathode by 100 °C.

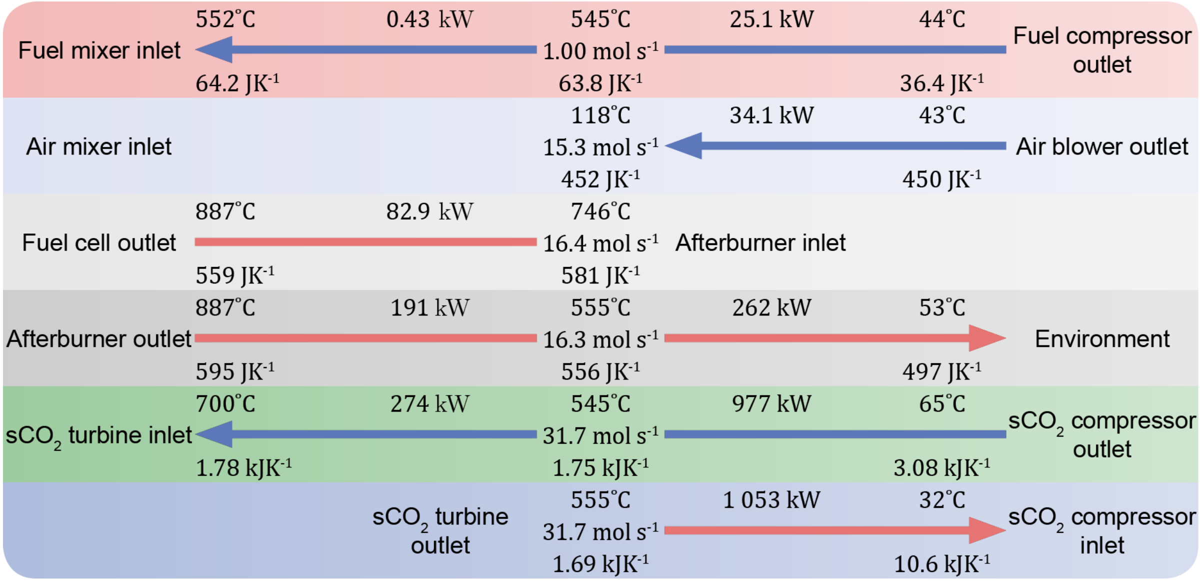

Figure C.11: *Heat flows (Case III.D: Cathode recirculation ratio, r_{ca} = 86%,ΔT_{hex} = 10 °C)*

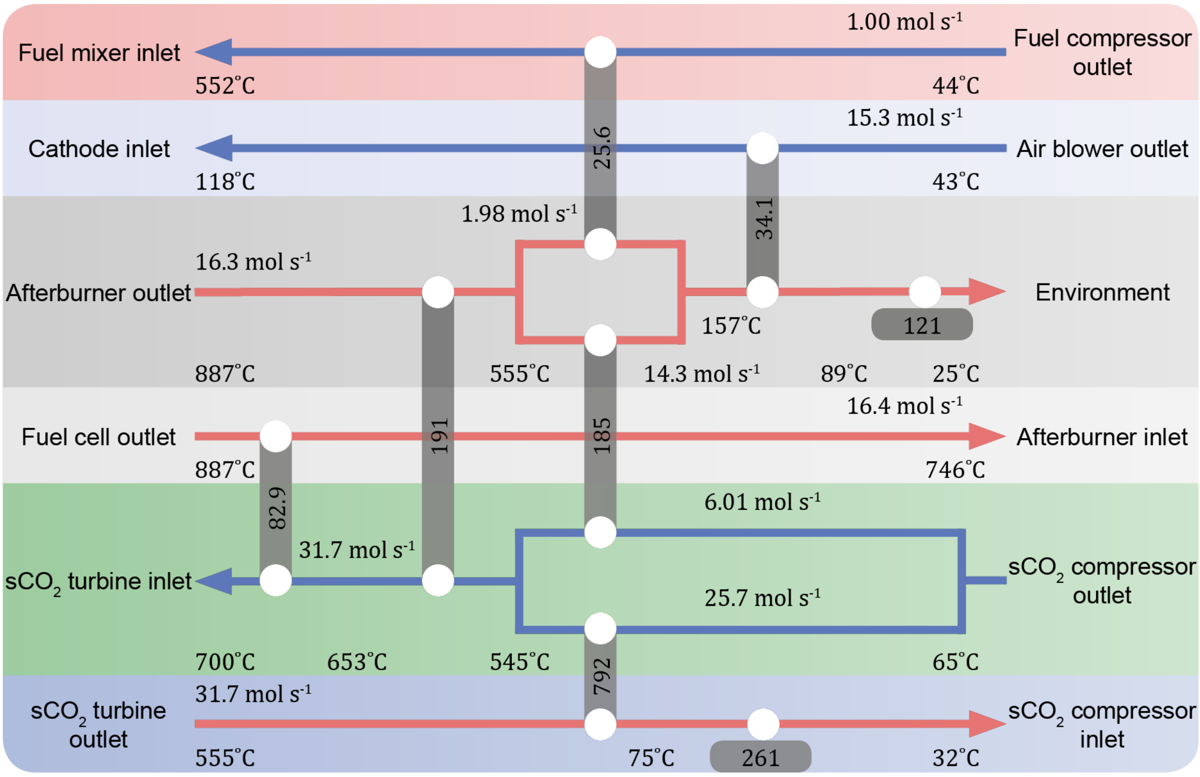

Figure C.12: *Heat exchanger netword (Case III.D: Cathode recirculation ratio, r_{ca} = 86%,ΔT_{hex} = 10 °C)*

C.5. Case IV: Recompression cycle + cathode recirculation (4.4)

The critical recirculation ratios mentioned in section C.5.1 to C.5.4 are valid for a minimal temperature difference of 15 °C.

C.5.1. Case IV.A ($0.6377 \leq r_{ca} \leq 0.6963$)

The points referred to in table C.20 to C.23 refer to the PFD in figure 4.28.

Point	$\dot{n}$ (mol s^{-1})	P (bar)	T (°C)	**Exergy**(kW)		
				Thermo mechanical	Chemical	Total
f1	1.00	1.01325	25.00	0.00	832.00	832.00
f2	1.00	1.24257	44.19	0.53	832.00	832.53
f3	1.00	1.21772	551.68	12.33	832.00	844.33
f4	3.85	1.21772	786.85	69.45	923.33	992.78
f5	5.83	1.15683	786.85	77.07	1141.28	1218.34
f6	2.99	1.11056	886.85	57.52	100.21	157.73
f7	2.85	1.11056	886.85	54.77	95.43	150.20
f8	2.85	1.21772	912.82	57.96	95.43	153.39
a1	30.23	1.01325	25.00	0.00	0.00	0
a2	30.23	1.18044	42.59	11.88	0.00	11.88
a3	30.23	1.17336	193.84	42.42	0.00	42.42
a4	30.23	1.15683	530.98	205.95	0.00	205.95
a5	95.34	1.15683	786.85	1193.40	0.61	1194.00
a6	28.40	1.11056	886.85	422.73	0.47	423.20
a7	65.11	1.11056	886.85	969.21	1.08	970.28
a8	65.11	1.15683	902.27	1001.39	1.08	1002.46
fg1	31.39	1.11056	886.85	480.00	87.04	567.04
fg2	31.39	1.08835	564.38	235.64	87.04	322.68
fg3	7.29	1.03393	642.87	67.51	1.28	68.79
fg4	22.53	1.03393	642.87	208.61	3.96	212.57
fg5	1.39	1.03393	642.87	12.90	0.24	13.15
fg6	7.29	1.03071	554.89	53.27	1.28	54.55
fg7	29.83	1.01866	208.84	40.32	5.24	45.56
fg8	1.39	1.01395	66.25	0.26	0.24	0.50
fg9	29.83	1.01372	59.09	4.79	5.24	10.03
c1	26.41	80.00	32.00	250.13	531.06	781.19
c2	26.41	250.00	64.88	278.19	531.06	809.24
c3	37.31	248.61	193.84	491.94	750.28	1242.22
c4	4.12	248.61	193.84	54.28	82.78	137.06
c5	41.43	246.13	539.89	966.61	833.07	1799.67
c6	41.43	246.06	549.33	980.28	833.07	1813.35
c7	41.43	245.00	700.00	1211.59	833.07	2044.66
c8	41.43	81.63	554.89	886.64	833.07	1719.71
c9	15.02	80.42	79.88	150.22	302.01	452.23
c10	41.43	80.76	208.84	494.23	833.07	1327.30
c11	26.41	80.42	79.88	264.15	531.06	795.21
w1	1.00	1.01325	25.00	0.00	0.00	0.00
w2	1.00	1.03393	25.00	0.00	0.00	0.00
w3	117.41	1.01325	50.59	9.19	0.00	9.19

Table C.20: *State points (case IV.A: Recompression cycle + cathode recirculation , r_{ca} = 69.63% ,ΔT_{hex} = 15 °C)*

	Point	Concentration						
		CH_4	H_2	H_2O	CO	CO_2	O_2	N_2
Methane	f1-3	1.0000	0.0000	0.0000	0.0000	0.0000	0.0000	0.0000

Fuel mix	f4	0.2614	0.0480	0.4444	0.0285	0.2177	0.0000	0.0000
Syngas	f5	0.0019	0.4941	0.1713	0.2380	0.0947	0.0000	0.0000
Anode outlet	f6-8	0.0019	0.0649	0.6005	0.0385	0.2942	0.0000	0.0000
Air	a1-4	0.0000	0.0000	0.0313	0.0000	0.0003	0.2035	0.7649
Cathode inlet	a5-7	0.0000	0.0000	0.0327	0.0000	0.0003	0.1684	0.7987
Cathode outlet	a6-8	0.0000	0.0000	0.0333	0.0000	0.0003	0.1521	0.8143
Fuel cell exhaust	fg1-2	0.0002	0.0062	0.0873	0.0037	0.0283	0.1376	0.7368
Flue gas	fg3-9	0.0000	0.0000	0.0940	0.0000	0.0323	0.1330	0.7407
Carbon dioxide	c1-8	0.0000	0.0000	0.0000	0.0000	1.0000	0.0000	0.0000
Water	w1-3	0	0	1	0	0	0	0

Table C.21: *Gas compositions (case IV.A: Recompression cycle + cathode recirculation , r_{ca} = 69.63% ,ΔT_{hex} = 15 °C)*

	Inlet	**Outlet**	$\dot{W}/\dot{Q}$ (kW)	**Exergy destruction** (kW)	η_{ex} (%)
			SOFC		
Reformer	f4	f5	234.77		
Fuel cell	f5/a5	f6/a6	376.21		
Total	f4/a4	f6/a6		109.16	95.01
			sCO_2 Brayton cycle		
Turbine	c7	c8	312.33	12.62	96.12
LT compressor	c1	c2	34.09	6.04	82.29
HT compressor	c9	c3	54.89	7.09	87.08
Generator			212.18	11.17	95.00
			BoP		
Air blower	a1	a2	15.59	3.71	76.23
Fuel blower	f1	f2	0.69	0.16	76.33
Anode blower	f7/a5	f8	3.40	0.21	93.70
Cathode blower	a7	a8	34.36	2.18	93.65
Water pump	w1	w2	0.01	0.00	75.00
Fuel mixer	f3/f8	f4	0.00	4.94	99.50
Air mixer	a4/a8	a5	0.00	14.41	98.81
Exhaust mixer	f6/a6	fg1	0.00	13.89	97.61

Table C.22: *System components (case IV.A: Recompression cycle + cathode recirculation , r_{ca} = 69.63% ,ΔT_{hex} = 15 °C)*

	Hot stream		**Cold stream**		$\dot{Q}$	$\dot{Ex}_D$	η_{ex}	$\dot{U}$	A
	Inlet	**Outlet**	**Inlet**	**Outlet**	(kW)	(kW)	(%)	(W m^{-2} °C^{-1})	(m^2)
					STHE				
Fuel preheater	fg5	fg8	f2	f3	25.57	0.84	93.37	20	47.31
LT air preheater	fg7	fg9	a2	a3	135.39	4.99	85.96	20	428.08
HT air preheater	fg4	fg7	a3	a4	315.91	14.62	91.79	20	316.66
					PCHE				
LT heater	fg6	fg7	c4	c5	80.67	1.63	96.23	500	7.82
HT heater	fg3	fg6	c5	c6	21.57	0.57	96.00	500	1.00
Aft precooler	fg1	fg2	c6	c7	347.38	13.18	94.61	500	9.98
LT recuperator	c10	c11	c2	c3	288.70	9.85	87.67	754	22.21
HT recuperator	c8	c9+c10	c3	c5	731.12	13.80	96.48	754	47.37
Cooler	c11	c12	w2	w3	226.26	4.83	65.54	7000	11.30

Table C.23: *Heat exchangers (case IV.A: Recompression cycle + cathode recirculation , r_{ca} = 69.63% ,ΔT_{hex} = 15 °C)*

C.5.2. Case IV.B ($0 \leq r_{ca} \leq 0.6376$)

This case has the same design as case II.A. The difference is that the mass flow of the air feed and flue gas decrease as the recirculation ratio increases. The outlet temperature of the air feed also decreases. At the maximum recirculation ratio of this case, 63.76%, it would be possible to replace the LT and HT fuel preheater by a single fuel preheater. At this point, the temperature difference at the LT end is 5 °C. This is less than the imposed 15 °C but choice has been made to go for a design with one heat exchanger less from this point, case IV.A, section C.5.1.

Figure C.13 shows the heat exchanger network at a cathode recirculation ratio of 50%, table C.24 the key performance data at this point.

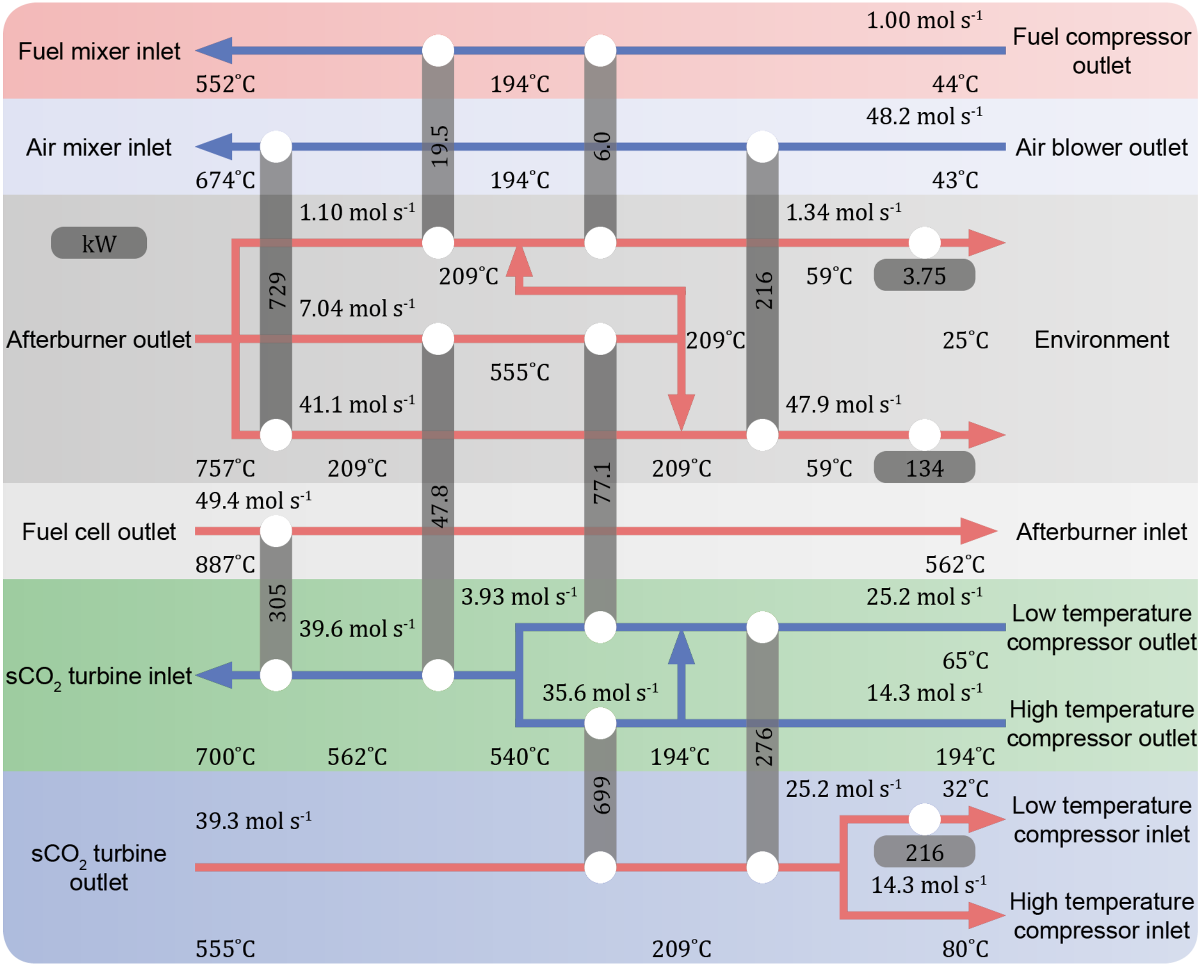

Figure C.13: *eat exchanger network (case IV.B: Recompression cycle + cathode recirculation , r_{ca} = 50%,ΔT_{hex} = 15 °C)*

Fuel cell power	378 kW
Generator power	203 kW
Auxiliary power consumption	53 kW
Net AC system power	528 kW
LHV AC efficiency	65.72 %
Thermodynamic efficiency	75.17 %
Second law efficiency	64.46 %
Thermodynamic cycle efficiency	50.79 %
sCO_2 cycle flow	39.6 mol s^{-1}
Total PCHE area	90 m^2
Total STHE area	1613 m^2
Number of heat exchangers	10

Table C.24: *Key performance data (case IV.B: Recompression cycle + cathode recirculation , r_{ca} = 50%,ΔT_{hex} = 15 °C)*

C.5.3. Case IV.C ($0.6964 \leq r_{ca} \leq 0.7593$)

In case IV.C, the recirculation ratio has increased to such an extent that it is no longer possible to adjust the outlet temperature of the afterburner to avoid the use of an additional heat exchanger as in case II.A, IV.A and IV, delineated in section 4.2.4. Figure C.14 shows that heat to the HP sCO_2 is now supplied by four heaters and two recuperators. The flow of the flue gas is split after the first heater and again after the second.

Fuel cell power	376 kW
Generator power	214 kW
Auxiliary power consumption	54 kW
Net AC system power	535 kW
LHV AC efficiency	66.68 %
Thermodynamic efficiency	76.28 %
Second law efficiency	65.44 %
Thermodynamic cycle efficiency	50.79 %
sCO_2 cycle flow	41.7 mol s^{-1}
Total PCHE area	91.7 m^2
Total STHE area	712 m^2
Number of heat exchangers	10

Table C.25: *Key performance data (case IV.C: Recompression cycle + cathode recirculation , r_{ca} = 72.5%,ΔT_{hex} = 15 °C)*

This case has a higher efficiency than case IV.A and a smaller PCHE area. However, the system is significantly more complex, it has more heat exchangers and flow splits. It is therefore not chosen as the best setup in case IV.

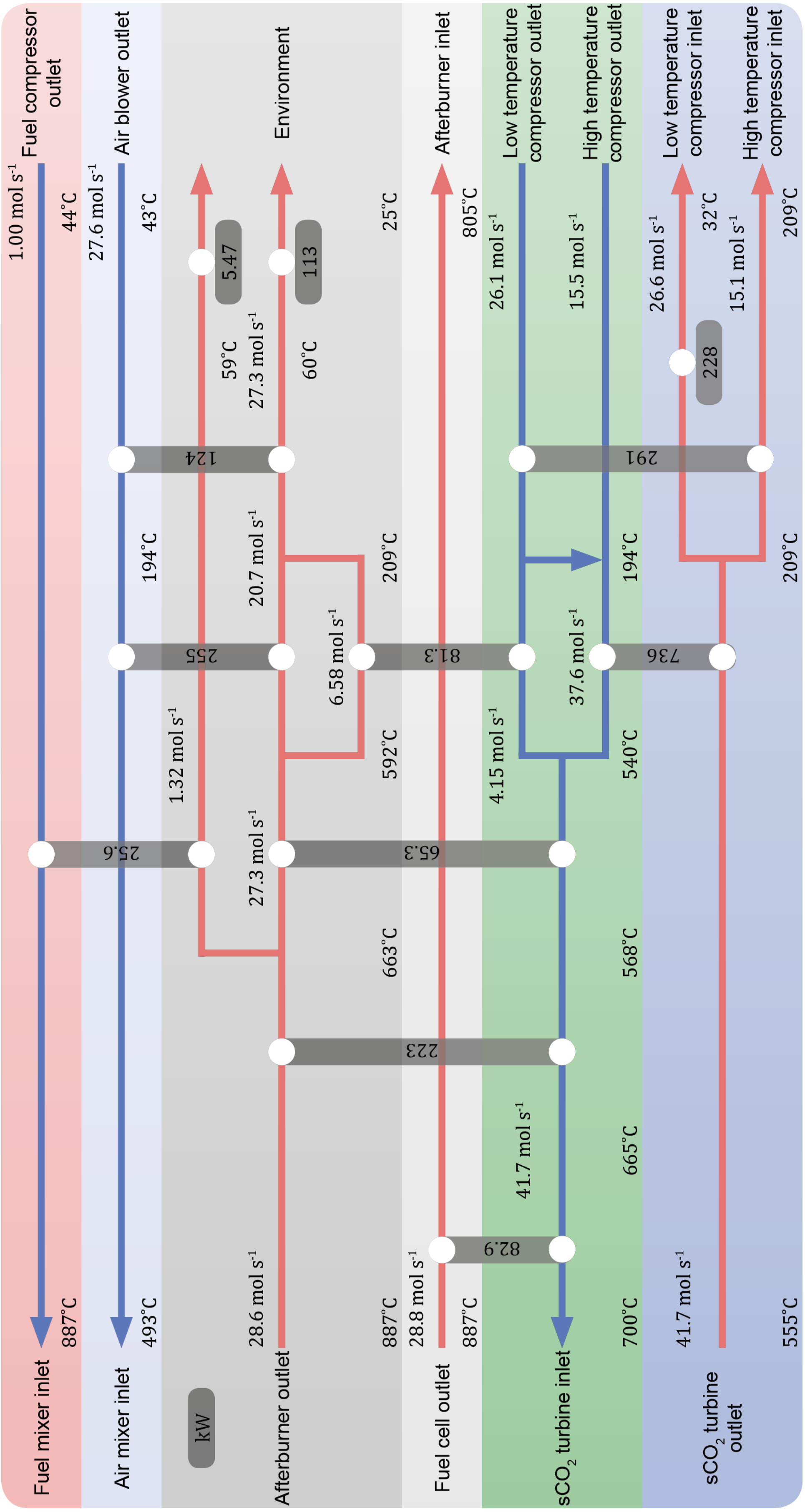

Figure C.14: *Heat exchanger network (case IV.C: Recompression cycle + cathode recirculation ,* r_{ca} *= 72.5%,*ΔT_{hex} *= 15 °C)*

C.5.4. Case IV.D ($0.7594 \leq r_{ca} \leq 0.8241$)

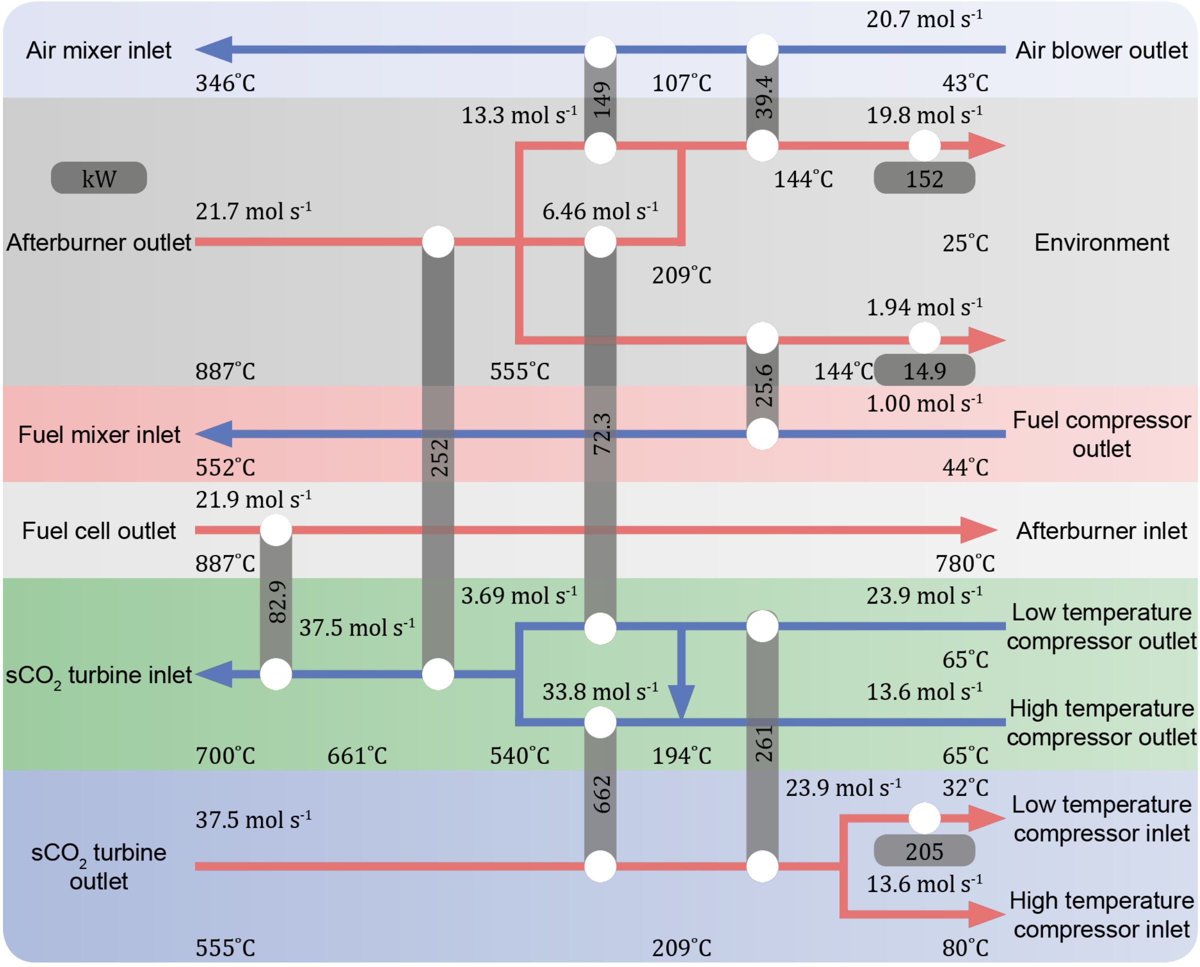

Figure C.15: *Heat exchanger network (case IV.D: Recompression cycle + cathode recirculation , r_{ca} = 80%,ΔT_{hex} = 15 °C)*

At a recirculation ratio of 75.94%, the lower limit of this case, the pinch temperature *jumps* to the interval temperature of the TOT. The mass flows through the sCO_2 starts to decreases significantly for higher recirculation ratio from here, decreasing the efficiency of the system. Figure C.15 shows the design for this case. At the upper limit of this case, a recirculation ratio of 82.41%, the inlet temperature of the air of the LT air preheater is equal to the inlet temperature of the air feed. A design with one less air preheater is case IV.E, section C.5.5.

Fuel cell power	373 kW
Generator power	192 kW
Auxiliary power consumption	55 kW
Net AC system power	510 kW
LHV AC efficiency	63.60 %
Thermodynamic efficiency	73.12 %
Second law efficiency	62.35 %
Thermodynamic cycle efficiency	50.79 %
sCO_2 cycle flow	37.5 mol s^{-1}
Total PCHE area	87 m^2
Total STHE area	176 m^2
Number of heat exchangers	9

Table C.26: *Key performance data (case IV.D: Recompression cycle + cathode recirculation , r_{ca} = 80%,ΔT_{hex} = 15 °C)*

C.5.5. Case IV.E ($0.8242 \leq r_{ca} \leq 0.8730$)

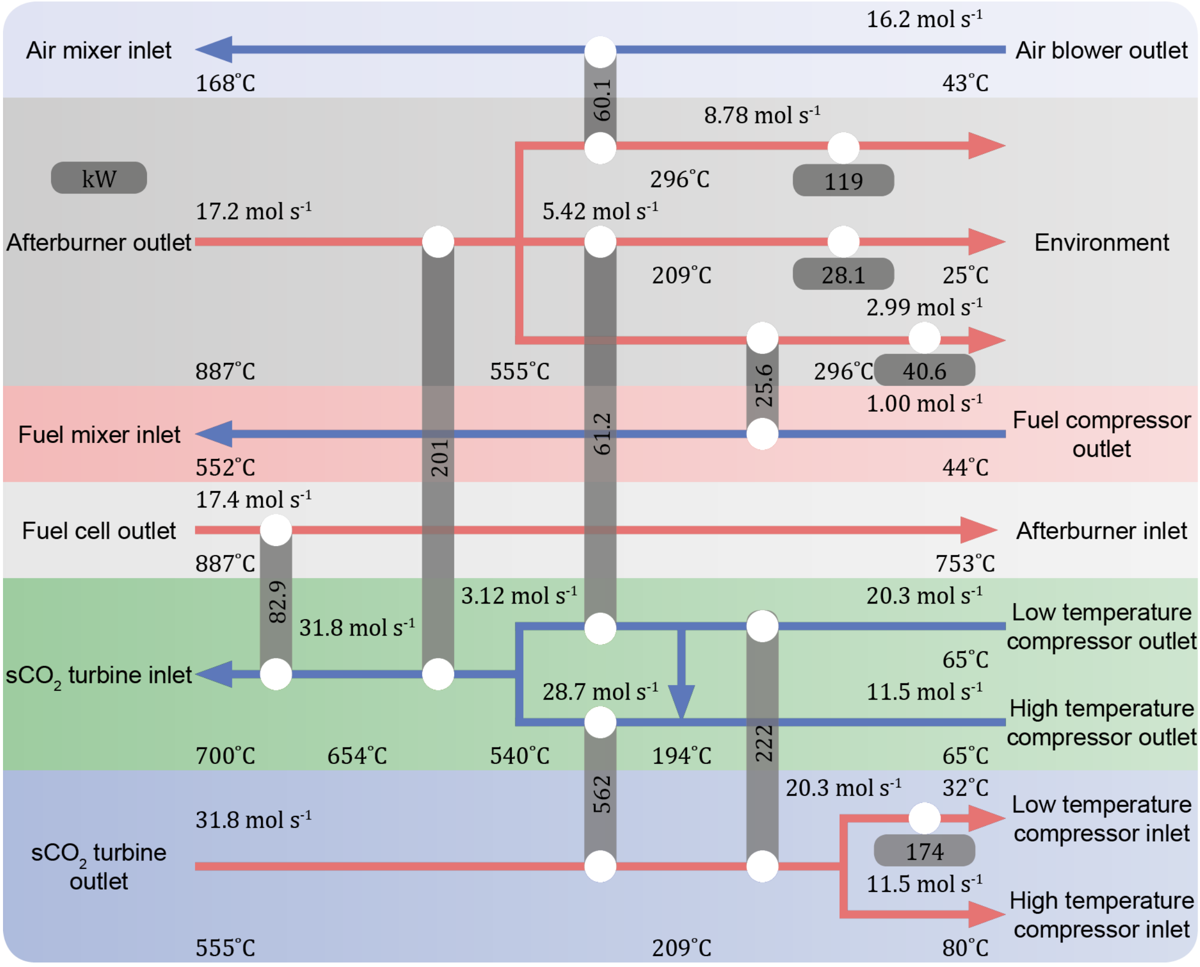

Figure C.16: *Heat exchanger network (case IV.E: Recompression cycle + cathode recirculation, r_{ca} = 85%,ΔT_{hex} = 15 °C)*

As mentioned before, case IV.E only differs from IV.D in that it has one air preheater less. At the maximum recirculation ratio, 87.30%, the outlet of the air blower mixes straight with the outlet of the cathode in order for the cathodic air to cool down with 100 °C. Not a single air preheater is necessary in this case.

Fuel cell power	370 kW
Generator power	163 kW
Auxiliary power consumption	55 kW
Net AC system power	477 kW
LHV AC efficiency	59.47 %
Thermodynamic efficiency	68.86 %
Second law efficiency	58.21 %
Thermodynamic cycle efficiency	50.79 %
sCO_2 cycle flow	31.8 mol s^{-1}
Total PCHE area	74 m^2
Total STHE area	31 m^2
Number of heat exchangers	8

Table C.27: *Key performance data (case IV.E: Recompression cycle + cathode recirculation, r_{ca} = 85%,ΔT_{hex} = 15 °C)*

C.6. Case V: Heat recovery steam generator (4.5)

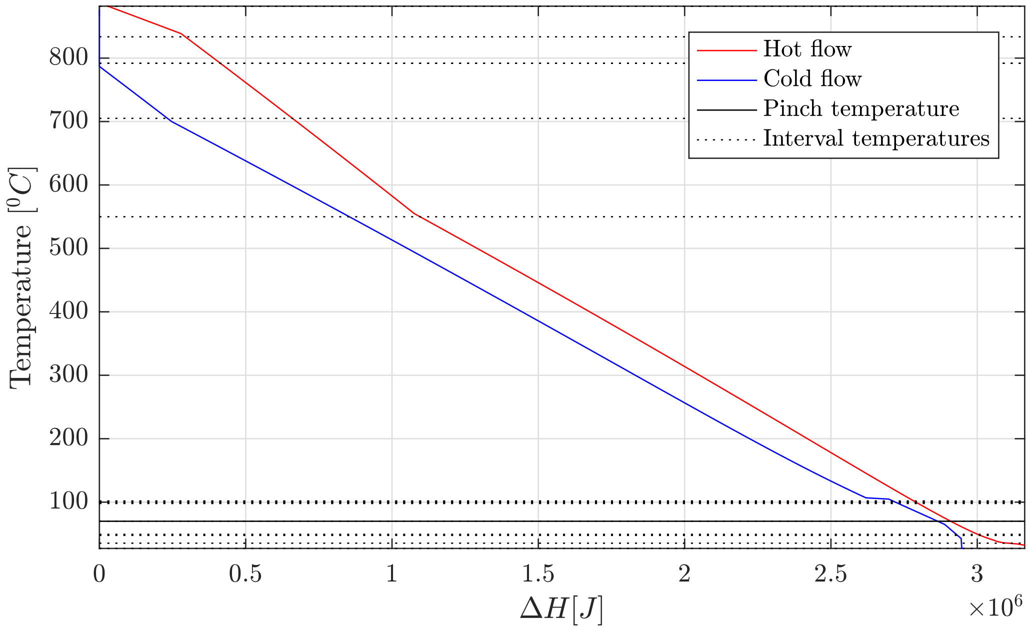

Figure C.17: *Pinch diagram (case V: HRSG, $\dot{n}_{fd}^{H_2O}$ =1.7 mol s^{-1}, ΔT_{hex} =10 °C)*

The points referred to in table C.28 to C.31 refer to the PFD in figure C.18.

Point	$\dot{n}$ (mol s^{-1})	P (bar)	T (°C)	**Exergy**(kW) Thermo mechanical	Chemical	Total
f1	1.00	1.01325	25.00	0.00	832.00	832.00
f2	1.00	1.24257	44.19	0.53	832.00	832.53
f3	1.00	1.23093	455.16	8.69	832.00	840.69
f4	1.00	1.21772	786.85	23.46	832.00	855.47
f5	2.70	1.21772	786.85	49.18	829.54	878.72
f6	4.65	1.15683	786.85	58.49	1027.82	1086.32
f7	78.81	1.11056	886.85	1175.23	0.05	1175.28
a1	80.51	1.01325	25.00	0.00	0.00	0.00
a2	80.51	1.18044	42.59	31.65	0.00	31.65
a3	80.51	1.16628	502.72	504.62	0.00	504.62
a4	80.51	1.15683	786.85	1009.58	0.00	1009.58
a5	80.51	1.15683	786.85	1009.58	0.00	1009.58
fg1	83.46	1.11056	886.85	1261.30	141.23	1402.53
fg2	83.46	1.08835	838.56	1154.18	141.23	1295.41
fg3	9.82	1.03393	886.85	147.60	-0.16	147.44
fg4	1.98	1.03393	886.85	29.72	-0.03	29.69
fg5	66.85	1.03393	886.85	1004.68	-1.06	1003.62
fg6	5.39	1.02538	554.89	38.53	-0.09	38.45
fg7	1.26	1.02538	554.89	9.02	-0.02	9.00
fg8	72.01	1.02538	554.89	514.95	-1.14	513.81
fg9	5.39	1.01403	74.88	0.91	-0.09	0.82
fg10	1.26	1.01403	74.88	0.21	-0.02	0.19
fg11	72.01	1.01347	50.22	6.11	-1.14	4.97
fg12	4.51	1.03393	886.85	67.76	-0.07	67.69
fg13	4.51	1.02647	598.60	36.48	-0.07	36.41
fg14	4.51	1.01492	113.98	1.76	-0.07	1.69
fg15	4.51	1.01370	60.26	0.51	-0.07	0.44

c1	22.84	80.00	32.00	216.35	459.32	675.67
c2	20.02	250.00	64.88	210.83	402.47	613.30
c3	2.83	250.00	64.88	29.78	56.85	86.62
c4	22.84	246.39	502.72	503.82	459.32	963.14
c5	22.84	245.77	590.47	574.00	459.32	1033.32
c6	22.84	245.00	700.00	668.03	459.32	1127.35
c7	22.84	81.63	554.89	488.86	459.32	948.18
c8	22.84	80.40	74.88	227.30	459.32	686.62
w1	101.55	1.01325	25.00	0.00	0.00	0.00
w2	101.55	1.05503	25.00	0.01	0.00	0.01
w3	99.85	1.03393	49.58	7.23	0.00	7.23
w4	1.70	1.03393	49.58	0.12	0.00	0.12
w5	1.70	1.24048	105.74	1.20	0.00	1.20
w6	1.70	1.22664	105.42	15.77	0.00	15.77
w7	1.70	1.21772	786.85	40.33	0.00	40.33

Table C.28: *State points (case V: HRSG, $\dot{n}_{fd}^{H_2O}$ =1.7 mol s^{-1}, ΔT_{hex} =10 °C)*

	Point	**Concentration**						
		CH_4	H_2	H_2O	CO	CO_2	O_2	N_2
Methane	f1-4	1.0000	0.0000	0.0000	0.0000	0.0000	0.0000	0.0000
Fuel mix	f5	0.3704	0.0000	0.6296	0.0000	0.0000	0.0000	0.0000
Syngas	f5	0.0048	0.6658	0.1194	0.1741	0.0359	0.0000	0.0000
Anode outlet	f7	0.0048	0.0832	0.7020	0.0264	0.1836	0.0000	0.0000
Air	a1-4	0.0000	0.0000	0.0313	0.0000	0.0003	0.2035	0.7649
Cathode outlet	a5	0.0000	0.0000	0.0320	0.0000	0.0003	0.1863	0.7814
Fuel cell exhaust	fg1-2	0.0003	0.0046	0.0693	0.0015	0.0105	0.1759	0.7378
Flue gas	fg3-15	0.0000	0.0000	0.0742	0.0000	0.0123	0.1730	0.7405
Carbon dioxide	c1-8	0.0000	0.0000	0.0000	0.0000	1.0000	0.0000	0.0000
Water	w1-7	0	0	1	0	0	0	0

Table C.29: *Gas compositions (case V: HRSG, $\dot{n}_{fd}^{H_2O}$ =1.7 mol s^{-1}, ΔT_{hex} =10 °C)*

	Inlet	**Outlet**	$\dot{W}/\dot{Q}$ (kW)	**Exergy destruction** (kW)	η_{ex} (%)
			SOFC		
Reformer	f5	f6	215.54		
Fuel cell	f6/a4	f7/a5	367.12		
Total	f5/a4	f7/a5		97.47	94.84
			sCO_2 Brayton cycle		
Turbine	c6	c7	172.21	6.96	96.12
Compressor	c1	c2	29.48	5.22	82.29
Generator			135.59	7.14	95.00
			BoP		
Air blower	a1	a2	41.52	9.87	76.23
Fuel blower	f1	f2	0.69	0.16	76.33
Waterpump	w1	w2	0.01	0.00	75.00
Fuel mixer	f4/w7	f5	0.00	17.07	98.09
Exhaust mixer	f7/a5	fg1	0.00	21.20	98.51

Table C.30: *System components (case V: HRSG, $\dot{n}_{fd}^{H_2O}$ =1.7 mol s^{-1}, ΔT_{hex} =10 °C)*

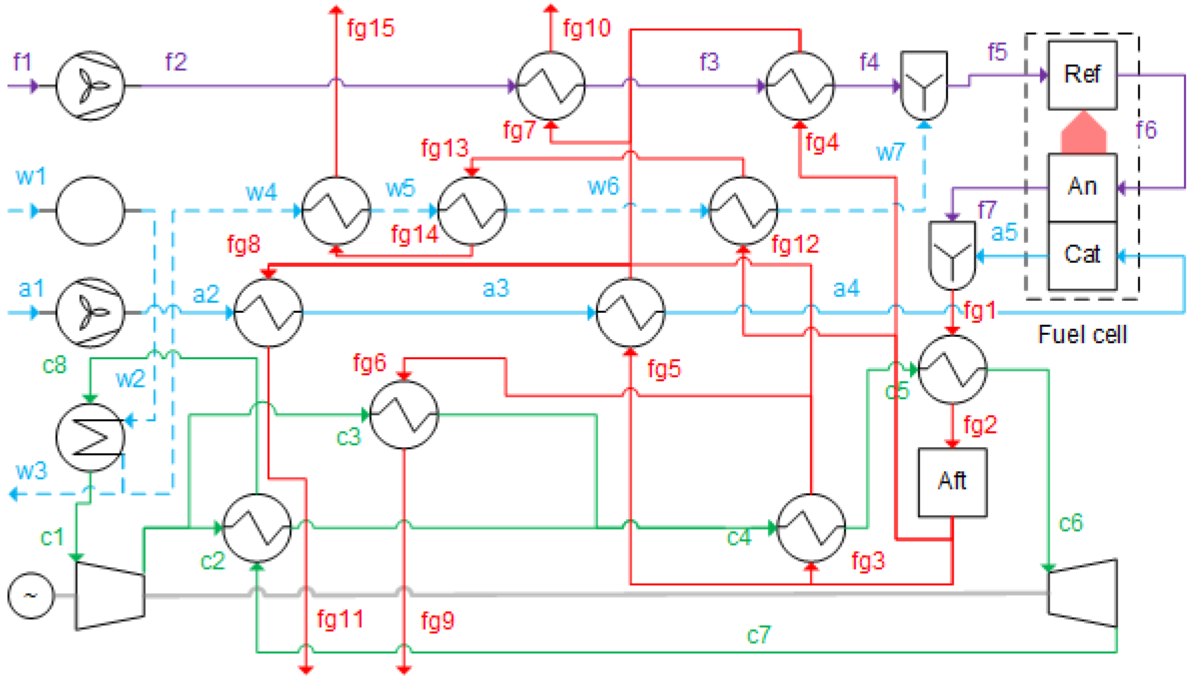

Figure C.18: *PFD (case V: HRSG, $\dot{n}_{fd}^{H_2O}$ =1.7 mol s^{-1})*

	Hot stream Inlet	Hot stream Outlet	Cold stream Inlet	Cold stream Outlet	$\dot{Q}$ (kW)	$\dot{Ex}_D$ (kW)	η_{ex} (%)	$\dot{U}$ (W m^{-2} °C^{-1})	A (m^2)
STHE									
LT fuel preheater	fg7	fg10	f2	f3	18.84	0.71	91.91	20	35.55
HT fuel preheater	fg4	fg7	f3	f4	22.26	0.80	94.88	20	11.66
LT air preheater	fg8	fg11	a2	a3	1128.79	35.87	92.95	20	2330.44
HT air preheater	fg5	fg8	a3	a4	752.70	21.60	95.90	20	509.13
Economizer	fg14	fg15	w4	w5	7.22	0.18	85.92	30	25.04
Boiler	fg13	fg14	w5	w6	68.62	20.14	41.98	30	17.81
Steam superheater	fg12	fg13	w6	w7	44.26	6.72	78.51	20	9.30
PCHE									
LT heater	fg6	fg9	c3	c4	80.51	5.05	86.58	500	3.22
HT heater	fg3	fg6	c4	c5	110.58	7.18	90.72	500	1.55
Aft precooler	fg1	fg2	c5	c6	139.57	13.09	87.78	500	1.29
Recuperator	c7	c8	c2	c4	570.04	30.92	88.18	754	17.78
Cooler	c8	c1	w2	w3	187.94	3.61	67.02	7000	9.82

Table C.31: *Heat exchangers (case V: HRSG, $\dot{n}_{fd}^{H_2O}$ =1.7 mol s^{-1}, ΔT_{hex} =10 °C)*

C.7. Case VI: Simplified heat exchanger networks (4.6)

C.7.1. Case VI.I: Simplified basic setup (4.6.1)

The points referred to in table C.32 to C.35 refer to the PFD in figure C.19.

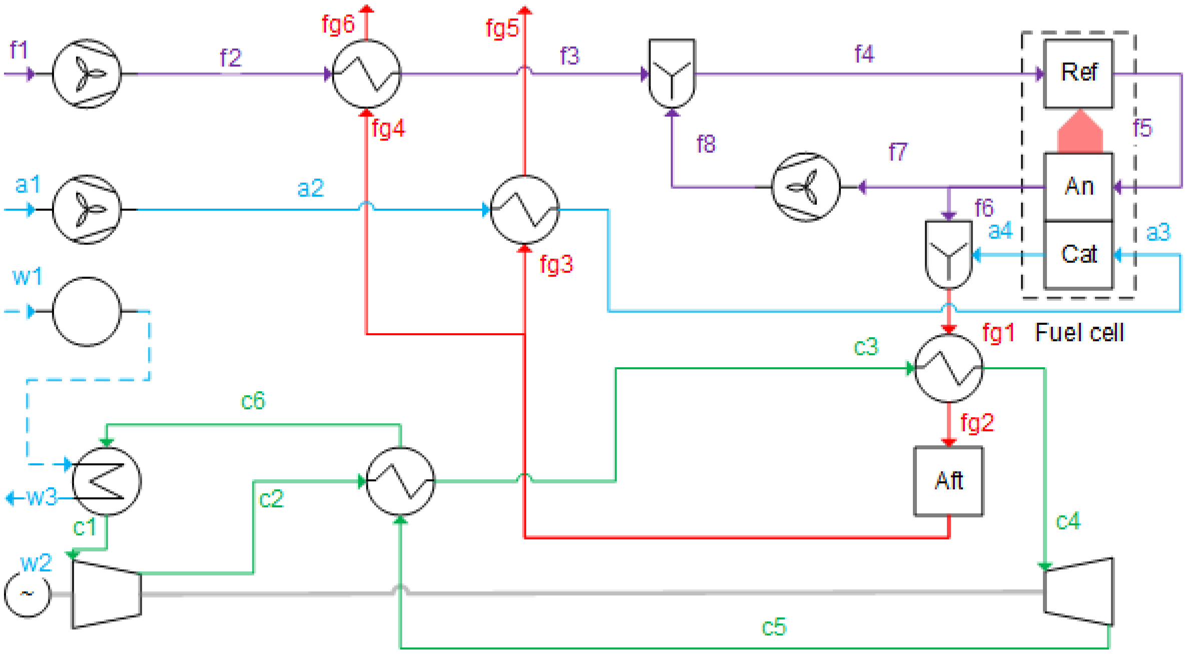

Figure C.19: *PFD (case VI.I: Case I simplified,* ΔT_{hex} = 10 °C)

Point	$\dot{n}$ (mol s^{-1})	P (bar)	T (°C)	**Exergy**(kW)		
				Thermo mechanical	Chemical	Total
f1	1.00	1.01325	25.00	0.00	832.00	832.00
f2	1.00	1.24257	44.19	0.53	832.00	832.53
f3	1.00	1.21772	551.68	12.33	832.00	844.33
f4	3.85	1.21772	786.85	69.45	923.33	992.78
f5	5.83	1.15683	786.85	77.07	1141.28	1218.34
f6	2.99	1.11056	886.85	57.52	100.21	157.73
f7	2.85	1.11056	886.85	54.77	95.43	150.20
f8	2.85	1.21772	912.82	57.96	95.43	153.39
a1	94.13	1.01325	25.00	0.00	0.00	0.00
a2	94.13	1.18044	42.59	37.00	0.00	37.00
a3	94.13	1.15683	786.85	1180.42	0.00	1180.42
a4	92.30	1.11056	886.85	1376.48	0.04	1376.52
fg1	95.29	1.11056	886.85	1433.19	83.26	1516.45
fg2	95.29	1.08835	771.32	1153.39	83.26	1236.65
fg3	94.03	1.03393	796.85	1186.77	2.11	1188.89
fg4	1.09	1.03393	796.85	13.79	0.02	13.82
fg5	94.03	1.01325	60.28	5.39	2.11	7.50
fg6	1.09	1.01325	60.28	0.06	0.02	0.09
c1	26.05	80.00	32.00	246.73	523.83	770.56
c2	26.05	250.00	64.88	274.40	523.83	798.23
c3	26.05	246.84	438.47	519.71	523.83	1043.55
c4	26.05	245.00	700.00	761.85	523.83	1285.68
c5	26.05	81.63	554.89	557.52	523.83	1081.35

c6	26.05	80.40	74.88	259.22	523.83	783.06
w1	115.81	1.01325	25.00	0.00	0.00	0.00
w2	115.81	1.03393	25.00	0.00	0.00	0.00
w3	115.81	1.01325	49.58	8.38	0.00	8.38

Table C.32: *State points (case VI.I: Case I simplified,* ΔT_{hex} = 10 °C*)*

	Point	**Concentration**						
Methane	f1-3	1.0000	0.0000	0.0000	0.0000	0.0000	0.0000	0.0000
Fuel mix	f4	0.2614	0.0480	0.4444	0.0285	0.2177	0.0000	0.0000
Syngas	f5	0.0019	0.4941	0.1713	0.2380	0.0947	0.0000	0.0000
Anode outlet	f6-8	0.0019	0.0649	0.6005	0.0385	0.2942	0.0000	0.0000
Air	a1-3	0.0000	0.0000	0.0313	0.0000	0.0003	0.2035	0.7649
Cathode outlet	a4	0.0000	0.0000	0.0319	0.0000	0.0003	0.1877	0.7801
Fuel cell exhaust	fg1-2	0.0001	0.0020	0.0497	0.0012	0.0095	0.1818	0.7556
Flue gas	fg3-5	0.0000	0.0000	0.0519	0.0000	0.0108	0.1804	0.7570
Carbon dioxide	c1-6	0.0000	0.0000	0.0000	0.0000	1.0000	0.0000	0.0000
Water	w1-3	0	0	1	0	0	0	0

Table C.33: *Gas compositions (case VI.I: Case I simplified,* ΔT_{hex} = 10 °C*)*

	Inlet	**Outlet**	$\dot{W}/\dot{Q}$ (kW)	**Exergy destruction** (kW)	η_{ex} (%)
			SOFC		
Reformer	f4	f5	234.77		
Fuel cell	f5/a3	f6/a4	379.66		
Total	f4/a3	f6/a4		109.08	94.98
			sCO_2 Brayton cycle		
Turbine	c4	c5	196.40	7.93	96.12
Compressor	c1	c2	33.63	5.96	82.29
Generator			154.63	8.14	95.00
			BoP		
Air blower	a1	a2	48.54	11.54	76.23
Fuel blower	f1	f2	0.69	0.16	76.33
Waterpump	w1	w2	0.01	0.00	75.00
Anode blower	f7	f8	3.40	0.21	93.70
Fuel mixer	f3/f8	f4	0.00	4.94	99.50
Exhaust mixer	f6/a4	fg1	0.00	17.80	98.84

Table C.34: *System components (case VI.I: Case I simplified,* ΔT_{hex} = 10 °C*)*

	Hot stream Inlet	Hot stream Outlet	Cold stream Inlet	Cold stream Outlet	$\dot{Q}$ (kW)	$\dot{Ex}_D$ (kW)	η_{ex} (%)	$\dot{U}$ (W m^{-2} °C^{-1})	A (m^2)
STHE									
Fuel preheater	fg4	fg6	f2	f3	25.57	1.92	85.99	20	19.04
Air preheater	fg3	fg5	a2	a3	2199.88	37.97	96.79	20	8090.01
PCHE									
Heater	fg1	fg2	c3	c4	377.11	37.66	86.54	500	2.99
Recuperator	c5	c6	c2	c3	650.10	52.98	82.24	754	15.17
Cooler	c6	c1	w2	w3	214.34	4.12	67.02	7000	11.20

Table C.35: *Heat exchangers(case VI.I: Case I simplified, ΔT_{hex} = 10 °C)*

C.7.2. Case VI.II: Simplified recompression cycle (4.6.2)

The points referred to in table C.37 to C.40 refer to the PFD in figure C.21.

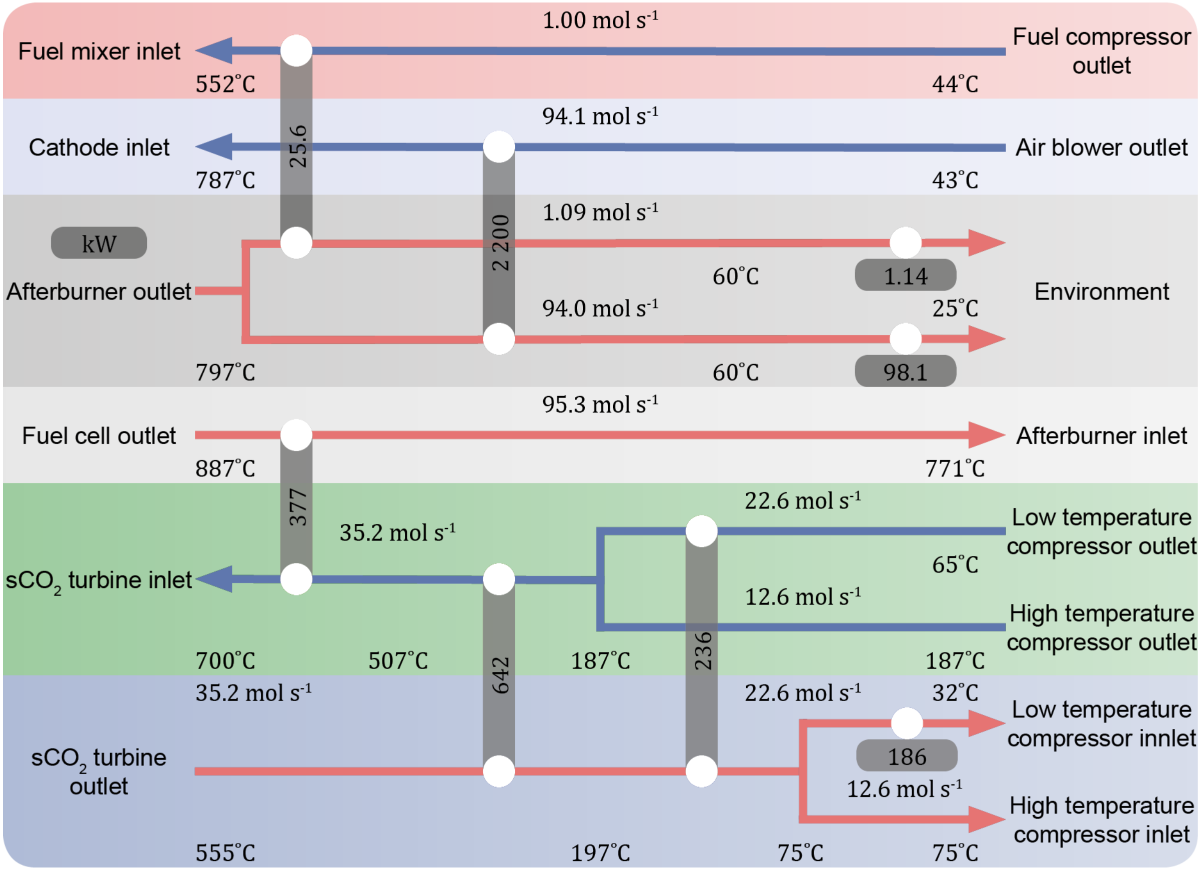

Figure C.20: *Heat exchanger network (case VI.II: Case II simplified, ΔT_{hex} = 10 °C)*

Fuel cell power	380 kW
Generator power	182 kW
Auxiliary power consumption	53 kW
Net AC system power	509 kW
LHV AC efficiency	63.42 %
Thermodynamic efficiency	72.63 %
Second law efficiency	62.05 %
Thermodynamic cycle efficiency	49.68 %
sCO_2 cycle flow	35.2 mol s^{-1}
Total PCHE area	68 m^2

Total STHE area	8109 m^2
Number of heat exchangers	6

Table C.36: *Key performance data (case VI.II: Case II simplified, ΔT_{hex} = 10 °C)*

Point	$\dot{n}$ (mol s^{-1})	P (bar)	T (°C)	**Exergy**(kW) Thermo mechanical	Chemical	Total
f1	1.00	1.01325	25.00	0.00	832.00	832.00
f2	1.00	1.24257	44.19	0.53	832.00	832.53
f3	1.00	1.21772	551.68	12.33	832.00	844.33
f4	3.85	1.21772	786.85	69.45	923.33	992.78
f5	5.83	1.15683	786.85	77.07	1141.28	1218.34
f6	2.99	1.11056	886.85	57.52	100.21	157.73
f7	2.85	1.11056	886.85	54.77	95.43	150.20
f8	2.85	1.21772	912.82	57.96	95.43	153.39
a1	94.13	1.01325	25.00	0.00	0.00	0.00
a2	94.13	1.18044	42.59	37.00	0.00	37.00
a3	94.13	1.15683	786.85	1180.42	0.00	1180.42
a4	92.30	1.11056	886.85	1376.48	0.04	1376.52
fg1	95.29	1.11056	886.85	1433.19	83.26	1516.45
fg2	95.29	1.08835	771.32	1153.39	83.26	1236.65
fg3	94.03	1.03393	796.85	1186.77	2.11	1188.89
fg4	1.09	1.03393	796.85	13.79	0.02	13.82
fg5	94.03	1.01413	60.28	5.59	2.11	7.70
fg6	1.09	1.01413	60.28	0.06	0.02	0.09
c1	22.55	80.00	32.00	213.60	453.50	667.10
c2	22.55	250.00	64.88	237.56	453.50	691.05
c3	35.19	248.67	186.88	458.20	707.64	1165.83
c4	35.19	246.36	507.00	781.29	707.64	1488.93
c5	35.19	245.00	700.00	1029.17	707.64	1736.80
c6	35.19	81.63	554.89	753.14	707.64	1460.78
c7	35.19	81.63	554.89	753.14	707.64	1460.78
c8	22.55	80.40	74.88	224.42	453.50	677.91
c9	12.64	80.40	74.88	125.76	254.14	379.90
w1	1.00	1.01325	25.00	0.00	0.00	0.00
w2	1.00	1.03393	25.00	0.00	0.00	0.00
w3	100.26	1.01325	49.58	7.25	0.00	7.25

Table C.37: *State points(case VI.II: Case II simplified, ΔT_{hex} = 10 °C)*

	Point	**Concentration**						
Methane	f1-3	1.0000	0.0000	0.0000	0.0000	0.0000	0.0000	0.0000
Fuel mix	f4	0.2614	0.0480	0.4444	0.0285	0.2177	0.0000	0.0000
Syngas	f5	0.0019	0.4941	0.1713	0.2380	0.0947	0.0000	0.0000
Anode outlet	f6-8	0.0019	0.0649	0.6005	0.0385	0.2942	0.0000	0.0000
Air	a1-3	0.0000	0.0000	0.0313	0.0000	0.0003	0.2035	0.7649
Cathode outlet	a4	0.0000	0.0000	0.0319	0.0000	0.0003	0.1877	0.7801
Fuel cell exhaust	fg1-2	0.0001	0.0020	0.0497	0.0012	0.0095	0.1818	0.7556
Flue gas	fg3-5	0.0000	0.0000	0.0519	0.0000	0.0108	0.1804	0.7570
Carbon dioxide	c1-8	0.0000	0.0000	0.0000	0.0000	1.0000	0.0000	0.0000
Water	w1-3	0	0	1	0	0	0	0

Table C.38: *Gas compositions (case VI.II: Case II simplified, ΔT_{hex} = 10 °C)*

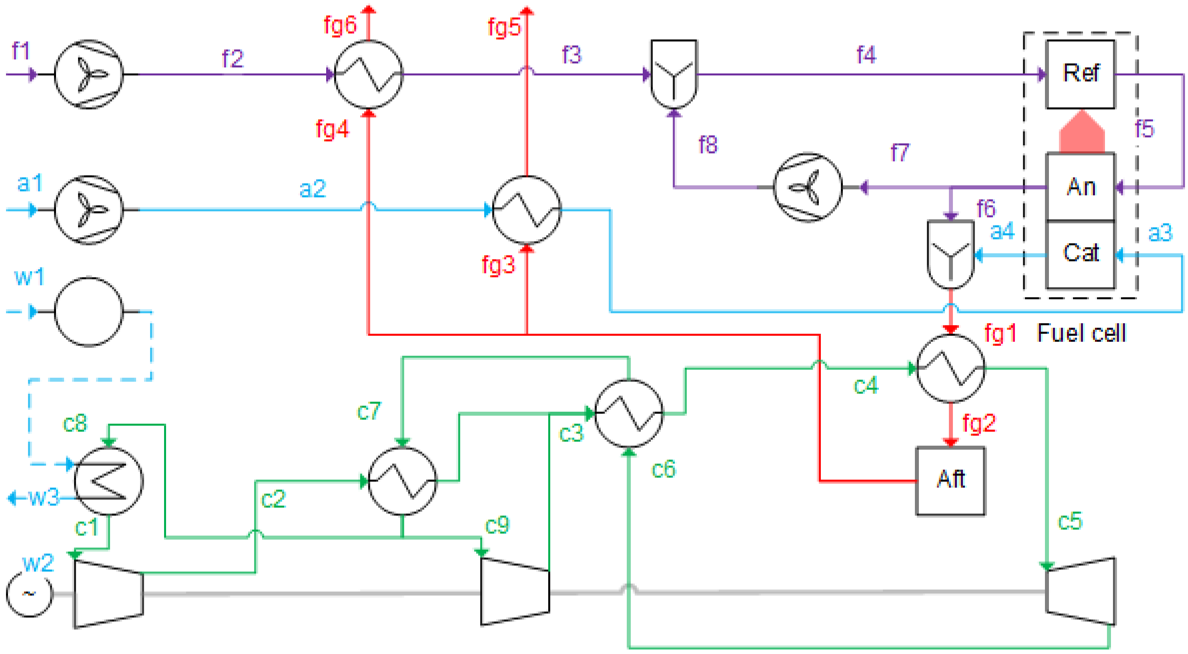

Figure C.21: *PFD (case VI.II: Case II simplified, ΔT_{hex} = 10 °C)*

	Inlet	**Outlet**	$\dot{W}/\dot{Q}$ (kW)	**Exergy destruction** (kW)	η_{ex} (%)
			SOFC		
Reformer	f4	f5	234.77		
Fuel cell	f5/a3	f6/a4	379.66		
Total	f4/a3	f6/a4		109.08	94.98
			sCO_2 Brayton cycle		
Turbine	c5	c6	265.31	10.72	96.12
LT compressor	c1	c2	29.11	5.16	82.29
HT compressor	c9	c3	44.65	5.85	86.89
Generator			181.97	9.58	95.00
			BoP		
Air blower	a1	a2	48.54	11.54	76.23
Fuel blower	f1	f2	0.69	0.16	76.33
Waterpump	w1	w2	0.00	0.00	75.00
Anode blower	f7	f8	3.40	0.21	93.70
Fuel mixer	f3/f8	f4	0.00	4.94	99.50
Exhaust mixer	f6/a4	fg1	0.00	17.80	98.84

Table C.39: *System components (case VI.II: Case II simplified, ΔT_{hex} = 10 °C)*

	Hot stream		**Cold stream**		$\dot{Q}$	$\dot{Ex}_D$	η_{ex}	$\dot{U}$	A
	Inlet	**Outlet**	**Inlet**	**Outlet**	(kW)	(kW)	(%)	(W m^{-2} °C^{-1})	(m^2)
					STHE				
Fuel preheater	fg4	fg6	f2	f3	25.57	1.92	86.00	20	19.04
Air preheater	fg3	fg5	a2	a3	2199.88	37.76	96.80	20	8090.01
					PCHE				
Heater	fg1	fg2	c4	c5	377.11	31.92	88.59	500	3.38
LT recuperator	c7	c8+c9	c2	c3	236.12	5.66	90.84	754	27.37
HT recuperator	c6	c7	c3	c4	642.10	18.13	94.69	754	27.66
Cooler	c8	c1	w2	w3	185.56	3.57	67.02	7000	9.69

Table C.40: *Heat exchangers (case VI.II: Case II simplified, ΔT_{hex} = 10 °C)*

C.7.3. Case VI.III: Simplified Cathode recirculation (4.6.3)

The points referred to in table C.42 to C.45 refer to the PFD in figure C.23.

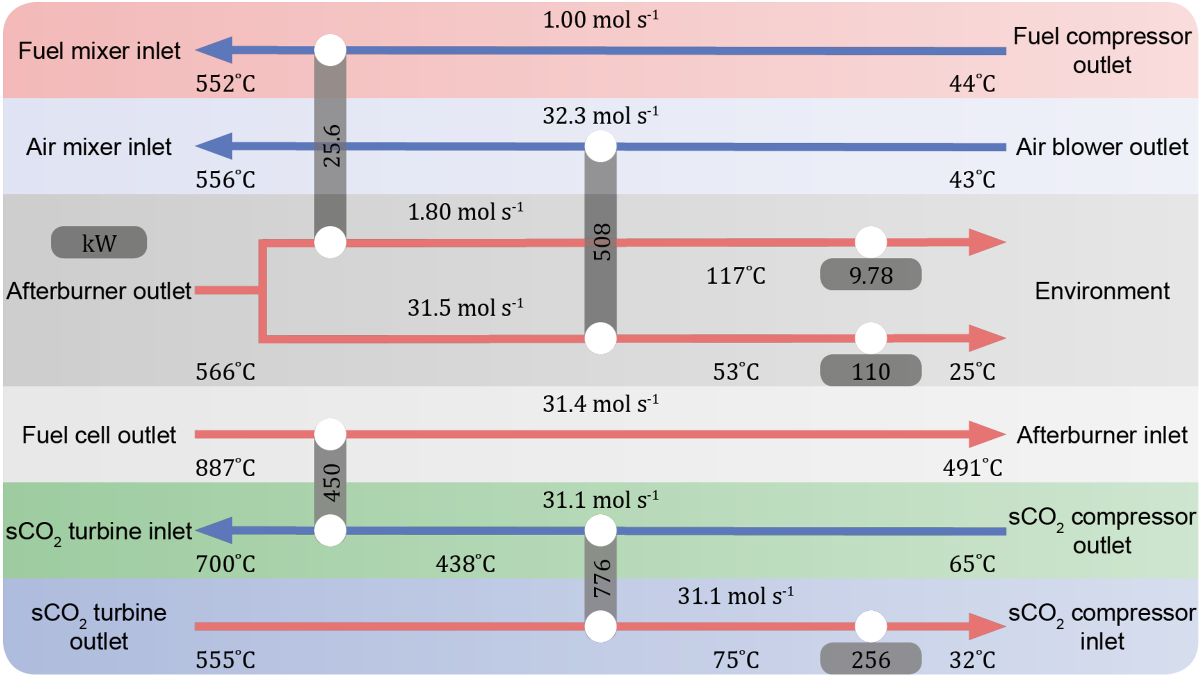

Figure C.22: *Heat exchanger network (case VI.III: Case III simplified, r_{ca} = 67.39% , ΔT_{hex} = 10 °C)*

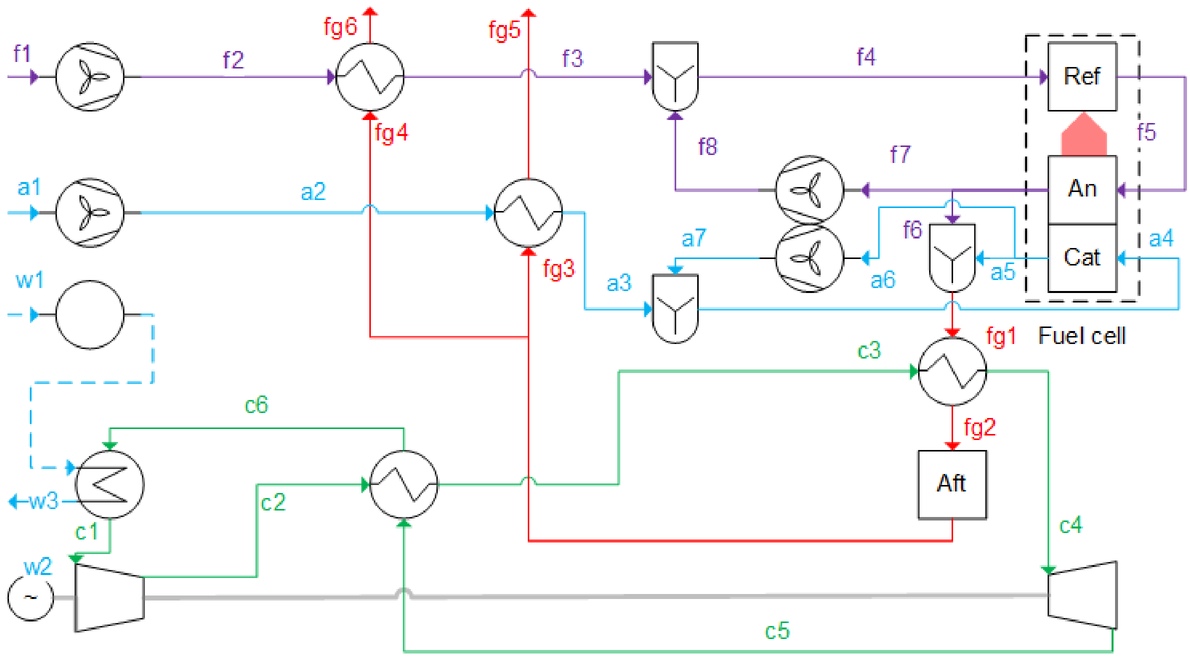

Figure C.23: *PFD (case VI.III: Case III simplified, ΔT_{hex} = 10 °C)*

Fuel cell power	377 kW
Generator power	185 kW
Auxiliary power consumption	54 kW
Net AC system power	507 kW

LHV AC efficiency	63.20 %
Thermodynamic efficiency	72.58 %
Second law efficiency	62.16 %
Thermodynamic cycle efficiency	43.16 %
sCO_2 cycle flow	31.1 $mol\,s^{-1}$
Total PCHE area	40 m^2
Total STHE area	2510 m^2
Number of heat exchangers	5

Table C.41: *Key performance data (case VI.III: Case III simplified, r_{ca} = 67.39% , ΔT_{hex} = 10 °C)*

Point	$\dot{n}$ ($mol\,s^{-1}$)	P (bar)	T (°C)	**Exergy**(kW) Thermo mechanical	Chemical	Total
f1	1.00	1.01325	25.00	0.00	832.00	832.00
f2	1.00	1.24257	44.19	0.53	832.00	832.53
f3	1.00	1.21772	551.68	12.33	832.00	844.33
f4	3.85	1.21772	786.85	69.45	923.33	992.78
f5	5.83	1.15683	786.85	77.07	1141.28	1218.34
f6	2.99	1.11056	886.85	57.52	100.21	157.73
f7	2.85	1.11056	886.85	54.77	95.43	150.20
f8	2.85	1.21772	912.82	57.96	95.43	153.39
a1	32.28	1.01325	25.00	0.00	0.00	0.00
a2	32.28	1.18044	42.59	12.69	0.00	12.69
a3	32.28	1.15683	555.78	236.32	0.00	236.32
a4	95.22	1.15683	786.85	1192.00	0.46	1192.47
a5	30.45	1.11056	886.85	453.35	0.43	453.78
a6	62.93	1.11056	886.85	936.93	0.88	937.81
a7	62.93	1.15683	902.27	968.03	0.88	968.91
fg1	33.44	1.11056	886.85	510.60	86.79	597.39
fg2	33.44	1.08835	490.83	199.94	86.79	286.74
fg3	31.47	1.03393	565.78	236.74	4.97	241.71
fg4	1.80	1.03393	565.78	13.55	0.28	13.83
fg5	31.47	1.01357	52.59	4.12	4.97	9.09
fg6	1.80	1.01602	117.11	0.82	0.28	1.11
c1	31.10	80.00	32.00	294.52	625.29	919.81
c2	31.10	250.00	64.88	327.55	625.29	952.84
c3	31.10	246.84	438.47	620.37	625.29	1245.66
c4	31.10	245.00	700.00	909.41	625.29	1534.69
c5	31.10	81.63	554.89	665.50	625.29	1290.79
c6	31.10	80.40	74.88	309.43	625.29	934.72
w1	138.24	1.01325	25.00	0.00	0.00	0.00
w2	138.24	1.03393	25.00	0.01	0.00	0.01
w3	138.24	1.01325	49.58	10.00	0.00	10.00

Table C.42: *State points (case VI.III: Case III simplified, r_{ca} = 67.39% , ΔT_{hex} = 10 °C)*

	Point	**Concentration**						
Methane	f1-3	1.0000	0.0000	0.0000	0.0000	0.0000	0.0000	0.0000
Fuel mix	f4	0.2614	0.0480	0.4444	0.0285	0.2177	0.0000	0.0000
Syngas	f5	0.0019	0.4941	0.1713	0.2380	0.0947	0.0000	0.0000
Anode outlet	f6-8	0.0019	0.0649	0.6005	0.0385	0.2942	0.0000	0.0000
Air	a1-3	0.0000	0.0000	0.0313	0.0000	0.0003	0.2035	0.7649

Cathode inlet	a4	0.0000	0.0000	0.0325	0.0000	0.0003	0.1718	0.7954
Cathode outlet	a5-7	0.0000	0.0000	0.0332	0.0000	0.0003	0.1555	0.8110
Fuel cell exhaust	fg1-2	0.0002	0.0058	0.0839	0.0034	0.0266	0.1416	0.7385
Flue gas	fg3-5	0.0000	0.0000	0.0901	0.0000	0.0303	0.1373	0.7422
Carbon dioxide	c1-6	0.0000	0.0000	0.0000	0.0000	1.0000	0.0000	0.0000
Water	w1-3	0.0000	0.0000	1.0000	0.0000	0.0000	0.0000	0.0000

Table C.43: *Gas compositions (case VI.III: Case III simplified, r_{ca} = 67.39% , ΔT_{hex} = 10 °C)*

	Inlet	Outlet	$\dot{W}/\dot{Q}$ (kW)	**Exergy destruction** (kW)	η_{ex} (%)
			SOFC		
Reformer	f4	f5	234.77		
Fuel cell	f5/a3	f6/a4	376.58		
Total	f4/a3	f6/a4		109.15	95.01
			sCO_2 Brayton cycle		
Turbine	c4	c5	234.43	9.47	96.12
Compressor	c1	c2	40.14	7.11	82.29
Generator			184.58	9.71	95.00
			BoP		
Air blower	a1	a2	16.65	3.96	76.23
Fuel blower	f1	f2	0.69	0.16	76.33
Waterpump	w1	w2	0.01	0.00	75.00
Anode blower	f7	f8	3.40	0.21	93.70
Cathode blower	f6	f7	33.21	2.11	93.65
Fuel mixer	f3/f8	f4	0.00	4.94	99.50
Air mixer	a3/a7	a4	0.00	12.76	98.94
Exhaust mixer	f6/a5	fg1	0.00	14.11	97.69

Table C.44: *System components (case VI.III: Case III simplified, r_{ca} = 67.39% , ΔT_{hex} = 10 °C)*

	Hot stream		**Cold stream**		$\dot{Q}$	$\dot{Ex}_D$	η_{ex}	$\dot{U}$	A
	Inlet	**Outlet**	**Inlet**	**Outlet**	(kW)	(kW)	(%)	(W m^{-2} °C^{-1})	(m^2)
					STHE				
Fuel preheater	fg4	fg6	f2	f3	25.57	0.92	92.77	20	79.61
Air preheater	fg3	fg5	a2	a3	507.75	8.98	96.14	20	2430.35
					PCHE				
Heater	fg1	fg2	c3	c4	450.15	21.63	93.04	500.00	8.36
Recuperator	c5	c6	c2	c3	776.02	63.25	82.24	754.00	18.11
Cooler	c6	c1	w2	w3	255.85	4.92	67.02	7000.00	13.36

Table C.45: *Heat exchangers (case VI.III: Case III simplified, r_{ca} = 67.39% , ΔT_{hex} = 10 °C)*

C.7.4. Case VI.IV: Simplified recompression cycle + cathode recirculation (4.6.4)

The points referred to in table C.47 to C.50 refer to the PFD in figure C.25.

Fuel cell power	377 kW
Generator power	216 kW
Auxiliary power consumption	54 kW
Net AC system power	539 kW
LHV AC efficiency	67.10 %
Thermodynamic efficiency	76.68 %
Second law efficiency	65.76 %

Thermodynamic cycle efficiency	49.68 %
sCO_2 cycle flow	41.7 mol s^{-1}
Total PCHE area	91 m^2
Total STHE area	2729 m^2
Number of heat exchangers	6

Table C.46: *Key performance data (case VI.IV: Case IV simplified, r_{ca} = 65.16% , ΔT_{hex} = 10 °C)*

Point	$\dot{n}$ (mol s^{-1})	P (bar)	T (°C)	**Exergy**(kW) Thermo mechanical	Chemical	Total
f1	1.00	1.01325	25.00	0.00	832.00	832.00
f2	1.00	1.24257	44.19	0.53	832.00	832.53
f3	1.00	1.21772	551.68	12.33	832.00	844.33
f4	3.85	1.21772	786.85	69.45	923.33	992.78
f5	5.83	1.15683	786.85	77.07	1141.28	1218.34
f6	2.99	1.11056	886.85	57.52	100.21	157.73
f7	2.85	1.11056	886.85	54.77	95.43	150.20
f8	2.85	1.21772	912.82	57.96	95.43	153.39
a1	34.33	1.01325	25.00	0.00	0.00	0.00
a2	34.33	1.18044	42.59	13.49	0.00	13.49
a3	34.33	1.15683	577.37	266.76	0.00	266.76
a4	95.11	1.15683	786.85	1190.82	0.35	1191.17
a5	32.49	1.11056	886.85	483.84	0.39	484.23
a6	60.78	1.11056	886.85	905.03	0.72	905.76
a7	60.78	1.15683	902.27	935.07	0.72	935.79
fg1	35.48	1.11056	886.85	541.07	86.56	627.64
fg2	35.48	1.08835	517.00	230.61	86.56	317.17
fg3	33.50	1.03393	587.37	267.01	4.79	271.79
fg4	1.81	1.03393	587.37	14.45	0.26	14.71
fg5	33.50	1.01359	52.59	4.08	4.79	8.87
fg6	1.81	1.01689	143.33	1.19	0.26	1.45
c1	26.71	80.00	32.00	252.98	537.09	790.07
c2	26.71	250.00	64.88	281.35	537.09	818.44
c3	41.68	248.67	186.88	542.66	838.08	1380.74
c4	41.68	246.36	507.00	925.31	838.08	1763.39
c5	41.68	245.00	700.00	1218.88	838.08	2056.96
c6	41.68	81.63	554.89	891.98	838.08	1730.05
c7	41.68	81.63	554.89	891.98	838.08	1730.05
c8	26.71	80.40	74.88	265.79	537.09	802.88
c9	14.97	80.40	74.88	148.95	300.99	449.93
w1	1.00	1.01325	25.00	0.00	0.00	0.00
w2	1.00	1.03393	25.00	0.00	0.00	0.00
w3	118.74	1.01325	49.58	8.59	0.00	8.59

Table C.47: *State points (case VI.IV: Case IV simplified, r_{ca} = 65.16% , ΔT_{hex} = 10 °C)*

	Point	**Concentration**						
Methane	f1-3	1.0000	0.0000	0.0000	0.0000	0.0000	0.0000	0.0000
Fuel mix	f4	0.2614	0.0480	0.4444	0.0285	0.2177	0.0000	0.0000
Syngas	f5	0.0019	0.4941	0.1713	0.2380	0.0947	0.0000	0.0000
Anode outlet	f6-8	0.0019	0.0649	0.6005	0.0385	0.2942	0.0000	0.0000
Air	a1-3	0.0000	0.0000	0.0313	0.0000	0.0003	0.2035	0.7649
Cathode inlet	a4	0.0000	0.0000	0.0324	0.0000	0.0003	0.1748	0.7925

Cathode outlet	a5-7	0.0000	0.0000	0.0331	0.0000	0.0003	0.1585	0.8081
Fuel cell exhaust	fg1-2	0.0002	0.0055	0.0809	0.0032	0.0251	0.1452	0.7400
Flue gas	fg3-5	0.0000	0.0000	0.0867	0.0000	0.0286	0.1412	0.7435
Carbon dioxide	c1-9	0.0000	0.0000	0.0000	0.0000	1.0000	0.0000	0.0000
Water	w1-3	0.0000	0.0000	1.0000	0.0000	0.0000	0.0000	0.0000

Table C.48: *Gas compositions (case VI.IV: Case IV simplified, r_{ca} = 65.16% , ΔT_{hex} = 10 °C)*

	Inlet	**Outlet**	$\dot{W}/\dot{Q}$ (kW)	**Exergy destruction** (kW)	η_{ex} (%)
SOFC					
Reformer	f4	f5	234.77		
Fuel cell	f5/a3	f6/a4	376.89		
Total	f4/a3	f6/a4		109.14	95.00
sCO_2 Brayton cycle					
Turbine	c5	c6	314.21	12.69	96.12
LT compressor	c1	c2	34.48	6.11	82.29
HT compressor	c9	c3	52.88	6.93	86.89
Generator			215.52	11.34	95.00
BoP					
Air blower	a1	a2	17.70	4.21	76.23
Fuel blower	f1	f2	0.69	0.16	76.33
Waterpump	w1	w2	0.00	0.00	75.00
Anode blower	f7	f8	3.40	0.21	93.70
Cathode blower	f6	f7	32.08	2.04	93.65
Fuel mixer	f3/f8	f4	0.00	4.94	99.50
Air mixer	a3/a7	a4	0.00	11.39	99.05
Exhaust mixer	f6/a4	fg1	0.00	14.32	97.77

Table C.49: *System components (case VI.IV: Case IV simplified, r_{ca} = 65.16% , ΔT_{hex} = 10 °C)*

	Hot stream		**Cold stream**		$\dot{Q}$	$\dot{Ex}_D$	η_{ex}	$\dot{U}$	A
	Inlet	**Outlet**	**Inlet**	**Outlet**	(kW)	(kW)	(%)	(W m^{-2} °C^{-1})	(m^2)
STHE									
Fuel preheater	fg4	fg6	f2	f3	25.57	1.45	89.04	20	30.25
Air preheater	fg3	fg5	a2	a3	563.89	9.66	96.33	20	2698.21
PCHE									
Heater	fg1	fg2	c4	c5	446.62	16.90	94.56	500	14.24
LT recuperator	c7	c8+c9	c2	c3	279.64	6.70	90.84	754	32.42
HT recuperator	c6	c7	c3	c4	760.46	21.47	94.69	754	32.76
Cooler	c8	c1	w2	w3	219.76	4.22	67.02	7000	11.48

Table C.50: *Heat exchangers(case VI.IV: Case IV simplified, r_{ca} = 65.16% , ΔT_{hex} = 10 °C)*

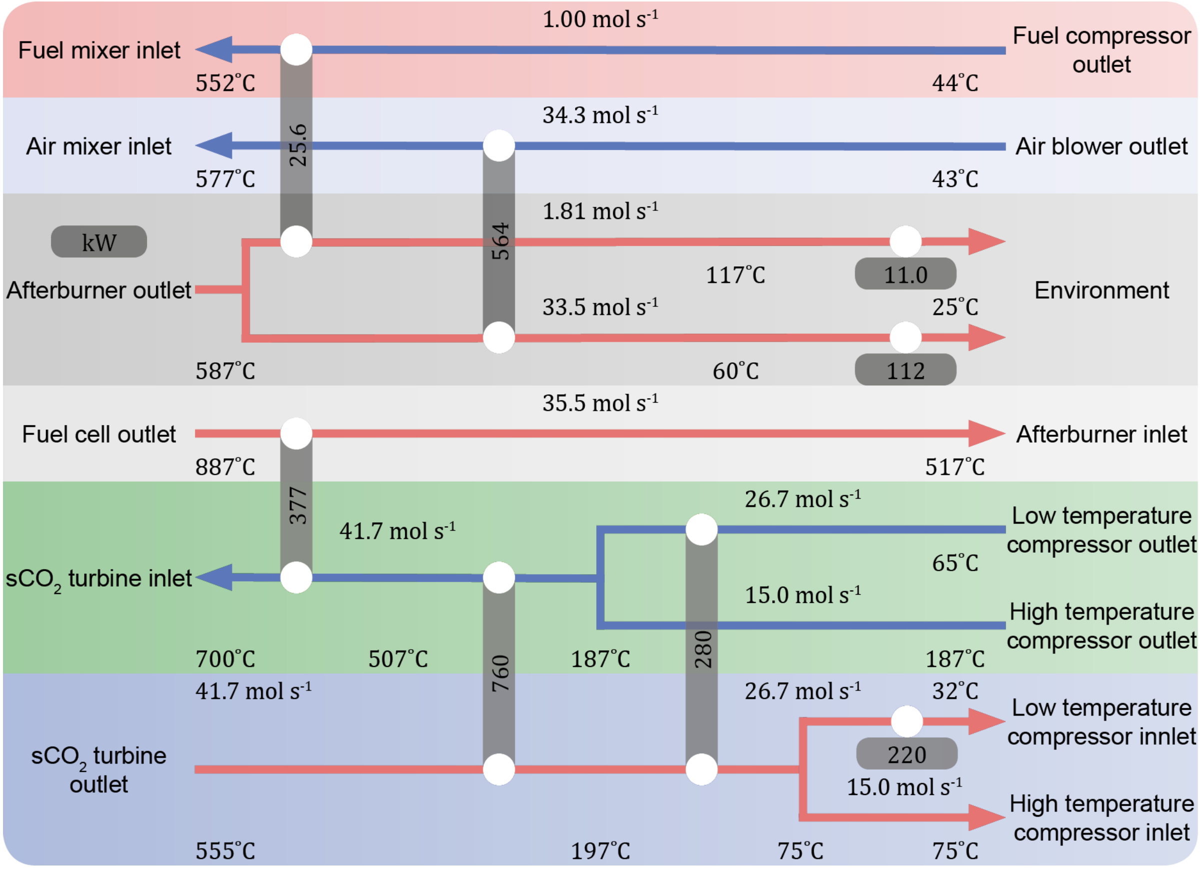

Figure C.24: *Heat exchanger network (case VI.IV: Case IV simplified,* r_{ca} *= 65.16% ,* ΔT_{hex} = 10 °C*)*

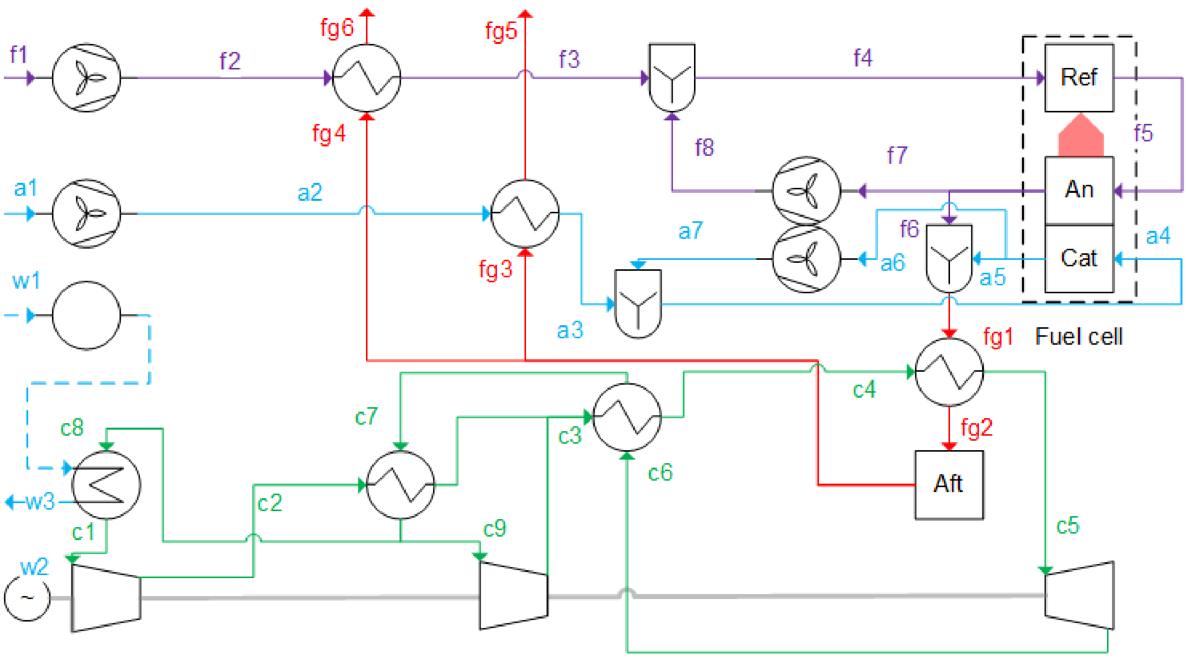

Figure C.25: *PFD (case VI.IV: Case IV simplified,* r_{ca} *= 65.16% ,* ΔT_{hex} = 10 °C*)*

C.7.5. Case VI.V: Simplified heat recovery steam generator (4.6.5)

The points referred to in table C.52 to C.55 refer to the PFD in figure C.27.

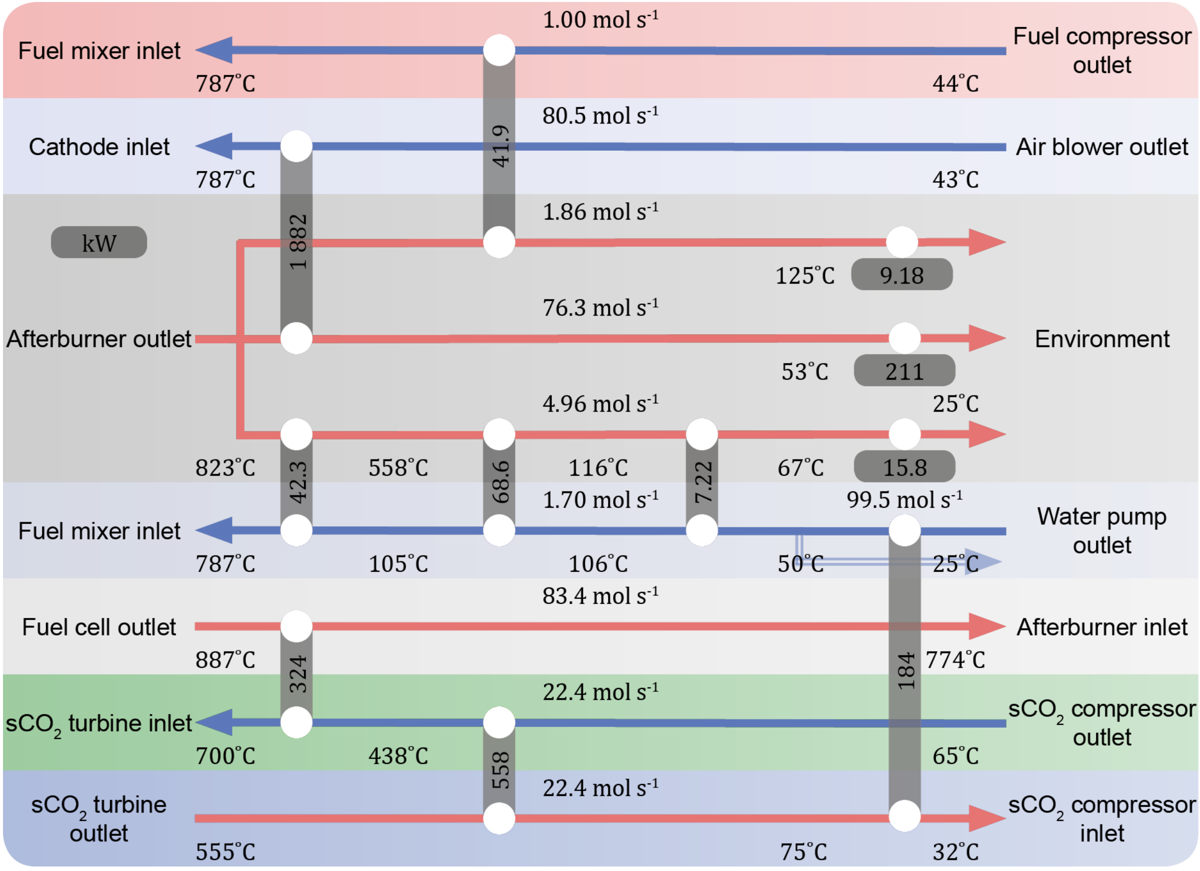

Figure C.26: *Heat exchanger network (case VI.V: Case V simplified, $\dot{n}_{fd}^{H_2O}$ = 1.7 mol s^{-1} , ΔT_{hex} = 10 °C)*

Fuel cell power	367 kW
Generator power	133 kW
Auxiliary power consumption	42 kW
Net AC system power	458 kW
LHV AC efficiency	57.03 %
Thermodynamic efficiency	64.57 %
Second law efficiency	55.86 %
Thermodynamic cycle efficiency	41.16 %
sCO_2 cycle flow	22.4 mol s^{-1}
Total PCHE area	25 m^2
Total STHE area	4547 m^2
Number of heat exchangers	8

Table C.51: *Key performance data (case VI.V: Case V simplified, $\dot{n}_{fd}^{H_2O}$ = 1.7 mol s^{-1}, ΔT_{hex} = 10 °C)*

Point	$\dot{n}$ (mol s^{-1})	P (bar)	T (°C)	**Exergy**(kW) Thermo mechanical	Chemical	Total
f1	1.00	1.01325	25.00	0.00	832.00	832.00
f2	1.00	1.24257	44.19	0.53	832.00	832.53
f3	1.00	1.21772	786.85	23.46	832.00	855.47
f4	2.70	1.21772	786.85	49.18	829.54	878.72

f5	4.65	1.15683	786.85	58.49	1027.82	1086.32
f6	4.65	1.11056	886.85	86.76	161.69	248.45
a1	80.51	1.01325	25.00	0.00	0.00	0.00
a2	80.51	1.18044	42.59	31.65	0.00	31.65
a3	80.51	1.15683	786.85	1009.58	0.00	1009.58
a4	78.81	1.11056	886.85	1175.23	0.05	1175.28
fg1	83.46	1.11056	886.85	1261.30	141.23	1402.53
fg2	83.46	1.08835	774.25	1020.81	141.23	1162.04
fg3	76.34	1.03393	822.93	1022.62	-1.21	1021.41
fg4	1.86	1.03393	822.93	24.95	-0.03	24.92
fg5	76.34	1.01355	52.59	6.93	-1.21	5.72
fg6	1.86	1.01534	125.30	0.88	-0.03	0.85
fg7	4.96	1.03393	822.93	66.43	-0.08	66.35
fg8	4.96	1.02655	558.35	35.84	-0.08	35.76
fg9	4.96	1.01511	115.76	2.00	-0.08	1.92
fg10	4.96	1.01390	66.93	0.68	-0.08	0.60
c1	22.37	80.00	32.00	211.88	449.85	661.73
c2	22.37	250.00	64.88	235.65	449.85	685.49
c3	22.37	246.84	438.47	446.31	449.85	896.16
c4	22.37	245.00	700.00	654.25	449.85	1104.10
c5	22.37	81.63	554.89	478.78	449.85	928.63
c6	22.37	80.40	74.88	222.61	449.85	672.46
w1	99.46	1.01	25.00	0.00	0.00	0.00
w2	99.46	1.05503	25.00	0.01	0.00	0.01
w3	97.76	1.03393	49.58	7.08	0.00	7.08
w4	1.70	1.24257	49.58	0.12	0.00	0.12
w5	1.70	1.24107	105.76	1.20	0.00	1.20
w6	1.70	1.22687	105.42	15.77	0.00	15.77
w7	1.70	1.21772	786.85	40.33	0.00	40.33

Table C.52: *State points (case VI.V: Case V simplified, $\dot{n}_{fd}^{H_2O}$ = 1.7 mol s^{-1}, ΔT_{hex} = 10 °C)*

	Point	Concentration						
Anode outlet	f6	0.0048	0.0832	0.7020	0.0264	0.1836	0.0000	0.0000
Air	a1-3	0.0000	0.0000	0.0313	0.0000	0.0003	0.2035	0.7649
Cathode outlet	a4	0.0000	0.0000	0.0320	0.0000	0.0003	0.1863	0.7814
Fuel cell exhaust	fg1-2	0.0003	0.0046	0.0693	0.0015	0.0105	0.1759	0.7378
Flue gas	fg3-10	0.0000	0.0000	0.0742	0.0000	0.0123	0.1730	0.7405
Carbon dioxide	c1-6	0.0000	0.0000	0.0000	0.0000	1.0000	0.0000	0.0000
Water	w1-7	0.0000	0.0000	1.0000	0.0000	0.0000	0.0000	0.0000

Table C.53: *Gas compositions (case VI.V: Case V simplified, $\dot{n}_{fd}^{H_2O}$ = 1.7 mol s^{-1}, ΔT_{hex} = 10 °C)*

	Inlet	**Outlet**	$\dot{W}/\dot{Q}$ (kW)	**Exergy destruction** (kW)	η_{ex} (%)
			SOFC		
Reformer	f4	f5	215.54		
Fuel cell	f5/a3	f6/a4	367.12		
Total	f4/a3	f6/a4		97.47	94.84
			sCO_2 Brayton cycle		
Turbine	c4	c5	168.66	6.81	96.12
Compressor	c1	c2	28.88	5.11	82.29
Generator			133.79	6.99	95.00

BoP					
Air blower	a1	a2	41.52	9.87	76.23
Fuel blower	f1	f2	0.69	0.16	76.33
Waterpump	w1	w2	0.01	0.00	75.00
Fuel mixer	f3/w7	f4	0.00	17.07	98.09
Exhaust mixer	f6/a4	fg1	0.00	21.20	98.51

Table C.54: *System components (case VI.V: Case V simplified,* $\dot{n}_{fd}^{H_2O}$ = 1.7 mol s^{-1}, ΔT_{hex} = 10 °C*)*

	Hot stream		**Cold stream**		$\dot{Q}$	$\dot{Ex}_D$	η_{ex}	$\dot{U}$	A
	Inlet	**Outlet**	**Inlet**	**Outlet**	(kW)	(kW)	(%)	(W m^{-2} °C^{-1})	(m^2)
STHE									
Fuel preheater	fg4	fg6	f2	f3	41.87	1.13	95.29	20	116.45
Air preheater	fg3	fg5	a2	a3	1881.49	37.75	96.28	20	4379.34
Economizer	fg9	fg10	w4	w5	7.22	0.25	81.17	30	18.08
Boiler	fg8	fg9	w5	w6	68.62	19.27	43.07	30	18.52
Steam Superheater	fg7	fg8	w6	w7	44.26	6.03	80.29	20	14.10
PCHE									
Heater	fg1	fg2	c3	c4	323.85	32.54	86.47	500	2.55
Recuperator	c5	c6	c2	c3	558.29	45.50	82.24	754	13.03
Cooler	c6	c1	w2	w3+w4	184.07	3.54	67.02	7000	9.62

Table C.55: *Heat exchangers (case VI.V: Case V simplified,* $\dot{n}_{fd}^{H_2O}$ = 1.7 mol s^{-1}, ΔT_{hex} = 10 °C*)*

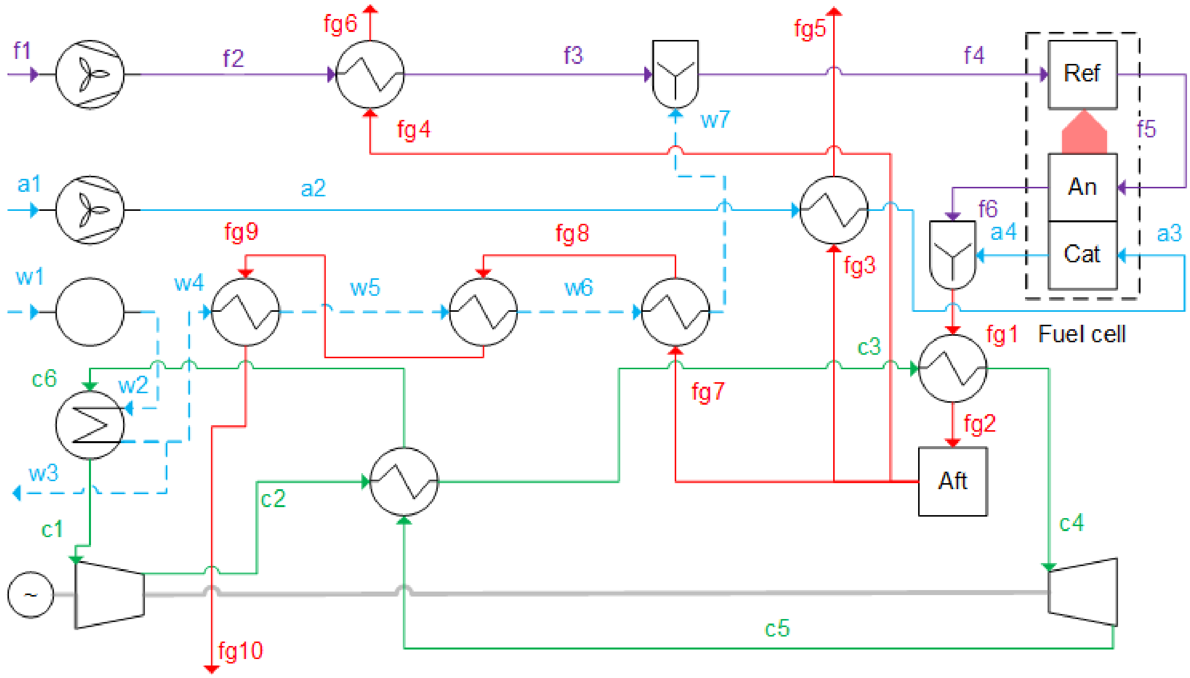

Figure C.27: *PFD (case VI.V: Case V simplified, $\dot{n}_{fd}^{H_2O}$ = 1.7 mol s^{-1}, ΔT_{hex} = 10 °C)*

C.8. Comparison (4.8)

	LHV efficiency(%)	**Number of Hex**	**PCHE area** (m^2)	**STHE area** (m^2)
Case I: Basic setup (4.1)	61.13	8	44	3778
Case II: Recompression cycle(4.2)	63.26	10	79	4467
Case III: Cathode recirculation (4.3)	63.52	7	45	508
Case IV: Recompression cycle + cathode recirculation (4.4)	66.58	9	100	792
Case V: Heat recovery steam generator (4.5)	57.37	12	34	2963
Case VI.I: Simplified basic setup (4.6.1)	60.01	5	29	8109
Case VI.II: Simplified recompression cycle (4.6.2)	63.42	6	68	8109
Case VI.III: Simplified Cathode recirculation (4.6.3)	63.2	5	40	2510
Case VI.IV: Simplified recompression cycle + cathode recirculation (4.6.4)	67.1	6	91	2729
Case VI.V: Simplified heat recovery steam generator (4.6.5)	57.03	8	25	4547
Case VII: Directly coupled GT (4.7)	62.38	2	0	2961

Table C.56: *Performance overview, (Case II and case IV refer to case II.A and case IV.A specifically)*